TAMPEREEN TEKNILLINEN YLIOPISTO
TAMPERE UNIVERSITY OF TECHNOLOGY

OULA JUUTILAINEN

QUANTITATIVE COMPARISON OF GLASS AND PLASTIC OPTICAL COMPONENTS IN MASS-PRODUCED IMAGING APPLICATIONS

Master of Science Thesis

Examiners: Assoc. Prof. (tenure track) Juha Toivonen and Dr. Johan Sand
Examiners and topic approved by the Faculty Council of the Faculty of Natural Sciences
on 28th of March 2018

ABSTRACT

OULA JUUTILAINEN: Quantitative Comparison of Glass and Plastic Optical Components in Mass-Produced Imaging Applications
Tampere University of Technology
Master of Science Thesis, 111 pages, 11 Appendix pages
November 2018
Master's Degree Programme in Science and Engineering
Major: Advanced Engineering Physics
Examiners: Assoc. Prof. (tenure track) Juha Toivonen and Dr. Johan Sand
Keywords: imaging, hybrid optics, thermal defocus, short wavelength transmittance, noise, simulation

Plastics have, in imaging applications, mostly replaced glass as the most common optical material. However, as there is a constant demand for better and better cameras, manufacturers are starting to hit limits of optical qualities of current polymer materials. This has raised interest towards hybrid optics, meaning lenses of a camera comprise of both glass and plastic elements rather than just one or the other.

In this thesis a wide range of physical and optical qualities of different optical glasses and plastics were studied via in order to later determine possible applications, in which hybrid optics could produce added value to the consumers. To achieve this goal, first a broad understanding on materials' properties was gathered via literature review, after which the two most promising topics were studied more in detail. At first it was settled upon a decision to compare short wavelength transmittance and its effects on noise creation in final image formation with a MATLAB simulation. Also the effects of temperature changes on focal length were studied.

It was found, that glasses are much more resistant to thermal defocus: in 10–50 °C temperature range plastics were at least ten times more affected. Also this difference would increase slightly exponentially, if temperature range was increased.

High transmittance was verified to reduce noise in final image. The biggest relative advantage was achieved in low light scenarios. As material differences go, for thin, well AR-coated plastics and glasses, transmittance differences are so tiny, that they only produce at maximum 0.8 % SNR difference for glass's advantage with six 0.4 mm lens stack. In one case, plastic even prevailed glass. However, it was found, that transmittances of plastics drop, when they are thermally aged, whereas glasses sustain high heats considerably better. Also AR-coatings for plastics may not be as efficient as ones for glasses. Thus results in this thesis are considered a best case scenario in terms of noise performance of plastics.

TIIVISTELMÄ

OULA JUUTILAINEN: Lasisten ja muovisten optisten komponenttien kvantitatiivinen vertailu massatuotetuissa kuvantamissovelluksissa
Tampereen teknillinen yliopisto
Diplomityö, 111 sivua, 11 liitesivua
Marraskuu 2018
Teknis-luonnontieteellinen tutkinto-ohjelma
Pääaine: Teknillinen fysiikka
Tarkastajat: Apulaisprof. Juha Toivonen ja TkT Johan Sand
Avainsanat: kuvantaminen, hybridioptiikka, polttovälin lämpötilariippuvuus, lyhyen aallonpituuden läpäisevyys, kohina, simulaatio

Muovimateriaalit ovat suurimmilta osin korvanneet lasit optisissa sovelluksissa. Kuluttajat kuitenkin vaativat jatkuvasti parempia ja parempia kameroita, joten nykyisten polymeerimateriaalien optisten ominaisuuksien rajat alkavat lähestyä, mikä onkin nostanut kiinnostusta hybridioptiikkaa kohtaan. Tämä tarkoittaa, että kameran linsseissä käytetään sekä muovi- että lasilinssejä vain jomman kumman materiaalin hyödyntämisen sijaan.

Tämän diplomityön tarkoituksena oli kerätä tietämystä, jota hyödyntamällä voitaisiin myöhemmin löytää sovellusalueita, joissa hybridioptiikka voisi tuoda lisäarvoa tuotteen loppukäyttäjälle. Tavoitteen saavuttamiseksi kerättiin ensin kirjallisuuskatsauksen keinoin laaja käsitys materiaalien optisista ja fysikaalisista ominaisuuksista, minkä jälkeen kahta lupaavinta aihetta tutkittiin tarkemmin. Näiksi aiheiksi valikoituivat lyhyen aallonpituuden läpäisevyyden tarkastelu MATLAB-simulaation keinoin sekä lämpötilan muutoksen vaikutus linssin polttoväliin hieman kevyemmin laskennallisin työkaluin.

Työn tuloksena huomattiin lasilinssin polttovälin olevan huomattavasti stabiilimpi kuin muovilinssin lämpötilan muuttuessa: 10–50 °C lämpötila-alueella muovilinssin polttoväli muuttui vähintään 10-kertaisesti verrattuna lasilinssiin. Tämä ero kasvaa myös lievän eksponentiaalisesti lämpötilavälin kasvaessa.

Korkean läpäisevyyden huomattiin vähentävän kohinaa loppukuvassa erityisesti huonosti valaistussa ympäristössä. Materiaaleja vertaillessa läpäisevyyserot olivat kuitenkin niin pieniä, että hyvin heijastuksenestopinnoitettujen kuusiosaisten lasi- ja muovilinssien välinen SNR-ero oli suurimmillaankin vain 0,8 % lasilinssin hyväksi. Yhden materiaaliparin kohdalla muovilinssi jopa päihitti lasilinssin. Muovien läpäisyominaisuuksien kuitenkin huomattiin heikkenevän rajusti pitkän lämpökäsittelyn seurauksena, kun taas lasit eivät tästä juuri kärsineet. Lasit voidaan myös mahdollisesti pinnoittaa muoveja tehokkaammin, joten työn tuloksia voidaan muovien osalta pitää niiden suorituskyvyn ylärajana.

PREFACE

On a slushy December morning I was walking to a meeting with three gentlemen. I had been contacted by one of them based on my advertisement in which I wrote I was searching for a topic and facilitator for my Master's Thesis. During the meeting we discussed, what the company they were all starting to work for, AAC Technologies, could offer me and what I could bring to the equation. As it turned out, these three men were to become my bosses: M.Sc. Eero Päivänsalo, M.Sc. Ossi Pirinen and M.Sc. Tuomas Punta. To you I will always be grateful for giving me a chance to show, what I got.

There are plenty of people, who have earned my gratitude along the Thesis process. First, I want to thank my examiners: Dr. Johan Sand for providing excellent guidance and help along the process whenever I needed it, and Assoc. Prof. Juha Toivonen for taking the time for me from his hyper-busy schedule whenever I asked for advice. Ossi also deserves a special mention as he was a huge help as I was trying to wrap my head around how digital cameras work. I would also like to thank all my colleges at AAC Technologies for creating an inspiring environment for me to work on my Thesis.

Finishing this Thesis also marks the end of my educational path. I would like extend my gratitude to all of my teachers along the way and especially mention my science teacher in upper secondary school, Mr. Jouni Malava, for inspiring me to pursue a career in natural sciences. As the final leg of the trail, Tampere University of Technology has provided me with uncountable number of unforgettable moments both inside and outside of lecture halls. For all of you new friends I made during the past six and a half years, thank you, as you made my time in the university incredible. Especially I want to thank all my fellow gentlemen in the orange overalls, guys at Kultahippu and other members of Hiukkanen.

Especially grateful I am to my mother, father and brother for providing me a nourishing environment to grow up in and for always standing by my side.

Lastly, Miia.
Thank you for always believing in me.

Tampere, November 19th, 2018

Oula Juutilainen

CONTENTS

LIST OF FIGURES

LIST OF TABLES

LIST OF ABBREVIATIONS AND SYMBOLS

In this thesis the vector quantities are written in **bolds** and scalar quantities in *italics*. Line over a quantity, for example $\overline{x}$, stands for arithmetic mean.

A-CA	Axial chromatic aberration
ADC	Analog-to-digital converter
AoI	Angle of incidence
APS	Active pixel sensor
AR	Anti-reflection
AWB	Auto white balance
BFL	Back focal length
CA	Chromatic aberration
CCD	Charge-coupled device
CIE	International Commission on Illumination (Fr. Commission internationale de l'éclairage)
CMOS	Complementary metal-oxide semiconductor
COC	Cyclo olefin copolymer
COP	Cyclo olefin polymer
CTE	Coefficient of thermal expansion
DPS	Digital pixel sensor
EM	Electromagnetic
FFL	Front focal length
FPN	Fixed-pattern noise
IR	Infrared
ISP	Image signal processing
L-CA	Lateral chromatic aberration
L-SA	Longitudinal spherical aberration
MOS	Metal-oxide semiconductor
MP	Megapixel
OPD	Optical path difference
OPL	Optical path length
PGM	Precision glass molding
PPS	Passive pixel sensor
PRNU	Photo-response non-uniformity
PSN	Photon shot noise
QE	Quantum efficiency
SA	Spherical aberration

SNR	Signal-to-noise ratio
STD	Standard deviation
T-SA	Transverse spherical aberration
UV	Ultraviolet
VIS	Visible light

a	Oscillation strength
$\mathbf{B}$	Magnetic flux density
B_j, C_j	Sellmeier coefficients
c	Speed of light in vacuum
C	Center of curvature
C	Capacitance
C_{ox}	Gate capacitance of a transistor
d	Distance
d_l	Thickness of a lens
$\mathcal{D}$	Refractive power of a surface
$\mathbf{D}$	Electric displacement field
$\mathbf{E}$	Electric field
E_0	Amplitude of the electric field
E_g	Optical band gap
E_R	Scalar electric field of the resultant wave
f	(Effective) Focal length
F	Focal point
$\mathbf{F}$	Arbitrary vector Field
h	Planck's constant
h_i	Distance between i:th vertex and principal point
H	Principal point
$\mathbf{H}$	Magnetic field
I	Irradiance
$\mathcal{I}$	Current
$\hat{\mathbf{i}}$, $\hat{\mathbf{j}}$	Unit vectors in the directions of Cartesian coordinate axises x and y
$\mathbf{J}$	Free current density
k	Wave number
k_B	Boltzmann constant
k_x, k_y, k_z	Components of wave vector in the directions of Cartesian coordinate axises
$\mathbf{k}$	Wave vector
K	Kelvin (temperature unit)
K	Stress-optical coefficient

$\mathcal{K}$	Constant for determination of $\frac{1}{f}$ noise
l	length
m_e	Mass of an electron
M_T	Transverse magnification
$\mathbf{M}$	Magnetization
n	Index of refraction
n_p	Number of photons
n_x	Number of statistical events
n_I	Imaginary part of complex index of refraction
n_R	Real part of complex index of refraction
$\tilde{n}$	Complex index of refraction
N	Nodal points
N_V	Number of particles in unit volume
$\mathbb{N}$	Natural numbers
$\mathcal{N}$	Noise
O	Optical center
$\mathbf{P}$	Polarisation density
q_e	Elementary charge
Q_E	Radiant energy
r	Interatomic distance
r_0	Equilibrium distance
$r_\perp$, $r_\parallel$	Fresnel coefficients for reflected light
$\mathbf{r}$	Place vector
R	Radius of curvature
$\mathcal{R}$	Reflectance
s_o, s_i	Object and image distances from respective principal points
S	Signal
t	Time
$t_\perp$, $t_\parallel$	Fresnel coefficients for transmitted light
T	Temperature
$\mathcal{T}$	Transmittance
T_p	Period
U	Voltage
v	Velocity
$\mathbf{v}$	Velocity vector
v_g	Group velocity
v_p	Phase velocity
V	Vertex
V_d	Abbe number

w	Width
x_o, x_i	Distance between object and image from respective focal points
y_i, y_o	Image and object height
Y	Young's modulus
$\mathbb{Z}$	Integers
x, y, z	Cartesian coordinates
α	Coefficient of thermal expansion
β	Angle
γ	Damping coefficient
δ	Total phase lag
ϵ	Relative permittivity
ϵ_0	Permittivity of vacuum
ϵ_p	Phase difference
θ_i	Angle of incidence
θ_r	Angle of reflection
θ_t	Angle of refraction
κ_x, κ_y, κ_z	Spring constants in Lorentzian model of an atom in the directions of Cartesian coordinate axises
λ	Wavelength
μ	Relative permeability
μ_0	Permeability of vacuum
μ_{abs}	Absorption coefficient
μ_x	Statistical mean
ν	Frequency
ν_P	Poisson's ratio
ρ	Free charge density
σ	Electrical conductivity
σ_s	Mechanical stress
σ_x	Standard deviation
Σ_{LC}	Circle of least confusion
Σ_p	Petzval surface
Σ_s	Sagittal (astigmatic) surface
Σ_t	Meridional (astigmatic) surface
Φ	Interatomic potential energy
Φ_E	Radiant flux
Φ_p	Electrical polarisability
ψ_0	Amplitude of a wave
Ψ	Wave function
ω	Angular frequency
ω_0	Resonance (angular) frequency

1. INTRODUCTION

From the telescopes of Galilei to prisms of Newton and microscopes of Zeiss and Abbe, for hundreds of years, optical components were exclusively fabricated out of glass. During the last few decades though, different types of plastics have started to replace it in many mass-produced applications, of which the most used ones are smart phone cameras, that millions and millions of people utilise daily. Plastics have some advantages over glass and maybe the most important one in nowadays' efficiency-driven economy is, that plastic components are cheaper and faster to produce in massive scales, that consumer products require. As materials though, plastics do not perform as well in wide range of physical and optical qualities. In some applications this problem can be avoided by appropriate optical design and material selection, but there is still a high demand for glass optical elements due to their versatility. Also due to advances in glass molding techniques, the volumes of glass elements manufactured have been increasing and prices then in turn declining making optical glass attractive again. This has given rise to hybrid optics, where some of the plastic lenses of optical system are replaced with glass, for example for better thermal stability and image quality. In some specific applications, where high precision and long product lifetime are of critical importance, even full glass solutions may come into play in the future.

To gain more understanding of the material differences and their fit for different consumer applications, in this thesis, wide range of different optical and physical properties of different optical polymers and glasses are studied in general level. The most interesting ones, thermal properties and short wavelength light transmittance, and their effects on image quality were then researched further via different computational methods and simulations. Also notable differences were found in birefringence and water absorption qualities and these, along with extension studies on thermal and transmittance properties, are presented to be studied further in future via experimental and computational methods.

In this thesis there are seven Chapters. In Chapter 2 wide range of different physical and optical properties of optical materials are reviewed and also some elementary properties of light itself are discussed. Also principles of lens systems, ray tracing and different aberrations are studied. In Chapter 3 principles of digital imaging systems are reviewed from different sources of light and noise properties of digital imaging sensors. In Chapter

4 there are explained how the calculations were made, simulations created and also what kind of limitations do these methods have and how they effect the results. Chapter 5 is focused then on the actual results received in the thesis and Chapter 6 these are discussed. Also some other factors, that would have effect on the usability and value addition of the materials in different applications are addressed. Finally, in Chapter 7 this thesis is summarised.

2. OPTICAL AND PHYSICAL PROPERTIES OF MATERIALS

When designing an optical system, one needs to account for several different optical and other physical properties of optical components. For example for lens system qualities such as refractive index, Abbe number, thermal expansion and different aberrations are vital to understand, since ignoring can have drastic effects on final image quality. Also, since optical components would be vain without light itself, some basic theory of electromagnetism needs to be understood too. In this Chapter some relevant physical properties of light and electromagnetic radiation in general are studied alongside with relevant optical and physical properties of optical plastics and glasses themselves.

2.1 Light and Electromagnetism

Light, as from nature, can be described as a disturbance in electromagnetic (EM) field carrying energy, so it is naturally a part of EM-radiation spectrum. As Max Planck found in the beginning of 20th century, EM-radiation is quantized to massless particles, namely photons, with each having quantized energy of [55]

$$E = h\nu = \frac{hc}{\lambda}, \tag{2.1}$$

where h is Planck's constant, ν the frequency, λ the wavelength and c the speed of light. As it can be seen from the frequency in the energy equation, photons are not particles in classical sense, but rather quantum particles with wave-like properties. This duality, called wave-particle dualism, or more precisely the wave characteristics of matter, are in modern physics and also in this thesis used to describe properties of light, atoms and electrons and EM-radiation in general.

As light can be characterized as waves, it is a solution to the classical wave equation [33, p. 36]

$$\nabla^2 \boldsymbol{\psi} = \frac{1}{\mathbf{v}^2} \frac{\partial^2 \boldsymbol{\psi}}{\partial t^2}, \tag{2.2}$$

where $\boldsymbol{\psi}$ is a complex wave function, $\mathbf{v}$ vector quantity of the velocity of the wave, and t time. One solution for this kind of differential equation is of following form; a harmonic wave function representing a plane wave as a function of space and time: [33, pp. 31-35]

$$\boldsymbol{\psi}(\mathbf{r}, t) = \psi_0 \cos(\mathbf{k} \cdot \mathbf{r} \mp \omega t). \tag{2.3}$$

Here ψ_0 is amplitude of the wave, $\mathbf{k}$ the wave vector and $\mathbf{r}$ the position vector of the plane in Cartesian space. Thus the scalar product of $\mathbf{k}$ and $\mathbf{r}$ defines the plane. Also the scalar product can be broken down to $\mathbf{k} \cdot \mathbf{r} = k_x x + k_y y + k_z z$, where x, y and z are Cartesian coordinates and k_x, k_y and k_z the corresponding components of the wave vector. The $\mp$-sign in between the scalar product and velocity component of the phase is there, since the plane can propagate to both positive and negative directions, respectively. This representation, even though it accurately represents a real wave, is not that commonly used since the trigonometric functions are pretty nasty to work with mathematically. Luckily, with some help from Leonhard Euler and complex analysis, one gets a complex exponential representation for a wave, that is of form

$$\boldsymbol{\psi}(\mathbf{r}, t) = \psi_0 e^{i(\mathbf{k} \cdot \mathbf{r} \mp \omega t)}, \tag{2.4}$$

where $i = \sqrt{-1}$ the imaginary unit. The exponent in total describes the phase of the disturbance. With this representation though ones needs to be extremely careful with mathematical operations and in the end one always needs to take the real part of the wave to make it represent an actual wave. [33, pp. 31-35]

If two waves $\boldsymbol{\psi_1}$ and $\boldsymbol{\psi_2}$ are both solutions to the equation 2.2, then it follows that the sum of the two $\boldsymbol{\psi_{1,2}} = \boldsymbol{\psi_1} + \boldsymbol{\psi_2}$ is also a solution for the wave equation. This is also true for more than two individual waves. This quality is called the superposition principle and in practice it means, that when two or more waves collide, they will form a resultant wave by, depending on the phase of the individual waves with respect to one another, either adding to or subtracting from each others. The waves will not permanently effect on each others and as soon as the encounter is over, the waves will go back to as they were before the encountering. [33, pp. 28-29]

Notationwise, when describing optical field, it is customary to omit the magnetic field and use just the electric field. Electric field has considerably greater impact on most

materials than magnetic field and thus this is a justified approximation [33, p. 60]. Futher simplification of the equation is done by assuming positive direction (with respect to Cartesian coordinate system) of propagation. Thus optical field simplifies to oscillating complex electric field, **E**. This is also one possible a solution to the classical wave equation 2.2 and of the similar form than general wave function 2.4:

$$\mathbf{E}(\mathbf{r}, t) = E_0 e^{i(\mathbf{k}\cdot\mathbf{r}-\omega t)}. \tag{2.5}$$

One of the most comprehensive ways to classically describe the behavior of EM-field are the Maxwell's equations. Here is one way of representing them in a modern differential form and as in a magnetic and polarisable medium: [28], [33, pp. 677-79]

$$\nabla \cdot \mathbf{E} = \frac{\rho}{\epsilon} \tag{2.6}$$

$$\nabla \cdot \mathbf{B} = 0 \tag{2.7}$$

$$\nabla \times \mathbf{E} = -\frac{\partial \mathbf{B}}{\partial t} \tag{2.8}$$

$$\nabla \times \mathbf{B} = \mu\mathbf{J} + \mu\epsilon\frac{\partial \mathbf{E}}{\partial t}, \tag{2.9}$$

where ρ free charge density, **B** magnetic flux density, **J** free current density and μ and ϵ relative permeability and permittivity, respectively. These vector quantities are related also via the following constitutive relations:

$$\mathbf{D} = \epsilon\mathbf{E} + \mathbf{P} \tag{2.10}$$

$$\mathbf{B} = \mu(\mathbf{H} + \mathbf{M}) \tag{2.11}$$

$$\mathbf{J} = \sigma\mathbf{E}, \tag{2.12}$$

where **D** is the electric displacement field, **P** polarisation density, **H** magnetic field, **M**

magnetization and σ electric conductivity.

Maxwell's equations, even though named after a Scottish physicist James Clerk Maxwell, were not his findings. Rather he saw something in already existing equations describing electricity and magnetism, that no-one else ever before him had. He was the one, who combined the discoveries of Carl Friedrich Gauss (equations 2.6 and 2.7), Michael Faraday (2.8) and André-Marie Ampere (2.9), added the second term to the right side of Ampere's law and with these equations was able to bring together theories of electricity and magnetism and characterize EM-field as waves. [26, pp. 220-222] This result is of such fundamental significance, that now Maxwell's footsteps are followed and it is found, how it really can be proven from these equations, that EM-field consists of oscillating waves. [33, pp. 677-679]

First a vacuum environment is considered to simplify the treatment. By definition there are no charges in a vacuum, so $\rho = 0$, $\sigma = 0$, and hence $J = 0$ and for this also the relation 2.6 equals zero. Also μ and ϵ are replaced with μ_0 and ϵ_0, permeability and permittivity of free space, respectively. Also then there is neither polarisation nor magnetization. As one wishes to show the wave nature of EM-light, one needs to manipulate the equation 2.8 to the similar form as the classical wave equation 2.2. This means one needs to form some second order partial derivatives. Hence curl is taken from both sides of the Faraday's law 2.8. Thus it becomes

$$\nabla \times (\nabla \times \mathbf{E}) = -\frac{\partial}{\partial t}(\nabla \times \mathbf{B}). \tag{2.13}$$

There is a following mathematical identity, where $\mathbf{F}$ is an arbitrary vector field,

$$\nabla \times (\nabla \times \mathbf{F}) = \nabla(\nabla \cdot \mathbf{F}) - \nabla^2 \mathbf{F}. \tag{2.14}$$

This can be used for the intermediate result 2.13. Also the free space version of Ampere's law with Maxwell's addition, 2.9, is substituted into 2.13, thus forming it as follows

$$\nabla(\nabla \cdot \mathbf{E}) - \nabla^2 \mathbf{E} = -\frac{\partial}{\partial t}\left(\mu_0 \epsilon_0 \frac{\partial \mathbf{E}}{\partial t}\right). \tag{2.15}$$

As it was pointed out earlier, in vacuum $\nabla \cdot \mathbf{E} = 0$. Thus the equation 2.15 simplifies to

$$\nabla^2 \mathbf{E} = \mu_0 \epsilon_0 \frac{\partial^2 \mathbf{E}}{\partial t^2}. \tag{2.16}$$

Here one can notice the remarkable similarity to the classical wave equation 2.2, and indeed by combining these two equations, one gets the velocity for an electric field in a vacuum as

$$v = \frac{1}{\sqrt{\mu_0 \epsilon_0}} \approx 3 \times 10^8 \; m/s. \tag{2.17}$$

The similar kind of treatment can also be done for magnetic field and it will lead to the same result for the wave characteristics and velocity of a magnetic field. As it has become clear later, this velocity has a special meaning in modern physics, and thus has its own notation, namely c, the speed of light in a vacuum.

With putting all of this together, Maxwell had for the first time shown the wave characteristics and intertwinedness of electric and magnetic fields on such a fundamental level. What makes his findings even more mind-bending, is that he made it with pen and paper, just trusting his mathematics without any experimental proof. At Maxwell's time in physics it was not that common to first postulate some theoretical result and later prove it experimentally. For this reason the theory was not approved at first, when Maxwell published his findings, but as time has passed, Maxwell's theory has been proven accurate time and time again.

Now it has been learnt, what light actually is how it behaves. However, thus far only vacuum conditions have been studied, so now focus is shifted to how light propagates in different media.

2.2 Propagation of Light in a Medium

In this Section the behavior of light in different media with different optical properties will be discussed. First the principles of wave-particle interaction are studied to understand, why light moves at different speeds in different media. This then leads to refractive index and to its wavelengths dependencies. Also polarisation of light and how its unusual effect on some materials will be discussed. Since normally materials react on changes in temperature, and optical glasses and plastics are not exceptions, also these properties are examined. Last the concept of haze is introduced.

2.2.1 Rayleigh Scattering

Scattering in general means, that radiation is forced to change its direction of propagation due to interaction with a particle. For now focus is on Rayleigh scattering: here a photon

is absorbed by a molecule and simultaneously the molecule emits a photon of the same wavelength as the initial one to some arbitrary direction. Using the wave characterization of light, this phenomenon can be explained by viewing a photon as a single EM-wavelet carrying energy. Also molecules are viewed as electrically polarised oscillators, meaning the charges in the electron cloud are not uniformly distributed. This creates differences in charge densities in the cloud. [33, p. 96]

The wavelet hits the molecule and the energy of the electric field makes the charges in the molecule vibrate at the same frequency as the electric field itself. Simultaneously the vibration makes the molecule emit a wavelet of the same frequency, and thus same energy, as the one it absorbed. This means there is no energy-loss in the scattering process, which makes it elastic.

As it was described earlier, scattered wavelet can be emitted to any direction. In a tenuous medium wavelets, that scatter laterally, are not interfering with each others as much as in a denser medium. This happens because the wavelets are nearly independent of each other due to relatively long distances between the scatterers. Good examples of this kinds of environments are the upper parts of atmosphere, where photons of shorter wavelengths scatter more than those of longer wavelengths, thus making sky blue. Why the sky is not some other coloured, has to do with the electronic resonance frequency, ω_0, of the molecules in atmosphere. In general the closer to the resonance frequency of a molecule the frequency of the radiation is, the higher will be the amplitude of the scattered wave and also the more the radiation will scatter. For molecules this resonance frequency lays in the ultraviolet (UV) range of EM-spectrum, which is closer to the blue and violet wavelengths of visible light. [33, pp. 96-97]

In an ideal dense and uniform medium, all other directions of scattered waves destructively interfere with each other and diminish, except for the forward scattering waves: they are always constructively interfering with each other, thus being the only ones prevailing. This is why in dense medium, such as most liquids and solids, the forward direction of scattering is the only meaningful direction of examining. To distinguish between the scattered and the initial waves, the scattered one is called the secondary wave and the initial the primary wave. When the secondary waves combine with each other and the remaining primary wave, this is called the resultant wave. Now, it is good to note, that in real world in most transparent objects, there is still some lateral scattering, even in the most uniform crystals. [33, pp. 96-101]

Not all EM-radiation induces scattering, though. When wavelength of the radiation is too long, that is, its energy is too low, the photons cannot be absorbed and will not interact with the molecule. This happens, since a photon does not have enough energy to excite

an electron from ground state to a higher state over the optical band gap, E_g: energy states are discrete, making them the only allowed energies for an electron to get excited to and thus the gaps between these states forbidden. [77]

Now as the Rayleigh scattering is just a special case of EM-waves scattering, it still describes accurately enough, what happens, when EM-wave encounters a small particle, like molecule. Next the effect scattering on the speed of light in a medium is discussed in more detail.

2.2.2 Phase and Group Velocity

As it was presented in Section 2.2.1, the forward scattered waves of EM-radiation are called secondary waves. As the initial, primary, waves, also the secondary waves move through free space between the molecules at the speed of light. Still it seems, that in medium the resultant of these waves, namely transmitted waves, are moving at some other, lower or sometimes even higher, velocity than the speed of light. This is due to phase differences in the combining primary and secondary waves, and the velocity of transmitted, resultant, wave is called phase velocity, v_p. [33, pp. 101-102] This describes the speed at which an individual phase of wave, for example the peak, is propagating and this can be mathematically represented for plane wave as [9, p. 19-21]

$$v_p = \frac{\omega}{k} = \frac{c}{\sqrt{\epsilon\mu}}, \tag{2.18}$$

where ω is angular frequency and k the wave number, which is the magnitude of the wave vector: $k = |\mathbf{k}| = \frac{2\pi}{\lambda}$. The angular frequency describes a rate at which a phase in a wave is changing, so $\omega = \frac{2\pi}{T_p} = 2\pi\nu$, where T_p is period. The equation 2.18 does not necessarily hold for an arbitrary non-planar wave, but with large enough frequencies, it's still a good approximation. As the wave vector points to the direction of propagation of EM-waves and is perpendicular to both electric and magnetic field ($E_z = H_z = 0$), this makes electric and magnetic fields transverse waves. To distinguish phase velocity from the velocity of the envelope of the wave packet, the latter is called group velocity [9, pp. 19-21], v_g:

$$v_g = \frac{\partial\omega}{\partial k}. \tag{2.19}$$

As it was said earlier, the phase velocity, and thus seemingly the velocity of light in a medium, can be larger than the speed of light. This still does not mean, that Einstein and his theory of relativity were wrong, since the phase itself cannot transfer any information.

As it is in the usual case, that the speed at which information can be transferred is the group velocity. Though, there is some research showing, that it is possible to reach superluminal group velocities in certain circumstances, but in those cases v_g cannot be interpreted as the speed at which the information is moving [18].

[33, pp. 101-104] In scattering process phase differences are formed, because the electron-oscillator will only be able to vibrate in the same phase as the initial wave at relatively low frequencies. At higher frequencies the electron-oscillator cannot keep up resulting to a phase difference between the primary and secondary waves, although the frequency stays the same. This phase difference is always, in real world, lagging, but in some cases it is namely said to be leading. Also contributing to the total phase difference between the primary and resultant waves is Huygens-Fresnel principle of diffraction. This states, that there is a 90° lag in phase of the resultant wave compared to the primary wave. This results from the merging of the primary and secondary waves [33, p. 102] [9, p. 416]. When these two factors contributing to the phase difference between primary and resultant waves are considered together, this leads to lag of 90° to 270°. In the situation, where the lagging from the electron-oscillator is 90° or more, and thus the resulting total lag, $\delta \geq 180°$, this is called a phase lead of $360° - \delta$. Both phase lead and lag are demonstrated in the figure 2.1.

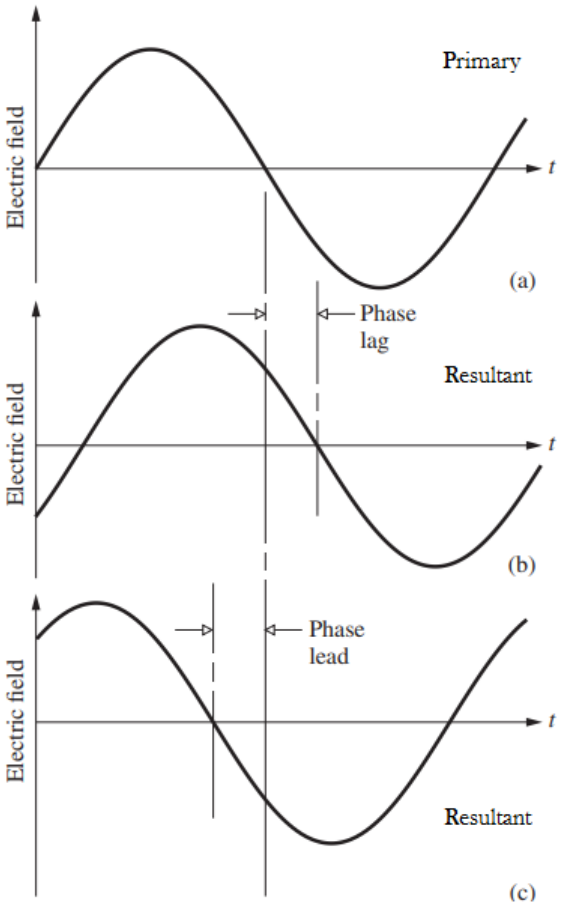

Figure 2.1 *Phase lag and lead demonstrated. The primary wave (a) compared to (b) and (c), the resultant wave. In (b) the resultant wave is lagging (reaches a certain point later) and in (c) it is leading (reaches a certain point earlier) the primary wave in phase. Based on [33, fig. 4.10].*

Now it still needs to be shown, that the phase difference is the responsible for the phase velocity and for that matter, that $v_p \neq c$ in non-free space. Assume a point P in space, to which the resultant wave arrives after its formation from primary and secondary waves. If light was moving in a vacuum, then it would arrive to this point without a phase difference with respect to the primary wave, which in this case would actually be the same wave as the resultant wave, and thus the electric field would be of form

$$E_R^{vacuum}(t) = E_0 \cos(\omega t), \tag{2.20}$$

where E_R^{vacuum} is the scalar resultant electric field at vacuum. This relation works for surfaces of any kind, but as for thick lenses go, there are two surfaces and some material in between, which needs to be considered.

Now if the point P was in a dielectric medium, this would cause a phase difference, ϵ_p,

due to the primary wave interacting with the molecules of the medium. If one assumes the phase difference being lagging, then the scalar electric field, E_R^{medium}, would be of form

$$E_R^{medium}(t) = E_0 \cos(\omega t - \epsilon_p). \tag{2.21}$$

Thus the as the phase is running late, the time, which it would take more to arrive at point P compared to the vacuum circumstances, would be $\Delta t = \frac{\epsilon_p}{\omega}$. Of course, if the phase difference would be positive, that is, if there was a phase lead of ϵ_p, then the wave would arrive to P time of Δt earlier. As speed is defined as distance traveled over time, this principle thus gives arise to the phase velocity and also the seemingly different speed of light in a medium, namely phase lagging causes $v_p < c$ and lead $v_p > c$. This then gives arise to the index of refraction, n. [33, pp. 102-104]

2.2.3 Index of Refraction and Dispersion

Refractive index is defined as the relation of phase velocity of light propagating in a medium, v_p, and speed of light in a vacuum [33, p. 101]

$$n = \frac{c}{v_p}. \tag{2.22}$$

As it is known from equation 2.18, phase velocity depends on the relative permittivity and permeability of the medium. When combining this with the equation 2.22, another representation for the refractive index is gotten:

$$n = \sqrt{\epsilon\mu}, \tag{2.23}$$

also known as Maxwell's formula [9, p. 14].

As noticed in Section 2.2.1, the amount of scattering depends on difference between the frequency of the wave and the resonance frequency of the electron-oscillator in the molecule. Hence this difference also effects on phase velocity and through that on refractive index, thus making it a function of angular frequency: $n(\omega)$.

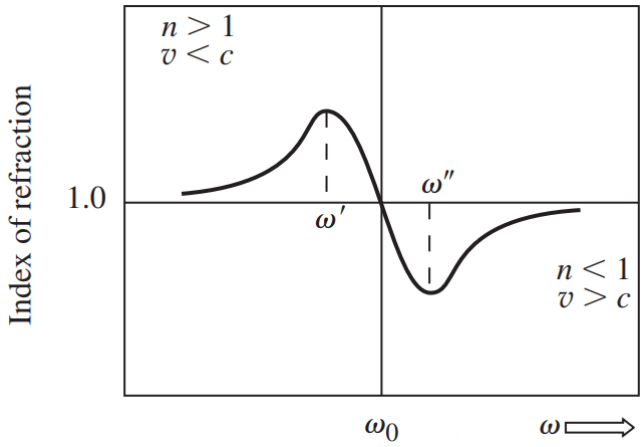

Figure 2.2 *The effect of the difference between the frequency of the EM-field and the resonance frequency of the electron-oscillator on refractive index, $n(\omega)$. Based on [33, fig. 4.9 c)].*

As it was described in the end of Section 2.2.2, phase velocity can be either greater or smaller than the speed of light. When this is combined with equation 2.22, it is clear, that when $v_p > c$, then $n < 1$, and the far more usual case when discussing about visible light; from $v_p < c$ it follows that $n > 1$. When one remembers, that phase lag and lead where the reasons for the phase velocity's difference from the speed of light, the relation between the frequency of the EM-field and refractive index now becomes obvious. This phenomenon is called dispersion and the relation between frequency of the wave and refractive index is demonstrated in the figure 2.2. There is a mathematical representation of the dependence of refractive index on the angular frequency in a tenuous medium, namely dispersion equation [33, p. 80]

$$n^2(\omega) = 1 + \frac{Nq_e^2}{\epsilon_o m_e}\left(\frac{1}{\omega_0 - \omega}\right), \tag{2.24}$$

where N is the total amount of contributing electrons in the molecule, q_e the elementary charge and m_e the mass of an electron.

The phenomenon of dispersion arises from the electric and magnetic dipoles in the molecules of the medium induced by the applied EM-field, which in turn polarises the considered molecule. As discussed earlier, the relative effect of magnetic field with respect to electric field is so insignificant, that it can be omitted. Now as in real world the particles are not really that isolated, especially in a denser medium, like liquids or solids, the dispersion equation 2.24 has to be modified to correspond: [33, pp. 78-81], [26, p. 417]

$$\frac{n^2-1}{n^2+2} = \frac{Nq_e^2}{3\epsilon_0 m_e} \sum_j \frac{a_j}{\omega_{0j}^2 - \omega^2 + i\gamma_j\omega}, \tag{2.25}$$

where j is a natural number, a_j are weighting factors called oscillation strengths, of particular electron-oscillators, which satisfy $\sum_j a_j = 1$ and γ_j corresponding damping coefficients. The sum in the equation considers all j oscillators and the number three in the denominator before the sum comes from the fact, that in a dense medium every molecule is affected by, not only the external electric field, but also the from the molecules surrounding it. This electric field from the molecules surrounding the considered molecule arises from the electrical polarisation of the molecules caused by the external electric field. Thus the local electric field is $\mathbf{E}_{local} = \mathbf{E} + \frac{\mathbf{P}(t)}{3\epsilon_0}$. [26, p. 417] The last term of the denominator in the sum represents the damping effect the medium has on the EM-field. Here one cannot surpass the fact, that into the representation of index of refraction, there has appeared the imaginary unit, i. The imaginary part of refractive index describes the attenuation, that is, the weakening of the amplitude, of EM-field in a medium. Basically complex refractive index, $\tilde{n}$, can be represented as [33, p. 141]

$$\tilde{n} = n_R - in_I, \tag{2.26}$$

where n_R is the real part of refractive index, which is usually nominated wit just n and n_I the imaginary part of refractive index. In ideal case, if $n_I = 0$, then attenuation does not happen in the dielectric and if the $n_R = 0$, then 100% of the incident EM-field would reflect back from the surface of the medium. [33, p. 141] Knowing this and with some help from the fantastic Mr. Feynman [26, pp. 415-418], one can now describe the propagation of electric field in the medium with the assumption, that it is polarised to only oscillate in x-direction and propagates in the z-direction. The electric field of this sort at the depth z can be written as

$$E_x = E_0 e^{i(\omega t - kz)}. \tag{2.27}$$

With the help of the equations 2.18 and 2.22 and some mathematical manipulation, the equation 2.27 can be written as

$$E_x = E_0 e^{i\omega\left(t - \frac{\tilde{n}}{c}z\right)},$$

and again using the definition of complex refractive index 2.26 as

$$E_x = E_0 e^{-\frac{\omega n_I z}{c}} e^{i\omega\left(t-\frac{n_R z}{c}\right)}. \tag{2.28}$$

Here, as one can see, the first exponential term is negative, which means the amplitude, E_0, is diminishing as the field penetrates deeper into the medium. This describes namely the attenuation of the field and the exponent of the second exponential then describes the phase of the field at depth z.

The time-averaged intensity of a field can be described with quantity of irradiance, I. This is written as a function of amplitude of the field [33, p. 60]

$$I = \frac{c\epsilon_0}{2} E_0^2, \tag{2.29}$$

meaning, that it is proportional to the second power of the amplitude of the field. Thus it is also a function of the imaginary part of refractive index, n_I,

$$I = \frac{c\epsilon_0}{2} E_0^2 e^{-\frac{2\omega n_I z}{c}}. \tag{2.30}$$

As it is known, the angular frequency, ω, is a function of wavelength, λ, of a wave and hence the refractive index can also be described in terms of the wavelength. This would suggest, that there is also a way to describe dispersion also with respect to wavelength. One relationship between the refractive index and wavelength, which is widely used with optical components and materials manufacturers is so called Sellmeier equation, named after Wolfgang von Sellmeier [78]

$$n^2(\lambda) = 1 + \sum_j \frac{B_j \lambda^2}{\lambda^2 - C_j}, \tag{2.31}$$

where B_j and C_j are medium dependent Sellmeier coefficients of said medium defined in the fitting process with least-squares approximation and λ the wavelength of the radiation. According to Tatian [72] it has been shown, that for transparent materials the equation corresponds accurately to measurement data of refractive index as a function of wavelength. It is also been determined, that in most cases $j = 3$ is enough of terms for an accurate fitting. The Sellmeier coefficients B_j and C_j are often given by manufacturers of glass and other optical materials for the determination of refractive indices in different wavelenghts.

Another widely used way to describe the dispersion of a optical material is Abbe number,

V_d, named after German Physicist Ernst Abbe, [33, p. 281]

$$V_d = \frac{n_d - 1}{n_F - n_C}. \tag{2.32}$$

Here n_d, n_F and n_C are refractive indices at different Fraunhofer lines, namely d (or D_3), F and C lines, respectively. Fraunhofer lines are spectral lines, whose wavelengths are very precisely known. Sometimes d-line can also be replaced with e-line, because it is easier to produce. Abbe number gives information on how dispersive materials are and basically larger the number is, less the material disperses light and vice versa. Usually manufacturers also give V_d-information together with refractive indices as in figure 2.3.

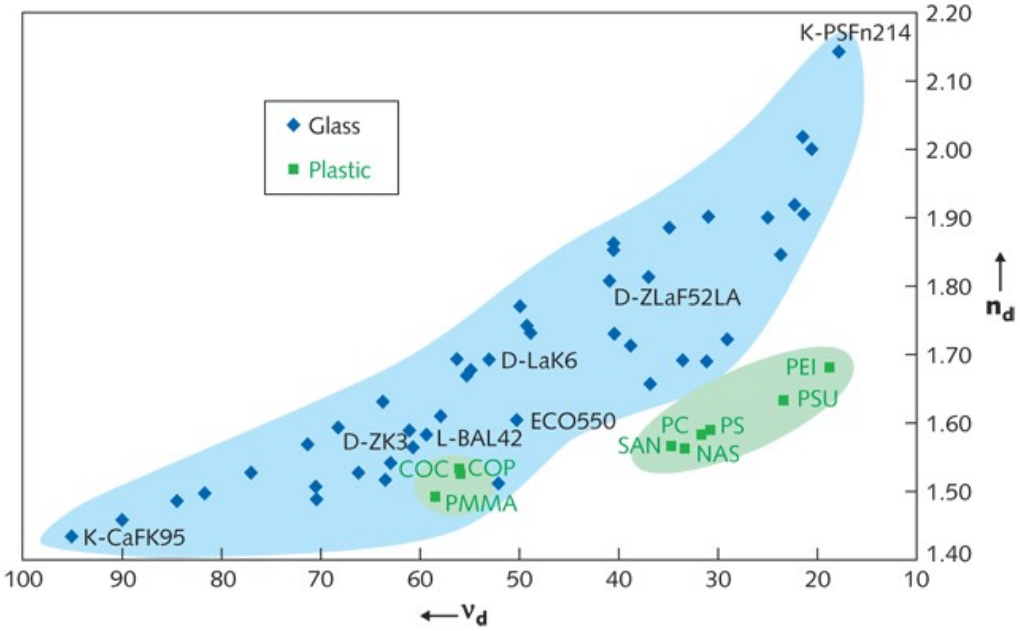

Figure 2.3 *Refractive index, n, as a function of Abbe number, V_d. Glasses are presented in blue and polymers in green. [71]*

Optical materials can be divided into two categories based on their Abbe numbers; flint and crown materials. Definition between the two is usually, that flint materials have Abbe number smaller than 50 and crown materials greater than 50. From the figure 2.3 one can also see, that the high refractive index and high Abbe number materials are made of glasses. The refractive indices of materials have been measured in Fraunhofer d-line, which lies at 587.56 nm wavelength.

The reason why optical designers are so interested in dispersion of different materials is, that when they are not accounted for, they can cause distortions in the imaging process called chromatic aberrations. They will be studied more in Section 2.5.2. There is also one other factor, which can induce unwanted dispersion called polarisation.

2.2.4 Polarisation

In this Subsection polarisation of light is discussed. It is, however, not to be confused with electric or magnetic polarisation of, for example, molecules or atoms. When focusing on only one ray of light propagating in z-direction, as this ray of light is emitted from a source, for example sun or light bulb, the electric and magnetic field will oscillate randomly in any arbitrary directions. In an isotropic medium this will happen on a plane perpendicular to the direction of propagation. Also, naturally, **E** and **H**-fields are perpendicular to each other. However, when medium is anisotropic, the **E**-field is not necessarily orthogonal with the propagation vector, **k**, but the electric displacement field, **D**, and both the magnetic flux and field, **B** and **H**, on the other hand always are. [33, p. 344]

For now the magnetic field is, again, omitted and concentration will be on the electric field. As mentioned, it can be oscillating to whichever direction on the plane as it propagates. This is a case of unpolarised light. Now when the light goes through some object, which only lets through a field oscillating in some particular fashion, for example linearly along x-axis, then any other way of oscillation cannot get through of the object. This object is now called a polarising filter or polariser. If the field is oscillating in the wanted direction, it passes through the filter unaltered, but if not only the component of field oscillating in the wanted direction will pass. The other components of the field are then absorbed by the filter. Thus when examining the field after a filter, it only oscillates in the direction the filter lets through. This light is now called polarised light and the process is described in figure 2.4.

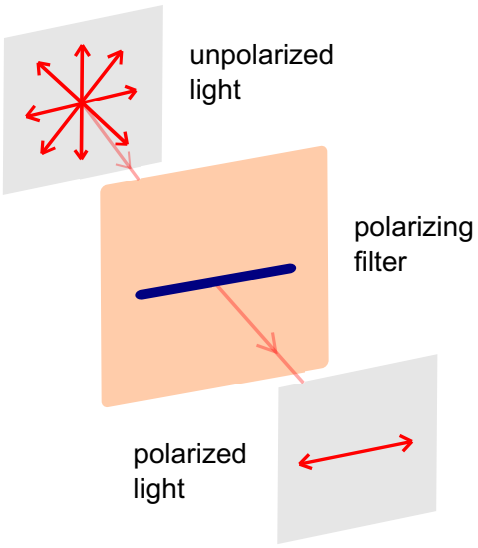

Figure 2.4 *Unpolarised light coming through a linearly polarising filter, which then linearly polarises light and absorbs the unwanted polarisations.*

But what happens to the electric field of the light as it polarises? When considering two

perpendicular initial **E**-fields both propagating to z-direction and are of forms [33, pp. 338-340]

$$\mathbf{E}_x(z,t) = \hat{\mathbf{i}} E_{0x} \cos(kz - \omega t) \tag{2.33}$$

and

$$\mathbf{E}_y(z,t) = \hat{\mathbf{j}} E_{0y} \cos(kz - \omega t + \epsilon_p), \tag{2.34}$$

where $\hat{\mathbf{i}}$ and $\hat{\mathbf{j}}$ are unit vectors in the directions of Cartesian coordinates x and y, respectively and $\mathbf{E}_x$ and $\mathbf{E}_y$ are the corresponding vector components of electric field. If the two fields are added together, the resultant field is gotten as

$$\mathbf{E}(z,t) = \mathbf{E}_x(z,t) + \mathbf{E}_y(z,t) = \hat{\mathbf{i}} E_{0x} \cos(kz - \omega t) + \hat{\mathbf{j}} E_{0y} \cos(kz - \omega t + \epsilon_p). \tag{2.35}$$

Now, from the equation 2.35 it can be seen, that if the phase difference is some multiple, $m \in \mathbb{Z}$, of 2π, that is, $\epsilon_p = m2\pi$, then the two fields are at same phase as equation 2.35 becomes

$$\mathbf{E}(z,t) = (\hat{\mathbf{i}} E_{0x} + \hat{\mathbf{j}} E_{0y})[\cos(kz - \omega t)]. \tag{2.36}$$

If on the other hand the condition would be $\epsilon_p = (2m + 1)\pi$, then the two fields would be at opposite phases as 2.35 would look like

$$\mathbf{E}(z,t) = (\hat{\mathbf{i}} E_{0x} - \hat{\mathbf{j}} E_{0y})[\cos(kz - \omega t)]. \tag{2.37}$$

These two situations of phase differences result in what is called a linear polarisation. The difference between the two situations described above is that the polarisation plane turns (not necessarily always) $90°$ and the cases have been depicted in figure 2.5.

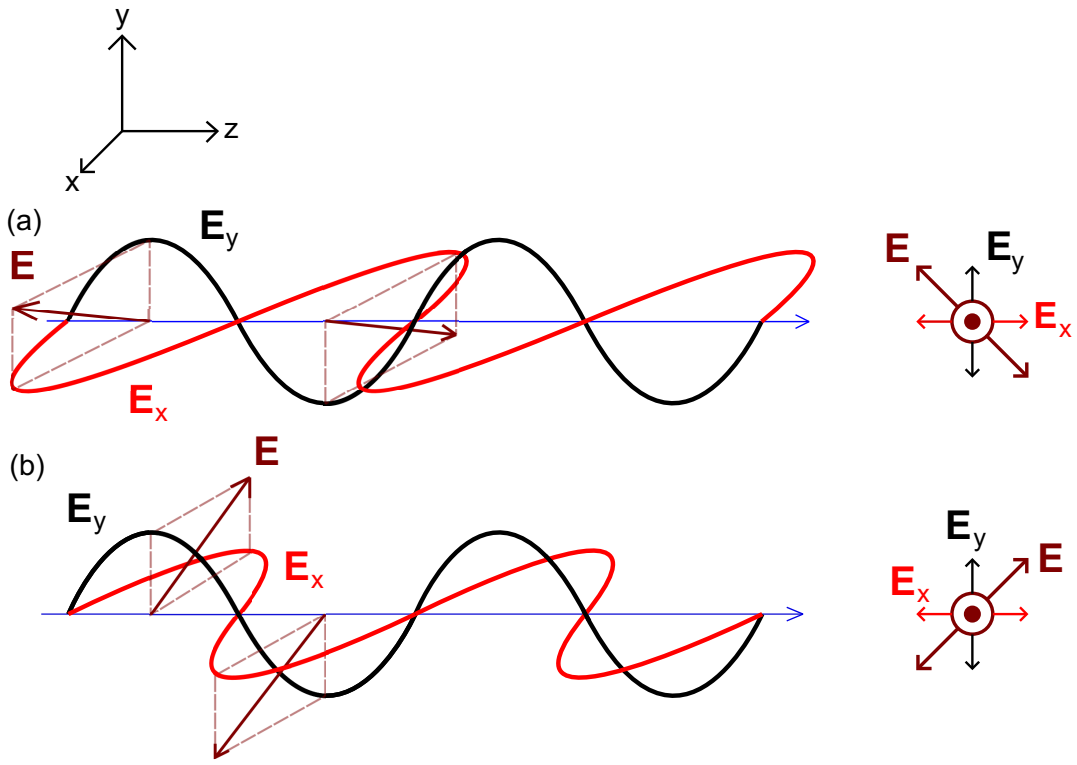

Figure 2.5 *Linearly polarised electric field represented with phase difference of (a) $\epsilon_p = 2m\pi$ and (b) $\epsilon_p = (2m+1)\pi$, where $m \in \mathbb{Z}$.*

If phase difference is some other than the two possibilities represented above, then one has a case of circular ($\epsilon_p = m + \frac{\pi}{2}$) or elliptical polarisation and the similar mathematical treatment could be used to define them as has already been done with linear polarisation. The circular polarisation is usually defined with handedness, that is, if $\epsilon_p = \frac{\pi}{2}$ it is called left-handed polarisation and for $\epsilon_p = -\frac{\pi}{2}$ it is called, logically, right-handed polarisation. [33, pp. 338-344] There are also more exotic polarisation forms, but they will not be studied more in depth here as for this thesis it is merely important to understand the concept.

2.2.5 Birefringence

As it was pointed out by Domíngues, Mayershofer, Garsia and Asara [20] and Zhang and Liu [86] in injection molding techniques for optical materials there appears local residual stress in molded materials, which makes them locally birefringent. This happens with both glasses and plastics, but the birefringence has been shown to be more severe in polymers [41]. Birefringence is a property of material, in which the refractive index of the material depends on the polarisation of light [33, p. 351]. To understand this phenomenon in more detail more about the crystalline structure of a solid material needs to be understood.

In some solid materials the crystalline structure is optically anisotropic. This means, that for incoming light it does not seem the same from all direction. This can be described for example with Lorentzian model of atoms, where positive nucleus is connected to negative electron cloud with springs in all three spatial dimensions and this is depicted in figure 2.6. Each dimension has its own spring constant, κ_x, κ_y and κ_z respectively, which means that the resonance frequencies are different in all spatial dimensions as depicted in figure 2.6. [33, p. 351]

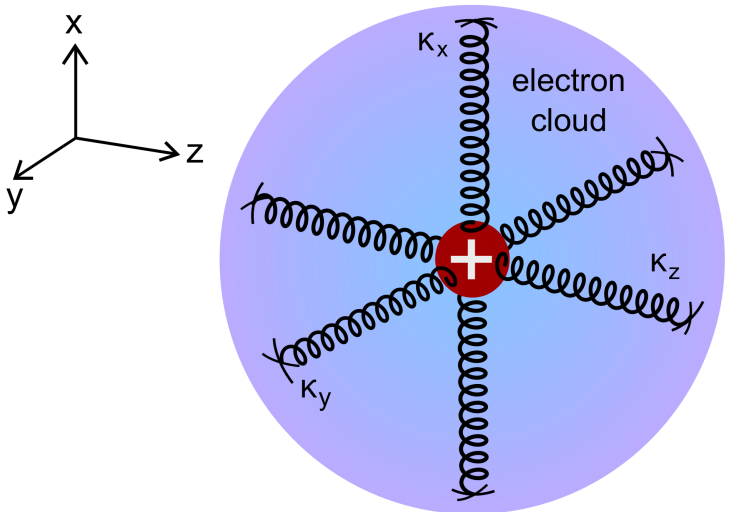

Figure 2.6 *Lorentzian model of an atom, where electrically positively charged nucleus is attached to the negative electron cloud with springs in every different spatial dimensions. Based on [33, Fig. 8.17].*

Suppose ,that light is coming to a medium made of Lorentzian atoms with a crystalline structure, in which the corresponding atomic springs align. Suppose that the **E**-field of light is oscillating in z-direction. Naturally due to different spring constants the electrons will oscillate, and thus reradiate, differently than if the field were to oscillate in x- or y-direction. This then means different phase velocities and thus different refractive indices for different linear polarisations of light. This phenomenon is called birefringence. [33, p. 351] [25, p. 316]

A well-known example of a birefringent material is calcite and in figure 2.7 it is clear how it seems to double the grid under the crystal. If one would put a linear polariser on top of the crystal at suitable angle, the other polarisation would disappear completely and when turned, the other would become visible, while the first one would little by little vanish.

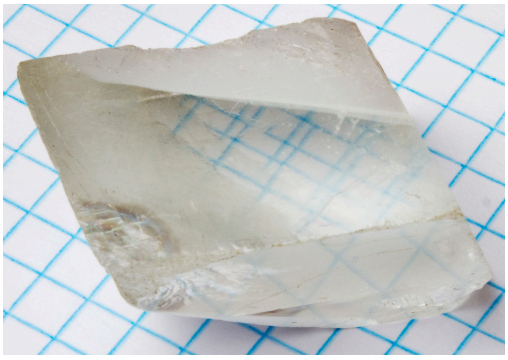

Figure 2.7 *Birefringent calcite crystal doubles the grid underneath it as it refracts the two different polarisations of light differently [4].*

Birefringence can also be induced into the materials with external stress. This stress can mainly be traced back to three origins: molding and cooling, coating and thermal compatibility with lens housing and mounting. Induced stress will effect different materials differently depending on how they can handle mechanical stress. The optical path length difference, OPD, is thus defined as [42]

$$\mathrm{OPD} = K d \sigma_s, \tag{2.38}$$

where K is material-dependent stress-optical coefficient, which usually has unit of mm^2/N, d ideal path length and σ_s mechanical stress. OPD is usually measured as nm/cm. According to Schott's Technical information sheet [63], the ISO 10110 standard instructs limits on OPD from stress induced birefringence in different optical applications as presented in table 2.1.

Table 2.1 *Instructions on stress birefringence induced OPD limits according to ISO-10110 standard according to Schott AG [63].*

Maximum OPD (nm/cm)	Application areas
<2	Polarisation instruments Interference instruments
5	Precision optics Astronomical optics
10	Photographic optics Microscopic optics
20	Magnifying glasses
no limitation	Illumination optics

As it is seen, tolerances for birefringence are really tight as it has drastic effects on sharpness of an image. Thus for lens and application manufacturers it is important to understand the phenomenon to be able to make proper material selection.

2.2.6 Haze

Haze is a measure of scattering of light in optical materials and it is usually property of plastics. It arises from uneven material surface, inconsistencies material structure, air pockets or other impurities, which will have an effect on light propagation in material. Haze is a function of thickness and thus, as refractive index is defined for different wavelengths, haze needs to be defined related to a specific thickness. [60, p. 28]

As haze is a measure of how much light scatters in transmission or in reflection, this basically means, it deteriorates image quality. Thus it needs to be noted in decisions concerning materials for optical design. On the other hand, as haze takes place due to surface imperfections, also coatings, such as anti-reflection coatings, which are highly used in optic elements, usually induce some level of haze as they produce fine texture on the surface. Most optical plastics represent at least 0.7 %, but usually between 1-3 %, transmission haze at thickness of 3 mm without any coatings as for glasses it is pretty much always between 0.3-1 %. [80], [19], [12].

Haze percentage is defines as [38]

$$\text{Haze} - \% = \frac{\mathcal{T}_{\text{diffused}}}{\mathcal{T}_{\text{tot}}} \times 100. \tag{2.39}$$

The equation defines haze percentage as the relation of transmitted diffused light and all transmitted light. Only light that has scattered more than 1.5 or 2.5° (depending on measurement method) of the direction of the chief ray is considered as haze [38].

2.3 Effects of External Factors on Material Properties

In this Section different factors effecting on physical and thus optical properties of materials are researched. Topics to be discussed are the effect of temperature, UV radiation and water absorption on optical glasses and plastics.

2.3.1 Thermal Properties of Matter and Refractive Index

In this Subsection are considered changes notable in materials or in their properties, when temperature of the material is changed. These include thermal expansion and change of refractive index and transmittance with temperature. Also concept of service temperature is introduced.

As a concept, thermal expansion may be familiar for most people, when discussing about metals and for example some thermometers make use of this property of matter. In the simplest of form, thermal expansion means the change in the size of an object with changing temperature and it is defined in one dimension as [34, p. 126]

$$\alpha \Delta T = \frac{\Delta l}{l}, \tag{2.40}$$

where α is the coefficient of thermal expansion (CTE), ΔT the temperature difference, Δl the difference in length of an object and l the initial length.

Thermal expansion is a universal property for all phases of matter, but in this thesis discussion is restricted in solid materials, since that is the form of optical components. The theoretical framework also only includes isotropic solids, that expand linearly.

In solid state atoms or molecules are organized in stiff lattice structure, in which they have a some interatomic distance, r, between each others. This is determined by the interatomic potential, Φ, which can be, for distances near the equilibrium distance, r_0, and thus the minimum potential, $\Phi(r_0)$, represented with Taylor's series [34, p. 71]

$$\begin{aligned} \Phi(r) = \Phi(r_0) + \frac{d\Phi(r_0)}{dr}(r - r_0) + \frac{1}{2}\frac{d^2\Phi(r_0)}{dr^2}(r - r_0)^2 + \\ \frac{1}{6}\frac{d^3\Phi(r_0)}{dr^3}(r - r_0)^3 + \cdots = \sum_{m=0}^{\infty} \frac{\Phi^{(m)}(r)}{m!}(r - r_0)^m. \end{aligned} \tag{2.41}$$

The first term describes the offset of absolute energy scale and thus can be here omitted. The second term, which describes the restoring electrical force, is zero at r_0. Third term tells us, that the restoring force depends linearly on the distance from r_0 and the fourth, cubic, term gives rise to the anharmonic, and thus asymmetric, nature of the potential energy as presented in figure 2.8. [34, p. 71]

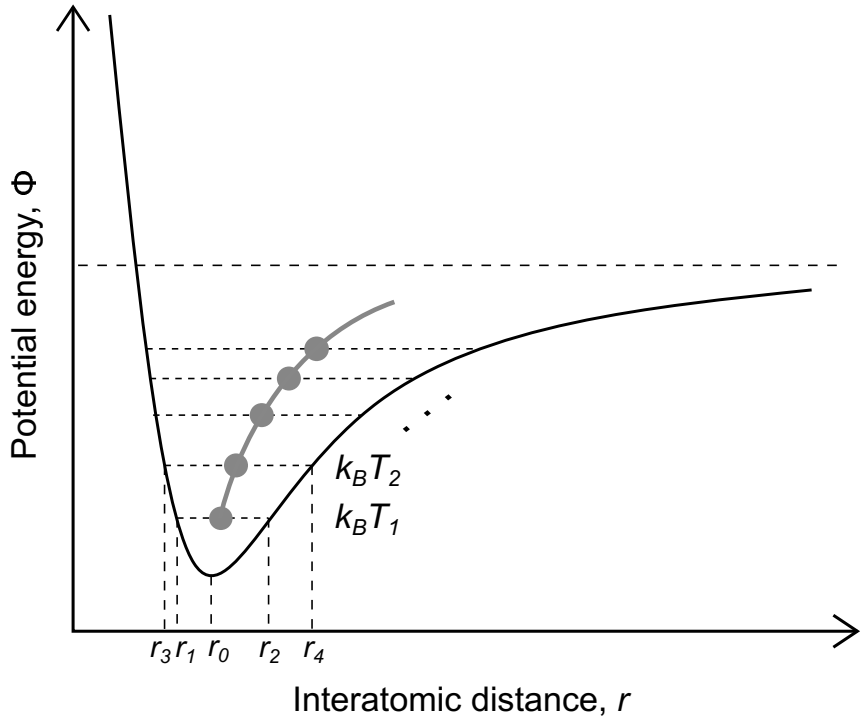

Figure 2.8 *Interatomic potential energy represented as a function of interatomic distance,* $\Phi(r)$. *Based on [34, Fig. 4.12].*

The figure 2.8 depicts the interatomic potential as a function of distance, $\Phi(r)$. The atoms can oscillate between the end points of the temperature line, for example at T_1 between r_1 and r_2. Though for any temperature, T_i, there is a certain mean energy for an atom, k_BT_i, which are depicted with gray dots. As one can see, due to the asymmetricity of the potential, the mean energies shift to longer interatomic distances as temperature rises ($T_i < T_j$). This then in turn leads to the macroscopic expansion of a material as its temperature rises. [34, pp. 127-128]

In table 2.2 there have been represented coefficients of thermal expansion of some common optical plastics and glass. There it can be seen, that usually for plastics, the coefficients are about one order of magnitude greater.

Table 2.2 *Thermal properties of some common plastic materials compared to a common glass material (N-BK7) [60].*

Material	α $\left(\times 10^{-6} \frac{1}{°C}\right)$	Service temperature (°C)	$\frac{dn}{dt}$ $\left(\times 10^{-6} \frac{1}{°C}\right)$
N-BK7	7.1	>400	3
PMMA	60	85	-105
COC	60	150	-101
NAS	58	80	-115
PC	68	120	-107

One term used to describe the temperature related performance of a optical material is service temperature. This is the temperature after which the material starts to lose its optical performance in some fashion for example due to structural degradation. These temperatures are not absolute, though, since they do not have an unambiguous definition. Thus they can change a bit between different material producers depending on their own definitions of the matter. [59, p. 130] These temperatures are also presented in table 2.2, where one can notice, that the service temperatures for optical plastics are significantly lower than the ones for glass. This fact needs to be very carefully considered, when planning an optical design for higher temperature applications.

Not only the dimensions of an object change with temperature, but also its refractive index is related to thermal changes: $\frac{dn}{dT}$. This relation is called thermo-optic coefficient. Thermal change of refractive index occurs at some level in all optical materials and is tied to the thermal expansion of a material and electrical polarisability, Φ_p, of material: [56]

$$\frac{dn}{dT} = \frac{\left(n^2 - 1\right)\left(n^2 + 2\right)}{6n}\left(\Phi_p - \alpha\right) \tag{2.42}$$

According to Pokrass, Burshtein and Gvishi [56], the relation 2.42, introduced by Prod'homme in 1960, is the most widely accepted mathematical tool to analyze thermal dependency of refractive index.

As already mentioned, the thermo-optic coefficient depends on both electrical polarisability and thermal expansion of material. In inorganic materials, that is, in this case non-carbon-based materials, the electrical polarisability and thermal expansion coefficient are relatively close in value. For example in silica-based glasses the case is usually, that polarisability prevails over thermal expansion resulting in positive thermo-optic coefficients. On the other hand in organic polymers, like the ones presented in 2.2, coefficient of thermal expansion dominates and thus thermo-optic coefficients turn negative as can

be seen from the table 2.2. [40], [56]

Last matter discussed in this Subsection is the dependence of transmittance on temperature. This matter seems to be something, that is, within optical material producers, well quantitatively identified, but no unambiguous and detailed explanation seems to be presented: When temperature rises, the UV edge of transmittance curve shifts towards longer wavelengths and respectively IR edge to shorter wavelengths. This means, that wavelength region of high transmittance gets narrower the higher the temperatures rise. [64]

For plastics, this shift can be noticed, when materials are kept exposed to constant elevated temperatures for long periods of time (some hundreds of hours). As plastics tend to change their colour when exposed to high temperatures for a long period of time, this could be a tell from increased absorption of light in certain parts of visible spectrum. Also in favor of increased absorption would speak, that refractive index of material and hence reflectance of material (discussed further in Section 2.4.4), does not change that significantly with temperature.

For optical grade glasses there is not that much literature to be found about this phenomenon. Some research made in the 1960's and 70's ([7], [30]) study the effects of thermal aging on fused silica or quartz, but these are not suitable for precision molding due to their high glass transition temperatures. Fortunately interest in high-power white light LEDs has shown light to the subject matter in resent years: It seems that glasses do not lose their transmittance properties as much as optical grade plastics, as shown in [43]. Also the findings for low transmittance losses of glass are back by Tsai et al. [76].

With these limited resources it seems, that glasses lose around 5% of their transmittance when exposed to temperatures up to 250°C for 1000 hours. Plastics seem to lose their transmittance a lot faster and in lower temperatures as their transition temperatures do not reach over 150 °C. At 120 hours the losses are already around 10% and they gradually rise to over 20% when heat exposure time gets to 500 hours. [43] When thermal aging time reaches 2000 hours at 125 °C or 1000 hours at 135 °C, some grades of optical plastics seem to lose almost all of their transmittance in visible regions [84].

As there is still very limited amount of studies to be found on the subject, it would be definitely an interesting one to study further in future. Especially as cameras on dashboards of cars are subjected to high temperatures, even over 100 °C, for thousands of hours cumulatively during the lifetime of a car, decrease in lens transmittance can have substantial effects on functionality of the camera.

2.3.2 Water Absorption

Water absorption comes mostly in question with plastic materials. This will happen at some level with all optical plastics and depending on the extent of it, there might be notable consequences. These might be for example increasing of physical dimensions, and thus change in density. This will also effect the refractive index as stated by Lorentz-Lorenz formula [52]

$$\frac{n^2 - 1}{n^2 + 2} = \frac{4\pi}{3} N_V \Phi_p, \tag{2.43}$$

where N_V is number of particles in unit volume. For example for acrylic put in 50 °C and 90 % humidity for two weeks, the refractive index will decrease by 0.001. Although, acrylic is the worst case scenario even for plastics, this fact needs to be considered when designing robust precision optical systems. The best plastics will perform more than an order of magnitude better, so this problem could be evaded with proper material selection, with of course all the other variables in mind. [60, pp. 25-26]

2.3.3 Photodegradation

Photodegradation is a term used for degradation of optical and material properties of plastics or glasses due to UV or some other high energy element of sun light. Here UV radiation in particular is discussed, since it is the most significant high energy radiation coming from Sun to the surface of the Earth. Degradation manifests itself as structural deterioration, loss of transmission, due to increase in haze and decrease in gloss, and color changes. The first is mainly problem with plastic and even the latter two happen with remarkably shorter UV exposure in plastics than in glass as for glass it could take decades and for plastics there are notable effects in couple of months of constant exposure. [54], [1], [75]

The structural degradation in polymers arises, since the energy of UV radiation is close to the dissociation energy of bonds in polymers. Thus UV light can break these bonds and create free radicals, which then in turn react with oxygen in atmosphere. This causes lightening of the molecular weight of the polymer and weakens the structure of it by, for example, making it more brittle. [24], [54] The radiation also induces surface erosion, which then in turn can increase the haze, as already learnt, since one key reason for haze is uneven surface of a component [75].

Normally the effect of color change in plastics is mainly yellowing and in glasses more on the bluish and purple side. In plastics this can be attributed to creation of conjugated

bond sequences, which then absorb blue wavelengths of visible light, thus turning the plastic more yellow [82]. Although after certain amount of radiation, the plastic will start bleaching, which in turn reduces yellowing. The point at which it happens, depends on the humidity of the environment and the time decreases when humidity increases. The study made with polycarbonate had photobleaching to start in 42 % relative humidity after about 1500 hours of radiation [75], but this depends on the radiation intensity and material properties, so the numbers here are not to be generalized for every polymer besides the order of magnitude.

In glasses the coloring is attributed to formation of internal defects, color centers, that absorb shorter wavelengths of the visible spectrum [1]. Hence basically this means, that for plastics the color changes need to be accounted for in longer term use, such as automotive applications or others, where the exposure to sun light is continuous. Also it has been found, that yellowing increases with humidity [75].

The transmittance problems with glass can also be traced to color centers, but as for color change, the formation of these will take decades [1]. For plastics also the increased absorption of yellow wavelengths reduces transmittance. Also the structural degradation and surface erosion increase scattering in the surface and also inside the plastic component. In the study of Tjandraatmadja and Burn [75], it was found, that for polycarbonate the transmission reduced by 4-5 % in 2000 hours of radiation and haze increased by 4.5-5.5 % in the same time. The samples performed better in drier conditions. Also it was found, that relative surface gloss decreased by 5 % after 2000 hours of radiation. Gloss means that light will reflect from the material surface as reflection law 2.45 states. The decrease in gloss means here, that the light will diffuse more on the surface of the radiated plastic and thus the haze will increase and transmission decrease.

Thus it can be seen, that UV light has some nasty effects on polymers in general. It still needs to be noted, though, that there are ways to lessen the effects of photodegradation. For example the UV absorption can be increased or the formation of free radicals can be reduced by dopants in the polymer materials. Hence dopant concentrations need to be determined for specif applications and thus UV conditions in mind.

2.4 Geometrical Optics

Now some basic principles on how light propagates in a medium have been established, so it is time to get familiar with how it behaves in an actual optical environment. Geometrical optics is defined as manipulation of rays of light through bodies of matter without taking into consideration any diffractive behavior. [33, p. 159]

In this Section first some basic reflection and refraction laws are discussed, then behavior of light and image forming in thick lenses is considered. After that the basics of analytical ray tracing is studied and last Fresnel equations are glimpsed.

2.4.1 Refraction and Reflection

Lenses are by far the most used optical components. Hence now a generalized picture of how light rays propagate through a lens is depicted: A lens is formed of two surfaces with some material in between. On these surfaces a ray of light can do two things; either refract or reflect and on most material interfaces there will be both in some ratio. Also it needs to be noted, that all of the rays; incident, refracted and reflected, lie on the same plane, called the plane of incidence [33, pp. 109-110]. This is depicted in figure 2.9.

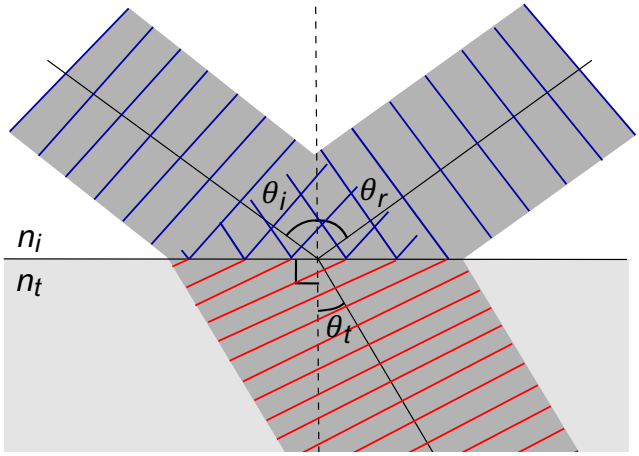

Figure 2.9 *Reflection and refraction on the interface of the mediums with different refractive indices, n_i and n_t. Angle of incidence, θ_i, equals angle of reflection, θ_r and refraction angle θ_t is dictated by Snell's law in equation 2.44.*

From upper secondary school it has been taught a general rule of how light transmits through a surface in geometric fashion, with different refractive indices, n_i and n_t, on each side of the interface. This relation is called Snell's law or law of refraction [33, p. 109]

$$n_i \sin\theta_i = n_t \sin\theta_t, \tag{2.44}$$

where θ_i and θ_t are the angle of incidence and angle of refraction with respect to the normal of the surface. On the other hand, when light does not transmit through a surface, it will reflect in the same angle, θ_r, as the angle of incidence, θ_i, was for incoming light. This is called law of reflection and both this and law of refraction have been depicted in figure 2.9 [33, p. 106]

$$\theta_i = \theta_r. \tag{2.45}$$

The phenomenon of reflection is due to light scattering backwards from the closely binded particles in the matter. This will happen, when the change in refractive indices is very rapid: if the index change has a gradient over a distance of about a wavelength, there is hardly any reflection and when the change happens in less than $\frac{\lambda}{4}$ of a distance, most of the rays will reflect. Of course if the change in refractive indices happens at some rate in between the aforementioned, there will be both refraction and reflection in some ratio. There is also a semantic difference in whether the light is reflected from optically denser or more tenuous medium. The former situation is called external and latter internal reflection. [33, pp. 104-105]

2.4.2 Lenses

As mentioned in Section 2.4.1, the lenses are by far the most widely used optical component. In general, lens can bend light in two ways; it can either converge the beams or diverge. Which one happens, depends on the geometry of the surface of the lens and also on the refractive indices of the medium and lens material. The most likely scenario is, that the lens is made of optically denser material and also that light is coming from the medium to the lens. Hence this situation will be studied futher: When the surface is convex (from Latin: convexus, meaning arched) the light is converged and beams bend towards the normal of the surface and when the surface is concave (concavus, meaning hollow) the light is diverged, hence the beams refract away from the normal. To this also closely attaches the concept of focal point. It is the point from which the rays diverge in case of concave lens and to which they converge in case of convex lens. [33, p. 161]

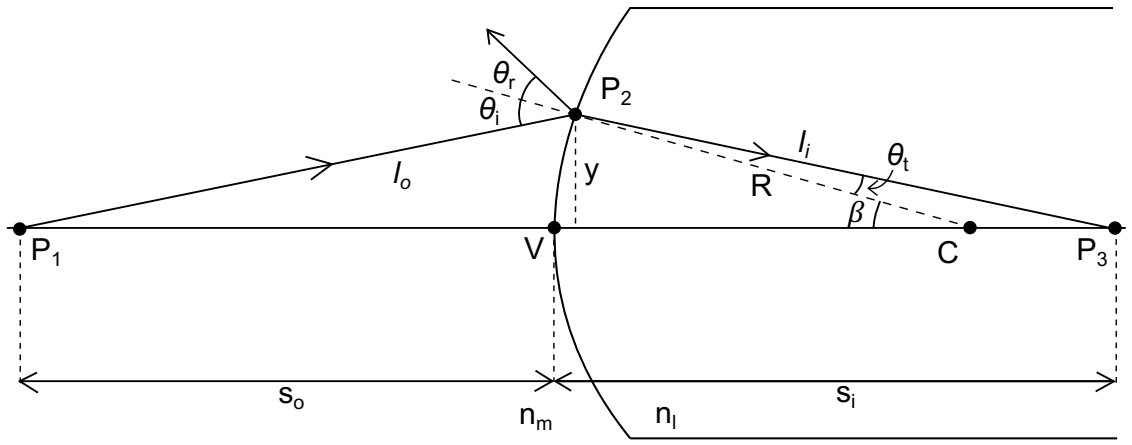

Figure 2.10 *Path of light between conjugate foci, P_1 and P_3, defining optical path length, OPL. Based on [33, Fig. 5.6].*

Here discussion is limited to spherical lenses: As it is already been defined, the speed of light depends on the medium it is propagating in. This occurs, because materials have different indices of refraction. Thus there has been defined a measure, with which one can determine phase differences and thus diffraction behavior of light in media. This measure is called optical path length, OPL, [33, p. 163]

$$OPL = l_o n_m + l_i n_l, \tag{2.46}$$

where l_o is the distance from the object to some point on the surface of the lens, l_i the distance from the point to the image plane and n_m and n_l refractive indices for the first medium and lens material, respectively. This can also be described as the distance light would travel in vacuum in the same time it uses to travel in media and OPL has been depicted in figure 2.10. The points P_1 and P_3 in this figure are called conjugate points or conjugate foci. This means that an image at point P_1 will be projected to P_3 and vice versa so light paths are reversible. For conjugate points through a refraction on one surface it also holds, that [33, p. 163]

$$\frac{n_m}{l_o} + \frac{n_l}{l_i} = \frac{1}{R}\left(\frac{n_l s_i}{l_i} - \frac{n_m s_o}{l_o}\right), \tag{2.47}$$

where s_o and s_i are object and image distances, respectively, from the vertex, V of the lens and R the radius of curvature of the lens. Through paraxial approximation $\sin\beta \approx \beta$, which leads also to $l_o \approx s_o$ and $l_i \approx s_i$. Thus equation 2.47 can be simplified to [33, pp. 163-164]

$$\frac{n_m}{s_o} + \frac{n_l}{s_i} = \frac{n_l - n_m}{R}. \tag{2.48}$$

As mentioned, this approximated relation holds only for small angles β, and when used for general situation will produce aberrations, but more on them in Section 2.5.

In the figure 2.11 have been depicted several optical quantities, which are important in analysis of lenses and lens systems. The quantities and their meanings have been then explained in table 2.3.

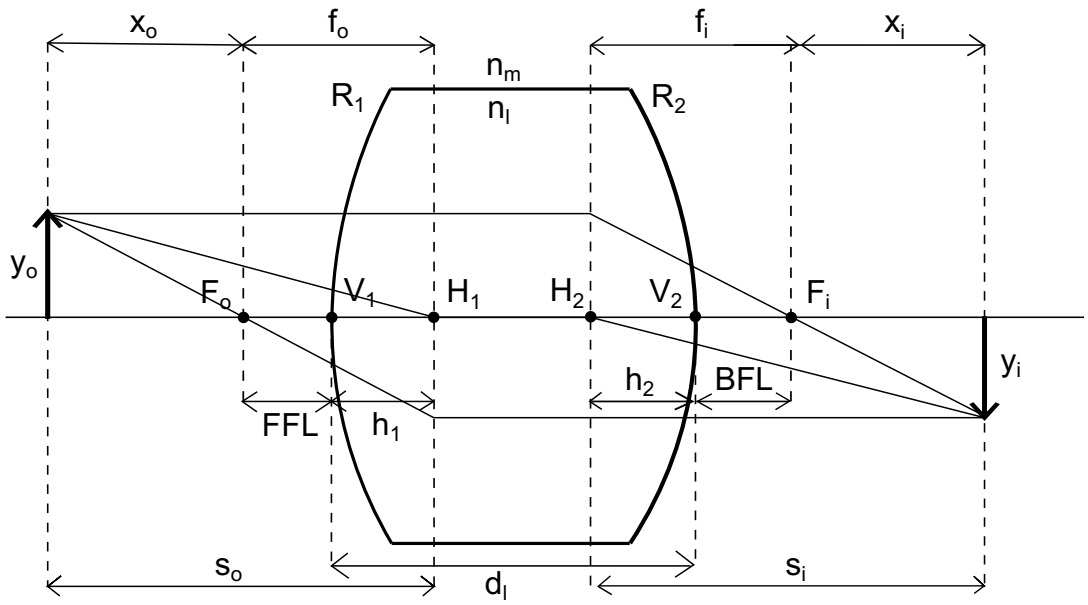

Figure 2.11 *Important quantities for analyzing lenses and lens systems. Quatities are explained in table 2.3. Based on [33, Fig. 6.5].*

Table 2.3 *Important optical quantities and their abbreviations.*

Abbreviation	Meaning
F_o, F_i	Front and back focal points
V_1, V_2	Vertices of front and back surfaces
H_1, H_2	First and second principal points
R_1, R_2	Radii of curvature of the front and back surfaces
FFL, BFL	Front and back focal lengths
f_o, f_i	(Effective) front and back focal lengths
x_o, x_i	Distances from object and image to F_o and F_i
h_1, h_o	Distances between V_1 and H_1 and V_2 and H_2
s_o, s_i	Distances from object and image to H_1 and H_2
y_o, y_i	size of object and image
N_1, N_2	First and second nodal points
d_l	thickness of the lens
O	Optical center

It is good to note, that when the lens is surrounded by the same medium, the effective front and back focal lengths, f_o and f_i, are equal. Thus it is marked $f_o = f_i = f$. Also to be noted is, that these quantities have specific sign conventions, which need to be carefully considered in calculations, since they vary a bit from quantity to quantity. The conventions have been presented in table 2.4 and they are marked so, that light is supposed to be coming

from the left of the lens.

Table 2.4 *Sign conventions used in geometrical optics [33, Table 5.1].*

Quantity	sign convention
s_o, f_o	+ left of V
x_o	+ left of F_o
s_i, f_i	+ right of V
x_i	+ right of F_i
R	+ if center of curvature is right of V
y_o, y_i	+ above optical axis

From the quantities in figure 2.11 and table 2.3, the focal points F_o and F_i and principal points H_1 and H_2 are called cardinal points. The principal planes determined by principal points represent the planes, where the light is thought to refract in a lens and focal points are so called infinite conjugates. This means, that when light comes from an object, which lies at infinity, light propagates parallel with optical axis, the rays will converge into the back focal point of the lens. Also light originating from front focal point of the lens will be parallel with the optical axis after refraction from the lens. There are also two more cardinal points, called nodal points, N_1 and N_2. They lie on the points where optical axis and the extensions of incoming and outgoing light cross. In the medium the actual refracted light must also cross the optical center, O, of the lens. [33, p. 255] Cardinal points have been represented in figure 2.11 and the abbreviations have also been presented in table 2.3.

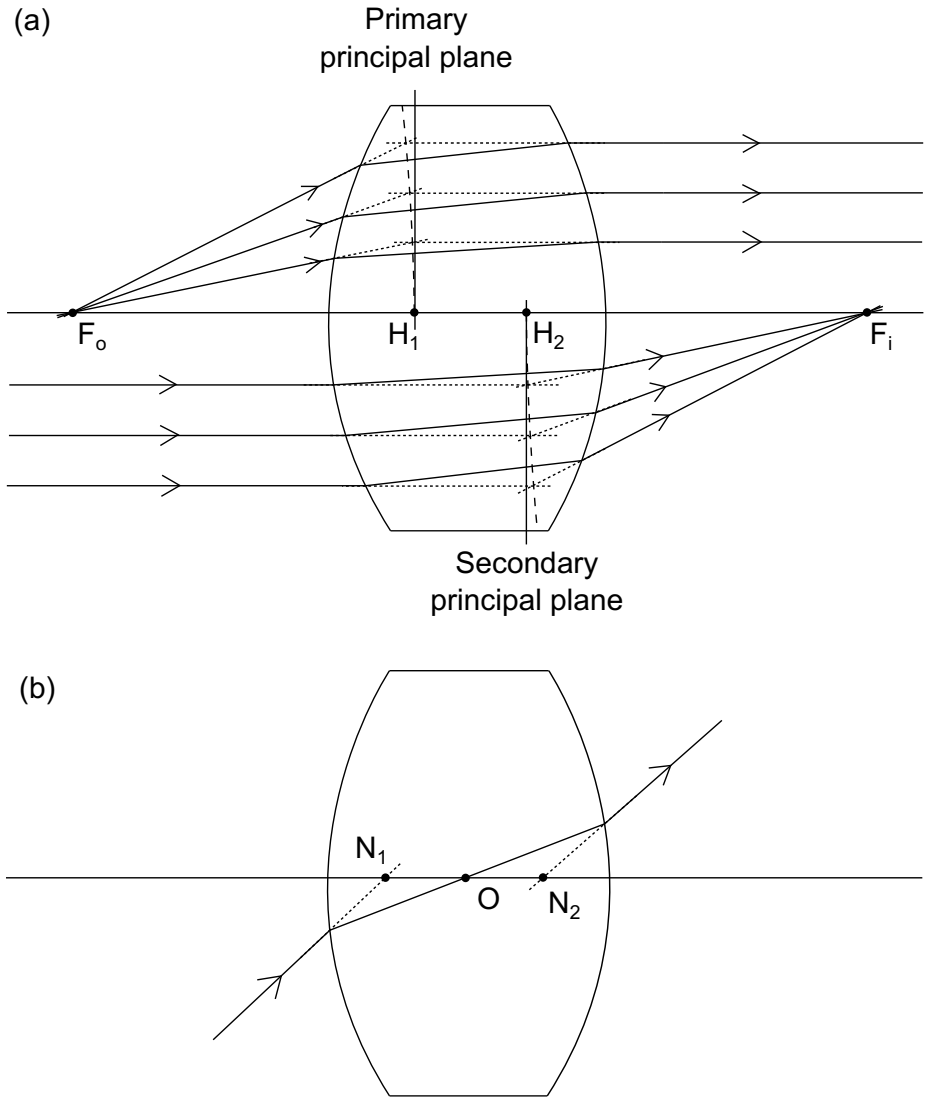

Figure 2.12 *Cardinal points of a lens: in (a) are portrayed focal points, principal points and principal planes and in (b) nodal points. Based on [33, Fig. 6.1] and [33, Fig. 6.2].*

The nodal points and principal points will take equal places, if on both sides of the lens there is the same medium. Also one can notice from figure 2.12 (a), that the principal planes are not actually planes, but they are curved slightly. Depending on the geometry of the lens, they can either lay inside or outside of the lens. The reasoning for all of these points is to give one information for ray tracing and with knowledge of the locations of these cardinal points, one can calculate the trace of a ray.

To determine the (effective) focal lens, f, of a lens, one can use lens-maker's formula [33, p. 257], [53]

$$\frac{1}{f} = \left(\frac{n_l}{n_m} - 1\right)\left[\frac{1}{R_1} - \frac{1}{R_2} + \frac{\left(\frac{n_l}{n_m} - 1\right) d_l}{n_l R_1 R_2}\right]. \tag{2.49}$$

Normally the situation is, that the lens lies in air, where refractive index can be approximated to $n \approx 1$. Thus the lens-maker's formula simplifies to

$$\frac{1}{f} = (n_l - 1)\left[\frac{1}{R_1} - \frac{1}{R_2} + \frac{(n_l - 1)\, d_l}{n_l R_1 R_2}\right]. \tag{2.50}$$

From this point onwards assumption is made, that the lens is surrounded by air, since that is the far likeliest situation. The principal points are connected to focal length with following equations [33, p. 257]

$$h_1 = -\frac{f(n_l - 1)d_l}{R_2 n_l}, \tag{2.51}$$

$$h_2 = -\frac{f(n_l - 1)d_l}{R_1 n_l}. \tag{2.52}$$

There is also a Newtonian form of a lens equation, which connects the distances between object and image with their respective focal points, x_o and x_i, to focal length, f, [33, p. 257]

$$x_o x_i = f^2. \tag{2.53}$$

As it is known from the applications of lens, such as cameras, telescopes and magnification glasses, lenses possess an ability to seemingly change the size of the imaged object. This quality is called magnification and transverse or lateral (with respect to the optical axis) magnification can be intuitively calculated from the ratio of the image and object sizes. From the geometry of image formation also other relations can be deduced [33, pp. 257-258]

$$M_T = \frac{y_i}{y_o} = -\frac{x_i}{f} = -\frac{f}{x_o} = -\frac{s_i}{s_o}. \tag{2.54}$$

Next two lens systems with lenses L_1 and L_2 are considered. This kind of lens doublet

is depicted in figure 2.13, where there are also represented the cardinal points for the system. Worth noting is, that the distance between the two lenses, d, is defined to be from the secondary principal plane of the first lens to the primary principal plane of the second lens and not from vertex to vertex.

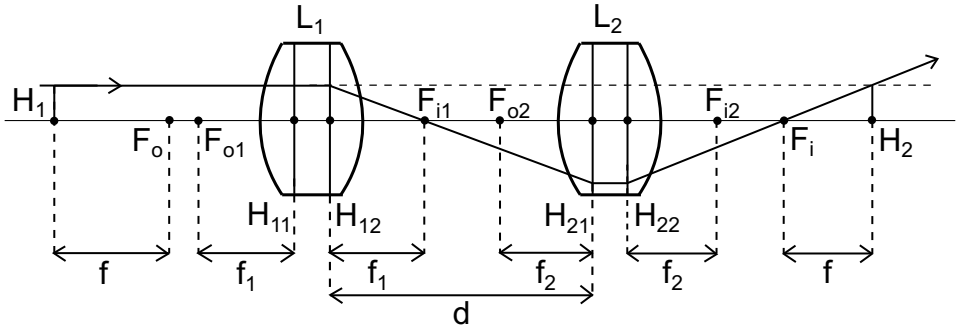

Figure 2.13 *Lens doublet with cardinal points of the system. Based on [33, Fig. 6.6].*

Mathematically the cardinal points this kind of doublet can be characterized as follows [33, p. 258]. The focal length of the system, f, is defined with focal lengths of individual lenses, f_1 and f_2, and the distance between lenses, d,

$$\frac{1}{f} = \frac{1}{f_1} + \frac{1}{f_2} - \frac{d}{f_1 f_2}. \tag{2.55}$$

Principal planes of the system are defined with following relations

$$\overline{H_{11}H_1} = \frac{fd}{f_2}, \tag{2.56}$$

$$\overline{H_{22}H_2} = -\frac{fd}{f_1}. \tag{2.57}$$

The transverse magnification of the system is defined to be the product of the two lenses, that is, [33, p. 258]

$$M_T = \left(-\frac{s_{i1}}{s_{o1}}\right)\left(-\frac{s_{i2}}{s_{o2}}\right) = -\frac{s_i}{s_o}. \tag{2.58}$$

For more than two lens system the same equations can be used so, that one first calculates necessary quantities for the first two lenses. Then one can use these combined quantities for the next lens and continue so for the rest of the lens system. This enables the examination of multiple lens systems, which are used for example in nowadays' mobile phone cameras.

2.4.3 Ray Tracing

When the light confronts discontinuity in medium, refraction and reflection take place. With evaluating these changes in direction of propagation of a ray of light, effectively the route it follows through a system of optical elements can be found. This method is called ray tracing. Since natural light does not consist of only one ray, but has all possible different wavelengths of light, there is no point on doing this by hand and there are really good optical designing softwares to do this. Anyway, these programs are using this same principle of ray tracing about to be described next.

A ray of light can be characterized with two numbers; the distance from optical axis, y, and the angle of its propagation with respect to optical axis, β. Light is also effected by the changes in optical densities of media it is propagating in according to Snell's law 2.44. This gives the principle followed through the process of tracing. The geometry needed is presented in figure 2.14.

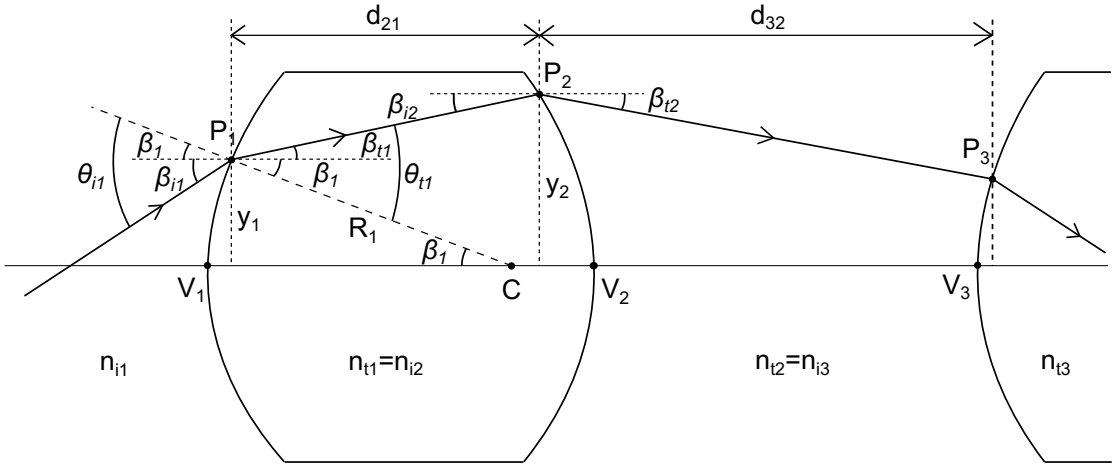

Figure 2.14 *Geometry of ray tracing. Based on [33, Fig. 6.8].*

Next the process of ray tracing referencing to figure 2.14 is discussed. First the Snell's law at point P_1 is considered. It can be written, that

$$n_{i1} \sin \theta_{i1} = n_{t1} \sin \theta_{t1} \tag{2.59}$$

The angles θ_{i1} and θ_{t1} can be broken down to two components, one of which is the part of the angle, which is above the direction of the optical axis, and the other one being the part, which lies beneath the direction of the axis. Also since β_1 is small, it holds, that $\beta_1 \approx \frac{y_1}{R_1}$. These modifications and some rearranging yields

$$n_{t1}\beta_{t1} = n_{i1}\beta_{i1} - \left(\frac{n_{t1} - n_{i1}}{R_1}\right) y_1, \tag{2.60}$$

where the term $\frac{n_{t1}-n_{i1}}{R_1}$ is called (refractive) power of surface and is marked with $\mathcal{D}_1$, simplifying the equation 2.60 to form known as refraction equation [33, p. 259]

$$n_{t1}\beta_{t1} = n_{i1}\beta_{i1} - \mathcal{D}_1 y_1. \tag{2.61}$$

After surface and point P_1 the ray propagates through medium to point P_2, the height of which can be determined with the help of known direction of propagation, β_{t1}, lateral distance, d_{21}, between the points and distance from optical axis to point P_1, y_1, as follows [33, p. 259]

$$y_2 = y_1 + d_{21}\beta_{t1}. \tag{2.62}$$

With this and equation 2.61 one can characterize the propagation of a ray of light through an optical system of different surfaces and media.

2.4.4 Fresnel Equations, Reflectance and Transmittance

Also to the understanding of the propagation of rays relate Fresnel equations. They are a way of deducing, how the amplitude of light distributes between the reflected and the refracted parts of it, when it confronts a interface of two media with different refractive indices. The equations describe the relative change in electric field amplitude of perpendicular ($E_{0\perp}$) and parallel ($E_{0\parallel}$) polarisations with respect to plane of incidence when the **E**-field confronts an interface. [33, pp. 123-125]

The Fresnel equations arise from continuity conditions on the border of two media. These conditions state, that the initial and reflected field components must be equal to the transmitted (refracted) component. The rigorous proof of the equations and boundary conditions is not presented here, but rather the principles and the relations, which Fresnel equations present for the angles of incidence, reflection, refraction and refractive indices of different media are shown. Although it can be said, that the boundary conditions differ for electric and magnetic fields and also for the parallel (subscript $\parallel$) and perpendicular (subscript $\perp$) polarisation states of the fields with respect to the plane of incidence. Again if magnetic field is omitted, Fresnel equations simplify quite a bit, and thus get forms of [33, pp. 123-125]

$$r_\perp = \left(\frac{E_{0r}}{E_{0i}}\right)_\perp = \frac{n_i \cos\theta_i - n_t \cos\theta_t}{n_i \cos\theta_i + n_t \cos\theta_t}, \tag{2.63}$$

$$r_\parallel = \left(\frac{E_{0r}}{E_{0i}}\right)_\parallel = \frac{n_t \cos\theta_i - n_i \cos\theta_t}{n_t \cos\theta_i + n_i \cos\theta_t}, \tag{2.64}$$

$$t_\perp = \left(\frac{E_{0t}}{E_{0i}}\right)_\perp = \frac{2n_i \cos\theta_i}{n_i \cos\theta_i + n_t \cos\theta_t} \tag{2.65}$$

and

$$t_\parallel = \left(\frac{E_{0t}}{E_{0i}}\right)_\parallel = \frac{2n_i \cos\theta_i}{n_t \cos\theta_i + n_i \cos\theta_t}. \tag{2.66}$$

Here $r_\perp$, $r_\parallel$, $t_\perp$ and $t_\parallel$ are Fresnel coefficients of reflection and transmission for perpendicular and parallel polarisations of electric field. Furthermore one can define the relation between irradiances (equation 2.29), I, of the reflected and incident and transmitted and incident beams, respectively reflectance, $\mathcal{R}$, and transmittance, $\mathcal{T}$. For transmittance one must also consider the difference in angles of incidence and refraction, but as for reflectance the angles equal, they will cancel out. Thus for reflectance it remains, that [33, p. 129]

$$\mathcal{R} = \frac{I_r}{I_i} = \frac{2v_r\epsilon_r E_{0r}^2}{2v_i\epsilon_i E_{0i}^2} = \left(\frac{E_{0r}}{E_{0i}}\right)^2 = r^2. \tag{2.67}$$

For normal angle of incidence this can be further simplified to

$$\mathcal{R} = \left|\frac{n_i - n_t}{n_i + n_t}\right|^2, \tag{2.68}$$

since at normal angle, reflection is indifferent on the polarisation of light and $\cos 0 = 1$.

For transmittance from similar treatment with irradiance, it follows that [33, p. 129]

$$\mathcal{T} = \frac{I_t \cos\theta_t}{I_i \cos\theta_i} = \frac{n_t \cos\theta_t}{n_i \cos\theta_i}\left(\frac{E_{0t}}{E_{0i}}\right)^2 = \left(\frac{n_t \cos\theta_t}{n_i \cos\theta_i}\right) t^2. \tag{2.69}$$

For transmittance and reflectance there also holds a relation, that

$$\mathcal{R} + \mathcal{T} = 1, \tag{2.70}$$

when no absorption occurs [33, p. 130].

Transmittance can be divided in internal and total transmittance, $\mathcal{T}_i$ and $\mathcal{T}_{tot}$ respectively. The former only takes into account absorption of light happening inside the material and latter, in addition, accounts for reflections on each surface of a lens and scattering inside a lens. Normally total transmittance for one lens element (thus having two surfaces) is around 90 % for visible light region. This can be calculated from equation 2.68, which gives for refractive index of 1.5 a 4 % reflection at each surface. There also stands a relation between internal and total transmittances [64]

$$\mathcal{T}_{tot} = \frac{2n_i n_t}{n_i^2 + n_t^2}\mathcal{T}_i. \tag{2.71}$$

Nowadays reflections can be avoided pretty sufficiently with appropriate anti-reflection (AR) coatings reducing the total reflectance to less than 1 % for a lens element over the visible wavelength region. AR-coatings will be further discussed in Section 3.3.

For imaging systems to be able to produce good quality images, it is crucial, that lens systems are as lossless as possible. This basically means good transmittance over the bandwidth in which lens system is designed to work. For consumer applications mass manufacturability is also of key importance. Thus one also needs to account for moldability of both glass and plastic materials being compared. This requirement cuts the material list a lot shorter, since besides the optical qualities, the materials need to be elastic or viscose enough, have CTE close to the one of the mold and so on.

As examples a couple of common moldable materials, which can be used in mass manufacturing, are considered. A division to a two categories based on Abbe number and refractive index of the material is made to make them comparable with one another, as it seems that with flint materials present lower transmittances in short wavelengths than crown materials. This can be qualitatively observed for example from Schott's glass catalogue [61].

As later in this thesis, the main objective is to compare the differences in transmittances of different materials, are the studied materials picked so, that their refractive indices match well. This is done, since in conversions between internal to total transmittances according to equation 2.71 the difference of indices could distort the results. Also the Abbe numbers are matched as well as possible, but it needs to be noted, that as it is usually prefered for

optical designs to have either low Abbe number and high refractive index or vice versa, it is hard to find glasses with as low Abbe numbers as those of plastics for corresponding refractive indices. The mismatch observable in figure 2.3 makes an apples-to-apples comparison with respect to just one variable really hard.

It is common for optical polymer manufacturers to provide transmittances for 3 mm and glass manufacturers for 10mm thickness. This causes differences in amount of light absorbed in materials. This mismatch is compensated by using Beer-Lambert law, proposed originally by Pierre Bouguer, to calculate internal transmittances for corresponding thicknesses for both glasses and plastics [10]:

$$\mathcal{T} = e^{-\mu_{abs} l}, \tag{2.72}$$

where μ_{abs} is absorption coefficient, also known as attenuation coefficient, and l the distance, that light travels in material. For two thicknesses, l_1 and l_2, of two materials with same absorption coefficient, with help of Beer-Lambert law, the relation between internal transmittances, $\mathcal{T}_{i1}$ and $\mathcal{T}_{i2}$, can be written as

$$\mathcal{T}_{i1} = \mathcal{T}_{i2} e^{\mu_{abs}(l_2 - l_1)}. \tag{2.73}$$

It is well known, that in mid- and long wavelength infrared regions of EM spectrum, plastic materials do not trasmit light well. In figure 2.15 are represented most common optical polymers and their respective transmittance curves.

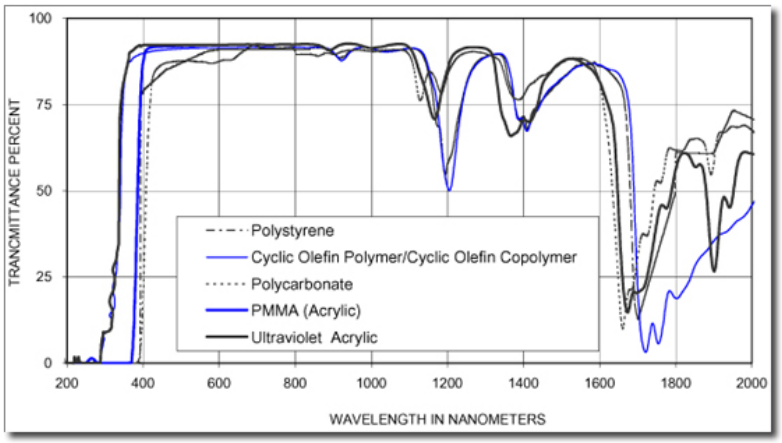

Figure 2.15 *Transmittances of different common optical polymers [31].*

Also in the UV region plastics have historically been week, but some manufacturers have

been able to reach the gap to glasses little by little. Best examples seem to be cyclic olefin polymers and copolymers, Zeonex being a good example, which exhibit glass-like transmittance in UV-A region (315-390 nm) as seen in 2.15.

Transmittance of IR-wavelengths in most consumer products has not been that important, since in most imaging solutions they are cut off with filters as it will be further explained in 3.3. Shorter wavelengths on the other hand are, maybe surprisingly, important for good image quality: as it will be discussed later on in Section 3.1 and demonstrated in figure 3.1, it is common, that spectral power of illuminants gets very weak the shorter the wavelengths get. This means that for imaging system that blues are naturally weaker and thus the color balance is harder to acquire. In low light scenarios this problem gets even worse resulting to blue noise in final image due to gaining in image processing process, which is further discussed in Section 3.7. This makes short wavelength transmittance interesting subject for studying.

2.5 Aberrations

Optical aberrations are deviations from ideal behavior of light in matter. They can be divided roughly into two categories depending on when they occur. First kinds of aberrations are called monochromatic aberrations, which means, they occur independent of the wavelength of light. Consequently the other types of aberrations are chromatic aberrations, which appear due to wavelength dependency of index of refraction. [33, pp. 266-267] In this Section first different monochromatic and then chromatic aberrations are discussed.

2.5.1 Monochromatic Aberrations

In this Subsection so called primary aberrations are discussed. They arise from first order approximation, which states basically the same thing as paraxial approximation. That is, that the angle at which the light travels compared to optical axis is relatively small. The name first order approximation comes from following expansion of sine function [33, p. 267]

$$\sin\beta = \beta - \frac{\beta^3}{3!} + \frac{\beta^5}{5!} - \frac{\beta^7}{7!} + \cdots \tag{2.74}$$

First order approximation only includes the first term, namely $\sin\beta \approx \beta$, of the expansion and this is only adequate for paraxial rays. There are also aberrations, which occur

also in higher order approximations and these are called higher-order aberrations, but as mentioned, discussion here is limited on only the primary ones.

First spherical aberrations, SA, are studied. First a third order approximation of equation 2.47 is taken. It is presented as

$$\frac{n_m}{s_o} + \frac{n_l}{s_i} = \frac{n_l - n_m}{R} + y^2 \left[\frac{n_m}{2s_o} \left(\frac{1}{s_o} + \frac{1}{R} \right)^2 + \frac{n_l}{2s_i} \left(\frac{1}{R} - \frac{1}{s_i} \right)^2 \right]. \tag{2.75}$$

Here it can be seen, that the additional term from first order approximation is proportional to the square of height of the point of refraction from optical axis, y. This means, that for convex surface the rays will focus closer to the second vertex as $|y|$ grows. Also this works to the other direction too and for concave lenses the marginal beams will focus further away from the vertex. Thus in short it can be said that the greater the aperture of a lens, the greater the SA for nonparaxial rays. [33, p. 267] This principle will work for just one refractive surface or a convex lens and it is presented in figure 2.16.

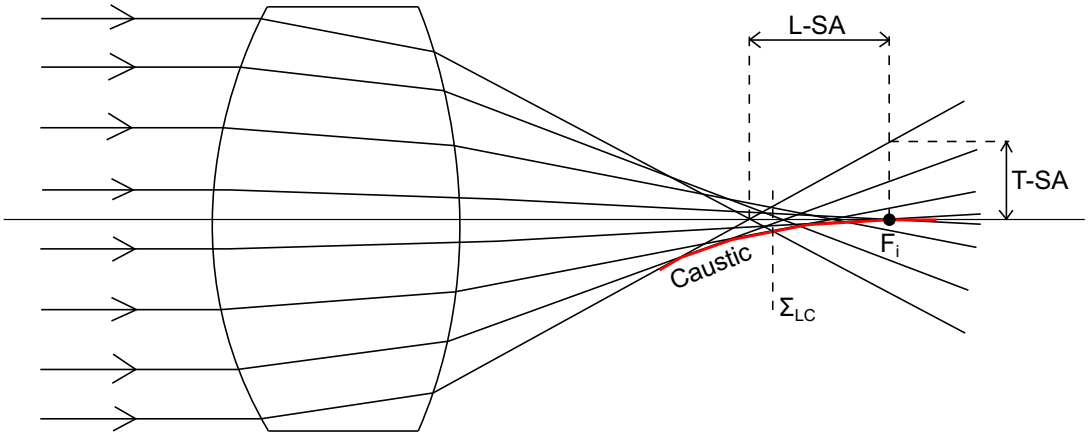

Figure 2.16 *In convex lens the light rays will focus too close to the second vertex of lens due to spherical aberration. Based on [33, Fig. 6.15 (a)].*

In figure the abbreviations L-SA and T-SA mean longitudinal and transverse spherical aberrations and caustic is the envelope on the edges of refracted rays. The Σ_{LC}, which is called the circle of least confusion, is placed on the crossing point of caustic and marginal rays. Usually this is the best place to view the image [33, p. 268].

Naturally SA will effect image quality. As the marginal rays do not focus on the focal point, the image will lose sharpness and the some intensity from a point image will shift to area around it. This can be lessened with either making the aperture smaller, but with that the amount of light the system gets in is also decreased. The amount of SA also varies with object distance and lens shape. Also for spherical lenses there can be found two

conjugate points with zero aberration with certain conditions on lens surfaces; the lens needs to be meniscus, that is, convex-concave. [33, pp. 268-269]

Next is discussed coma or comatic aberrations. They arise from the fact that principal planes are not actually flat, but curved as presented in figure 2.12 (a). When there is no SA, parallel light rays will focus at BFL distance from second vertex of a lens, but as the principal plane is curved, the effective focal lengths differ for rays at different distances, y, from optical axis. Thus transverse magnification will get distorted.

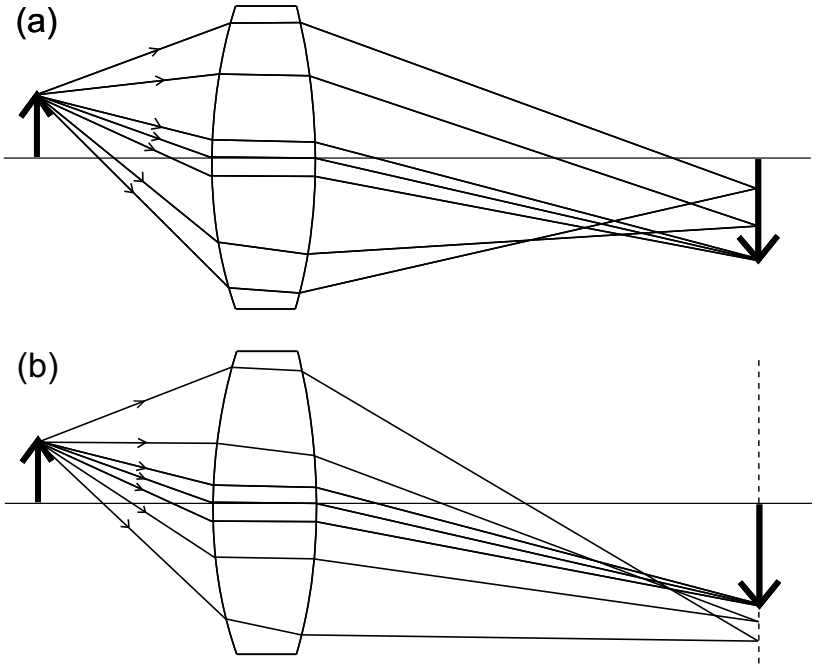

Figure 2.17 *(a) Negative and (b) positive coma. Based on [33, Fig. 6.22].*

As shown in figure 2.17, coma is defined to be positive, when marginal rays magnify the object too much and negative in opposite situation. As a rule of thumb it can be stated, that strongly concave positive-meniscus lens produces the most negative coma and convex-meniscus on the other hand the most positive coma. The optimal shape for a lens for minimum coma would be somewhat convex-planar and actually this is pretty close to the optimal shape for minimizing SA. There is though a slight problem with this and that is, that distance s_o is designed to infinity. This can be dodged though, with taking two such lenses. This lens system then can be designed to work with finite conjugate points. [33, pp. 271-273]

Third major monochromatic aberration studied is astigmatism. This means, that light rays from same source propagating in perpendicular planes with each other have different focal points as shown in figure 2.18.

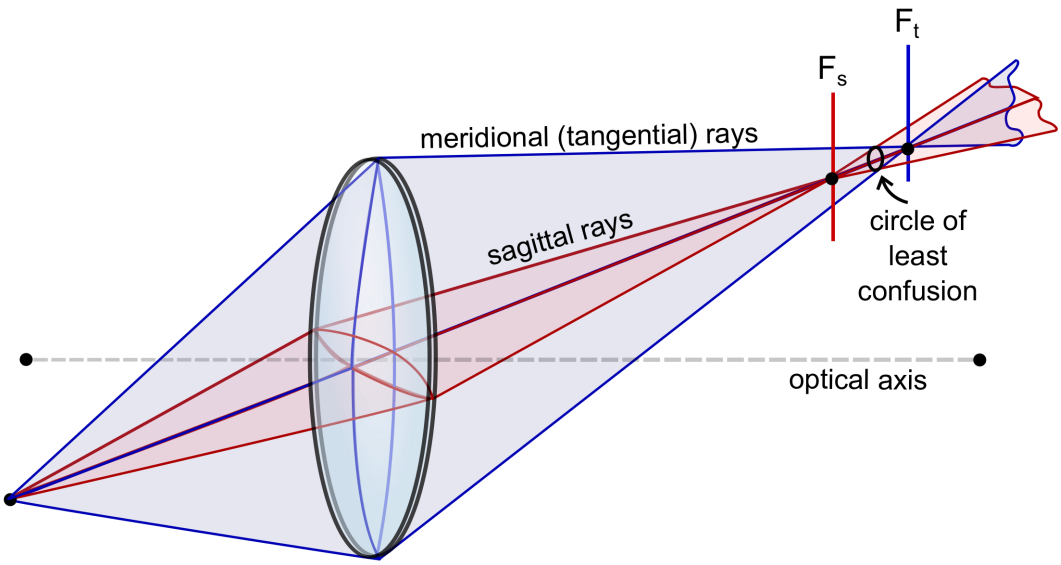

Figure 2.18 *Astigmastism manifests itself with different focal lengths for meridional and sagittal rays. Based on [39].*

Astigmatism arises, when the object point is out of the optical axis, which then in turn makes the lens seem asymmetric for different parts of a cone of rays incident from the object point. Thus different parts of the cone refract differently in the lens, which leads to different focal points of different components of the cone. The rays traveling in same vertical plane are called meridional or tangential rays and ray traveling perpendicular to this plane are called sagittal rays. The difference between focal points of sagittal and meridional rays, F_s and F_t respectively, are separated by astigmatic difference. This distance depends on the power of lens, $\mathcal{D}$, defined in equation 2.60 and the angle at which they incident; the further the object point lies from the optical axis, the larger the astigmatic difference will be. [33, p. 274]

The difference in focal lengths of different components of a light cone will effectively make the refracted ray somewhat ellipsoidal. At focal points F_s and F_t the cone will effectively turn into vertical and horizontal lines, respectively. In between these focal points there is a place at which the rays will again form a circle and this is called circle of least confusion, where the image has a circular blur compared to ellipsoidal, horizontal or vertical blur produced elsewhere. On focal points the images produced are called primary and secondary images in the order at which they occur from the lens. [33, p. 274]

Next monochromatic aberration studied is field curvature, also known as Petzval field curvature. This aberration arises from the fact, that lens can focus sharply only the paraxial rays on a paraxial image plane. The rays coming in an angle with respect to optical axis will not focus on this plane but rather, in case of positive lens, closer to the lens on so called Petzval surface, Σ_p. This effect gets stronger as the angle between optical

axis and the rays direction of propagation increases. Thus when an object is imaged on paraxial image plane, the center of the image is sharply in focus and the edges will appear out of focus. When the image plane is then brought closer to the lens, the edges will get sharper and the middle part of image will start to appear blurred. This works for positive lens and for negative lens, the image plane needs to be moved backwards to achieve sharp edges. [33, p. 276]

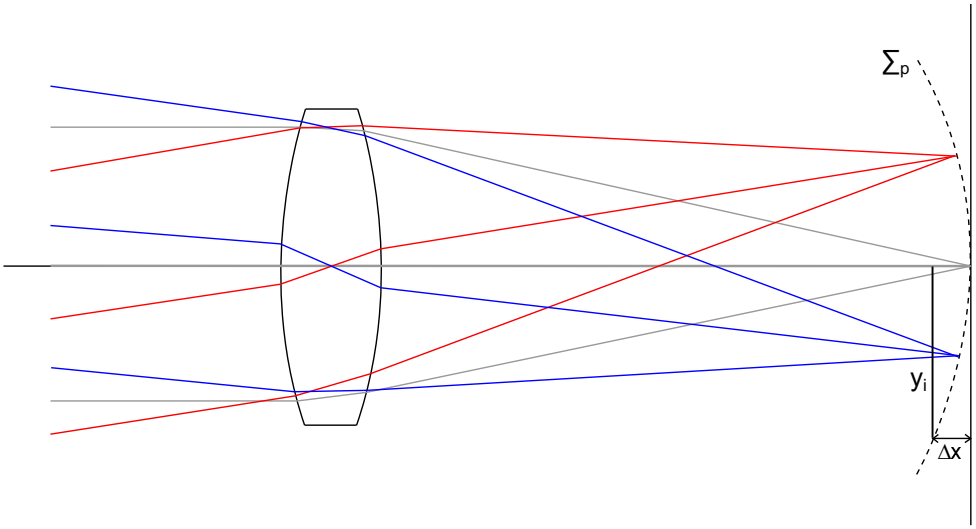

Figure 2.19 *Field curvature and Petzval surface, Σ_p, for positive lens.*

The displacement of Petzval surface from paraxial image plane, Δx, for image height y_i can be calculated for thin lens from Petzval sum [33, p. 276]

$$\Delta x = \frac{y_i^2}{2} \sum_{j=1}^{m} \frac{1}{n_j f_j}. \tag{2.76}$$

Here n_j and f_j are the refractive indices and focal lengths of m thin lenses forming the lens system. If Δx is made zero, this is so called Petzval condition, which indicates, that there is no field curvature. Thus with this and 2.55 in mind, it is possible to design a lens system with flat field and finite conjugate points. This is very important for example camera design, because the imaging sensors are usually flat. The field flattener for positive lens can be achieved with positioning negative lens after the positive. This can be done so, that is does not notably add to any other aberrations. [33, p. 276]

Also astigmatism produces curved image fields. Thus it is very closely related to the aberration produced by field curvature. As shown by figure 2.19, the field curvature gets worse the further from the optical axis is moved and the same happens with astigmatic surfaces, Σ_t and Σ_s referring to meridional and sagittal surfaces respectively. To lessen

the problem at hand, a field stop can be mounted to the system to cut off the edges of the field to decrease the aberrations on the edges.

The lens system with a stop can also be modified so, that it produces so called artificially flattened field shown in figure 2.20. There the surface of least confusion, Σ_{LC}, is made planar and thus the image plane is placed there.

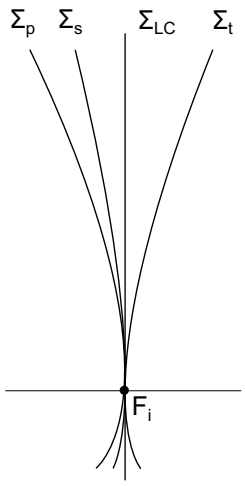

Figure 2.20 *Artificially flattened surface of least confusion, Σ_{LC}. Based on [33, Fig. 6.32 (b)].*

Last monochromatic aberration being discussed is distortion. This arises from non-uniform magnification power in the lens. When magnification power of edges of a lens is greater than near the optical axis, this is called positive or pincushion distortion (fig. 2.21 (a)) and when the M_T is greater in the neighborhood of the optical axis than on the edges, this is referred as negative or barrel distortion (fig. 2.21 (b)). Distortions are different from other aberrations discussed so far, since every point of distorted image is still sharply in focus and the image is just bended. [33, pp. 277-278]

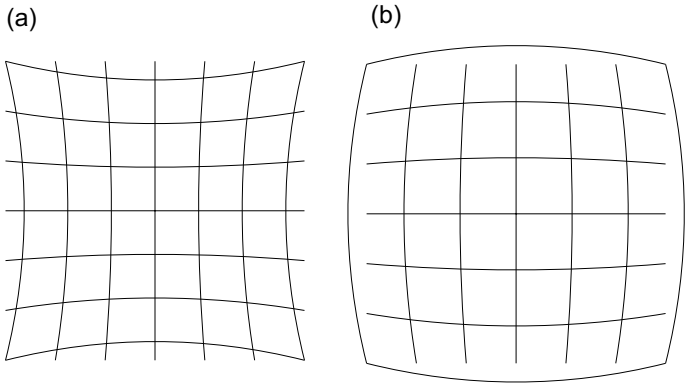

Figure 2.21 *(a) Pincushion and (b) barrel distortions, based on [81].*

Normally if lens is thin, there will not be very much distortion, but as the lens gets thicker,

the distortion becomes more and more prominent. Also adding a stop to the optical system will usually induce distortions, since the chief ray cannot always travel through principal points of a lens. Only when it is located at a lens or in the middle of two identical lens elements, it will not induce distortions. [33, pp. 277-278]

2.5.2 Chromatic Aberrations

The aberrations discussed in previous Subsection will take place even if the light was monochromatic as in for example lasers. Although even if it would make the theoretical reference frame of this thesis a lot of simpler, the fact of a matter is, that natural light has multiple wavelengths. As presented in Section 2.4, the path of light is depended on, among other things, the refractive indices of the media it propagates in. These in turn are depended on the wavelength of light as discussed in Section 2.2. This then makes also for example focal length of a lens depended on wavelength as seen in equation 2.49. This is the essence of chromatic aberrations, CA; the behavior of light is strongly attached to its wavelength and thus color.

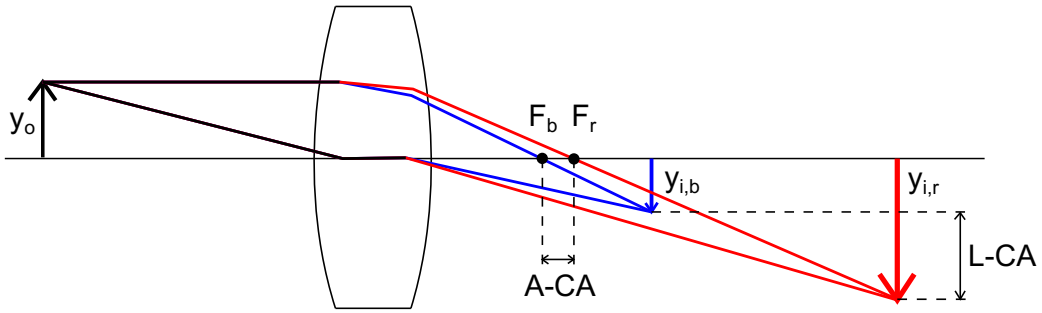

Figure 2.22 *Difference in light path and image formation for different wavelengths of light, here red and blue light. Based on [33, Fig. 6.38].*

Usually in the visible light region of wavelengths the refractive index is greater for light of shorter wavelengths. This results in shorter focal lengths and thus also shifts image plane closer to the lens in cases of converging lenses as seen in fig. 2.22. The difference in focal lengths resulting from the different refractive indices is known as axial chromatic aberration, A-CA, and the difference in image heights, in this figure $y_{i,b}$ for blue and $y_{i,r}$ for red image, as lateral chromatic aberration, L-SA. Thus from one object emitting natural light several images of different sizes and colors are formed. It is customary to design lenses in most imaging systems to focus sharply around 550nm wavelengths, which corresponds to yellowish green light. This is done, since human eye is most sensitive for light around that wavelength region. This then leads to the edges of the image being a bit blurred due to being out of focus. [33, p. 279-280]

Thus the goal for an optical system is usually to minimize, or ideally eliminate, the CA (and also all the previously described monochromatic aberrations), that is, total dispersion in the system. A system with no CA would be called achromatized and for two wavelengths, for example blue and red light, this can be produced with one positive and one negative lens. This then in turn would be called achromatic doublet. Effectively this means that the focal lengths of the two wavelengths, here for red and blue light, f_r and f_b respectively, would be equal.

A special case of thin compound lens is now considered. Here distance between lenses is zero, and object and image are at infinities. Also it is known, that wavelength and refractive index have roughly linear dependence in the visible region for most optical materials [33, p. 82]. Thus the focal lengths for compound lenses can be approximated to correspond to the focal length for yellow light, f_y. When combining this with focal length of system of two thin lenses (equation 2.55), the above paragraph and some mathematical action, it can be written [33, p. 280]

$$\frac{f_{2y}}{f_{1y}} = -\frac{\dfrac{n_{2b} - n_{2r}}{n_{2y} - 1}}{\dfrac{n_{1b} - n_{1r}}{n_{1y} - 1}}. \tag{2.77}$$

Here the f_{1x} and f_{2x} are focal lengths for first and second lens of the compound and n_{1x} and n_{2x} the refractive indices for the lenses and subtext $x \in b, y, r$. In this equation the the nominator and denominator of the right side are called the dispersive powers of lenses 2 and 1, respectively. These look pretty familiar already, since when comparing them to equation 2.32, it is noticed, that they are reciprocals of Abbe number. Thus

$$\frac{f_{2d}}{f_{1d}} = -\frac{V_{1d}}{V_{2d}}, \tag{2.78}$$

where subtext d corresponds to the Fraunhofer spectral d-line.

As it was mentioned earlier, one negative and one positive lens is needed to create a achromatic doublet. Now it is also known, that due to the equation 2.78, one needs to account for dispersive powers or Abbe numbers of the lenses. Hence one flint and one crown lens (flint and crown defined in Section 2.2) are needed to compensate for different dispersive powers of lenses.

In real world, as lenses are thick, one also needs to account for, that for different wavelengths the principal planes differ. Thus one cannot compensate for all dimensions of magnification

in lenses and thus it is usual, for practical reasons, to optimize the lateral CA and not axial CA. Also here only two colors (and their average) are achromatised, and for two lenses that is pretty much the best one can do. The more colors, or better wavelengths, is wanted to be achromatised, the more lenses are needed to make all compensations and corrections needed. [33, p. 283]

Also in real world, lenses are not always touching each others. In this situation it is called a separated achromatic doublet. For two such lenses made out of same material the distance, d, in between the two, that yields achromatization, can be written as [33, pp. 283-284]

$$d = \frac{f_{1d} + f_{2d}}{2}. \tag{2.79}$$

As it was the case for compound lenses, also in this case L-CA is well corrected, but A-CA might not be.

Now the aberrations independent of surroundings of an optical system have been studied. As lenses in a camera still are not in a vacuum, some outside stimuli need to be considered and for this thesis the most important one is temperature.

2.5.3 Thermal Defocus

Last aberration type studied in this Section is the effect of changing temperature to focal length of a lens. As it has been shown in Subsection 2.3.1, the changes in thermal conditions can have significant effects on the refractive index and geometrics of a lens depending on the lens material: thermal expansion is responsible for the geometrical change in a lens and also has a significant role in the thermo-optic coefficient, which is in charge of the refractive index change with temperature.

Now the thermal defocus, $\frac{df}{dT}$, can be characterized for thin lens in air as [58]

$$\frac{df}{dT} = -f\left(\frac{\frac{dn}{dT}}{n-1} - \alpha\right). \tag{2.80}$$

Since thermo-optic coefficient is dependent on wavelength of light, so is also thermal defocus. According to Sultanova, Kasarova and Nikolov [70], [69], thermo-optic coefficients of optical plastics generally decrease when wavelength of radiation increases, though in visible region the change is only some percentages. Also from Schott glass' optical glass data sheet [62] it also can be seen, that for glasses the general behavior is also similar.

Though, when looking at tables 2.2 and 5.1, it can be seen, that for plastics $\frac{dn}{dT}$ are negative. For glasses they are in most cases positive and also the absolute values are about two orders of magnitude smaller. Another factor effecting the thermal focal length change is CTE. As it can be seen from table 2.2, for plastics CTEs are about ten times higher than for glasses. Thus it can be qualitatively deduced when examining equation 2.80, that for glasses the two factors, CTE and thermo-optic coefficient, are in most cases canceling each others out, but for plastics they add up to the total effect of thermal defocus.

From equation 2.80 it can be noted, that relative thermal focal length change is indifferent of the focal length of a lens as it cancels out. Thus relative focal length change with temperature, defined as $\frac{df}{dT}$ divided by focal length, f, can be written as

$$\left(\frac{df}{dT}\right)_{rel} = -\frac{\frac{dn}{dT}}{n-1} + \alpha \tag{2.81}$$

Thus relative thermal defocus is indifferent also of lens geometry and only depends on material properties of a lens.

3. PRINCIPLES OF DIGITAL IMAGING SYSTEMS

Imaging system is thought to consist of different parts, which help to capture light from its surroundings and bring it to screen or film. Naturally digital and analog imaging systems differ somewhat with their structures and in this Chapter mainly digital imaging systems are discussed, since basically all mass-produced imaging products nowadays utilize digital technology.

When path of photons is considered from illuminant through the lenses to the sensor on and after which the photons are converted to electrons and digits. Then image signal processing (ISP) pipe further refines them to the form seen on the displays of mobile phones, surveillance units, digital cameras and so on. In this Chapter aforementioned path is studied in more detail and the foundations on which the simulation framework is built later on in the thesis is laid.

3.1 Illuminants

As it naturally is, different illuminants create different spectra of light. This can be seen even with bare eye, of course with different coloured lasers, but also when observing a good old light bulb, it create very yellowish or even reddish illumination and on the other hand for example LEDs in modern car head lamps can seem even bluish. As humans have natural born need to standardise and measure things, a somewhat extensive catalog of different standard illuminants, CIE illuminants, has been created. Here CIE stands from Commission internationale de l'éclairage, which is French for International Commission on Illumination.

First illumination standardised by CIE was so called A illuminant, which represents the spectrum of black body radiator at temperature of 2856 K. A more concrete description would be that it replicates the spectrum of incandescent light bulb. Another important light source, which needed to be standardised, was naturally Sun. This is represented by CIE D65 illuminant, which is more specifically defined as daylight at temperature 6500 K. CIE has also defined other illuminants in different classes, namely B, C, D, E and F: B and C where illuminants to represent daylight, but they were replaced by D series. E illuminants have equal energies at every wavelength within visible spectrum and hence

they do not have defined color temperature. Color temperature is defined for black body radiator with certain temperature and hence producing certain type of spectrum. F series consists of different fluorescent illuminants, which usually have some characteristic spikes in the illumination spectrum. [15] Also new L series based on white LEDs is expected to be published during 2018 and the aim of this series is to find new alternatives for old incandescent based standardisation and measurement systems due to banning and increase in prices of incandescent lighting [23].

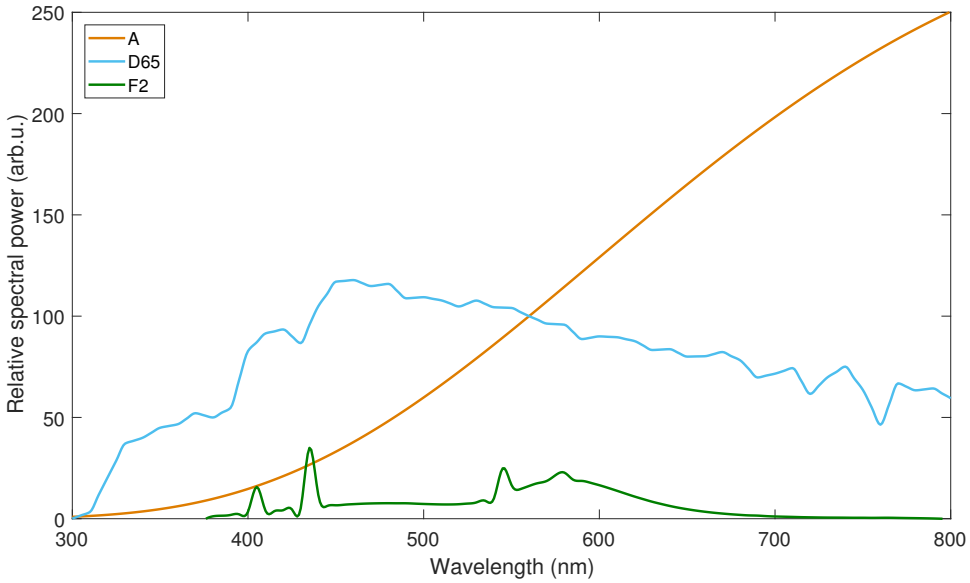

Figure 3.1 *Some important CIE illuminant spectra from different illuminant series: A, D65 and F2.*

As it can be seen from figure 3.1, both A and D65 illuminants have been normalised so, that they achieve 100 units of relative spectral power at 560 nm wavelength. This means, that they are not absolute measures of illumination and do not represent any specific spectral irradiances or radiant fluxes. Thus for these spectra to actually be useful, they need to be scaled to some meaningful level.

As it was pointed out in former paragraph, for example D65 illuminant, describing daylight, is set here so, that its power spectrum has value of 100 at 560 nm wavelength. If one looks for similar spectrum for actual sunlight on the surface of the Earth, it is found, that at 560 nm spectrum achieves power of 1.7860 $\frac{\mathrm{W}}{\mathrm{m}^2 \cdot \mathrm{nm}}$ [5]. Thus from these a scaling factor of $\frac{1.7860}{100} \frac{\mathrm{W}}{\mathrm{m}^2 \cdot \mathrm{nm}}$ is deduced. However, as sensor pixels, to which light hits in the camera, are around 1 $\mu\mathrm{m}^2$ of size, this factor is scaled to $1.7860 \cdot 10^{-14} \frac{\mathrm{W}}{\mu\mathrm{m}^2 \cdot \mathrm{nm}}$.

Further on the number of incoming photons is a factor in noise properties of an imaging system as presented in Section 3.5. Radiant flux, Φ_E, is defined as radiated or received

energy, Q_E, over time: [29]

$$\Phi_E = \frac{\partial Q_E}{\partial t}. \tag{3.1}$$

As energy of light consists of energies of individual photons, by combining equation 3.1 with Planck's law on energy of a photon in equation 2.1, for number of photons, n_p, it is deduced, that

$$n_p = \frac{\Phi_E \lambda t}{hc}. \tag{3.2}$$

Here time, t, effectively means the exposure time of the camera, that is, the time that camera lets light to the sensor. For example, if exposure time

3.2 Reflectance of an Object

Humans perceive colours of objects as the colours they reflect. Thus as one sees red rose or green leaf, they reflect mostly the wavelengths corresponding to these colours. Of course reflectance spectra of natural objects are not only sharply of any specific wavelength but broader spectra, where there is more reflectance on certain bands. In figure 3.2 are represented X-RITE's GretagMacbeth ColorChecker and reflectances of its blue, light grey (neutral 8), and white patches. ColorChecker is used for example for colour calibration and thus its reflectances are very well defined and known. [45]

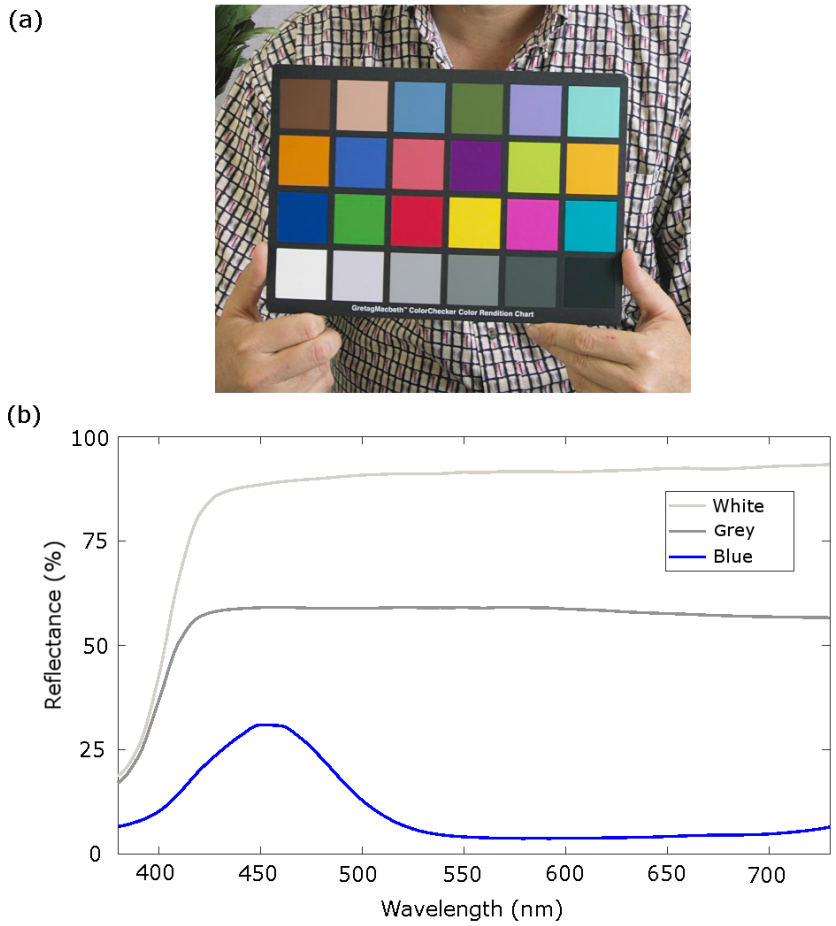

Figure 3.2 *(a) X-RITE's GretagMacbeth ColorChecker chart [44] and (b) reflectances of white, light grey (neutral 8) and blue patches of the chart.*

As objects reflect the light of the illuminant, this means, that light gets dimmed down, since not 100 % of the light is never reflected in a real world. From figure 3.2 (b) it can be noted, that shades of grey reflect light pretty evenly through visible spectrum, but for example blue has peak around 450 nm and already around 550 nm reflectance gets close to zero and thus the patch seems blue.

3.3 Lens System Transmittance, AR coating and IR cut-off filter

For single lens, transmittance as a physical property has already been covered in Section 2.4.4, hence in this Section the focus is on lens system transmittance, and what needs to be accounted for, when designing lens system. For example high end mobile cameras have up to six lenses per camera, which all need to be accounted for in calculating the total transmittance of the system. Also all of these lenses need to be coated (most common being AR-coating) for better optical performance, and these coatings will have effect on per lens, and thus per lens stack, transmittance.

AR-coatings have been shortly introduced in Section 2.4.4 and as already mentioned, they can reduce lens reflections down to <1 % for each lens in visible light region. This in turn means, that reflections of a lens system are somewhere around 4 to 6 % depending on the number of lenses in the system. Some AR-coating reflectance profiles are presented in figure 3.3.

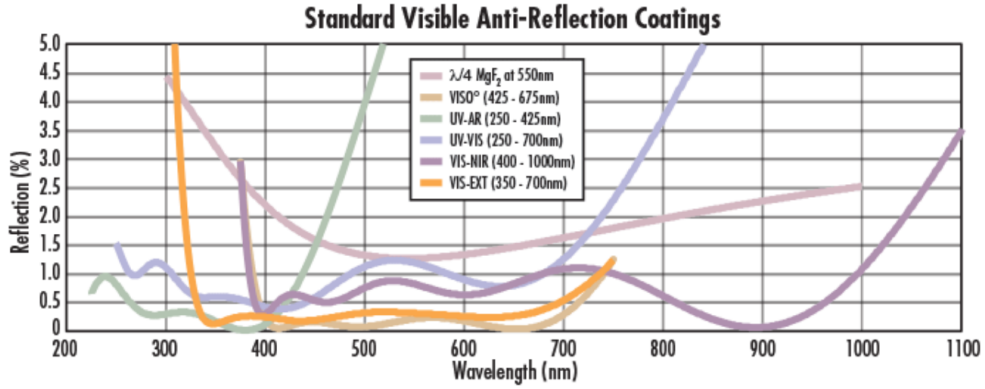

Figure 3.3 *Reflectances of some AR-coatings from Edmund Optics. Coatings have been done for N-BK7 glass substrate. [21]*

It needs to be noted though, that reflections here are calculated for normal angle of incidence (AoI) and they will increase when the AoI is increased. For example at 45°the reflectance will increase for around 0.5 - 5 percentage points per lens depending on the coating [21].

Maybe the simplest working principle of AR-coating to understand is the interference coating: the optical thickness of the coating layer is designed to be a quarter of a wavelength of light or some half multiple of it $\left(\frac{\lambda}{4}, \frac{3\lambda}{4}, \frac{5\lambda}{4}...\right)$. When coating layers get thicker though, the performance for single wavelength gets weaker. [6] Thickness of layer arises from the fact, that OPD between light travelling in the coating layer and light reflected from the surface of the coating needs to enable phase shift leading to destructive interference:

$$OPD = 2n_c d_c \cos\theta_c = \left(m - \frac{1}{2}\right)\lambda, \tag{3.3}$$

where n_c and d_c are refractive index and thickness of the coating and θ_c the reflection angle from the coating-substrate boundary and $m \in \mathbb{Z}$. These quantities have also been depicted in figure 3.4. This then means, that the phase difference of light beam reflected from coating and beam reflected from surface of the substrate is ideally exactly 180° making the the interference of two beams destructive. This principle is depicted in figure 3.4.

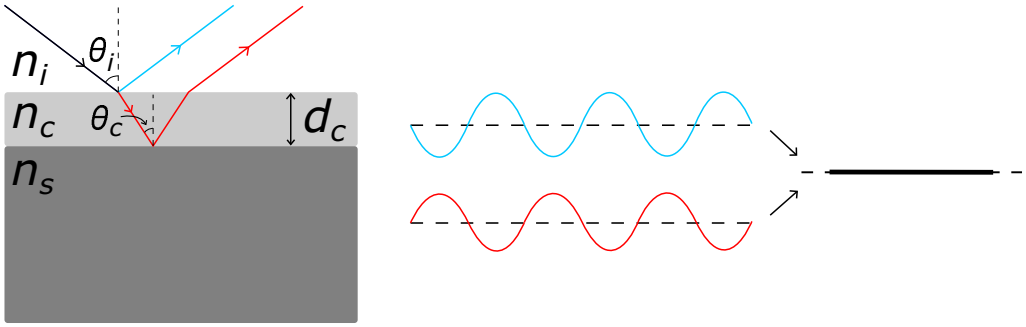

Figure 3.4 *In interference coating the beams reflected from surfaces of the coating layer and substrate destructively interfere and hence, ideally, eliminate the reflection of that wavelength.*

The index of refraction for coating needs to be chosen so, that it is between the indices of substrate and incident medium. Only then will it produce reflections on both sides of the coating thus resulting in interference of reflected beams. Ideal 180° phase shift is achieved with [6, pp. 166-168]

$$n_c = \sqrt{n_i n_s}. \tag{3.4}$$

As it can be deducted from equation 3.3, single thickness (layer) of coating works well only for very narrow bandwidth. This is not very useful in consumer products so wider bandwidth AR-coatings are needed. This problem can be addressed with multiple coating layers so in general it can be said, that the more layers AR-coating has, better it can perform. [6, pp. 166-168]

As AR-coatings need to be done from different materials than substrate itself, there are naturally differences in physical and optical properties of the materials. In different parts of the coating process and in the use of optical elements these differences can cause some problems with coating material durability. Major factor in these problems are changing temperatures in coating process itself and in user environment, since these changes change the physical dimensions of both coating and substrate. Since coating is usually grown via adhesion on to the substrate, these differences in, for example CTE, will result in differences in expansion rates, which then induces stress to thin coating layer. This stress can be quantified as follows [6, pp. 158-161]:

$$\frac{d\sigma_{s,c}}{dT} = \frac{Y_c}{1 - \nu_{P,c}} (\alpha_s - \alpha_c), \tag{3.5}$$

where $\sigma_{s,c}$ is the stress induced, Y_c Young's modulus and $\nu_{P,c}$ Poisson's ratio, all quantities of one coating layer, and α_s and α_c CTEs of substrate and coating layer, respectively.

As discussed in few occasions already in this thesis, plastics tend to have around one order of magnitude higher CTEs than glass materials. If one then takes a look at some common AR coating materials, such as MgF_2, ZrO_2 and SiO_2, it can be noticed, that their CTEs ($8 - 13 \times 10^{-6}$, 11×10^{-6} and 0.6×10^{-6}, respectively) correspond pretty well with those of glasses. Now by taking use of equation 3.5, it can be said, that plastics induce around 5-15 times more tensile stress to coating materials as they encounter thermal changes.

This can lead to cracking of coatings and thus weakening of their performance or altogether making them useless. Cracking and buckling of coating is presented in figure 3.5, former of which happens due to tensile stress caused by thermal variations and latter by insufficient adhesion and compression stress in growth phase of coating. Hence it is important in the design phase to match, in addition to optical properties, also CTEs of coating and substrate materials as well as possible.

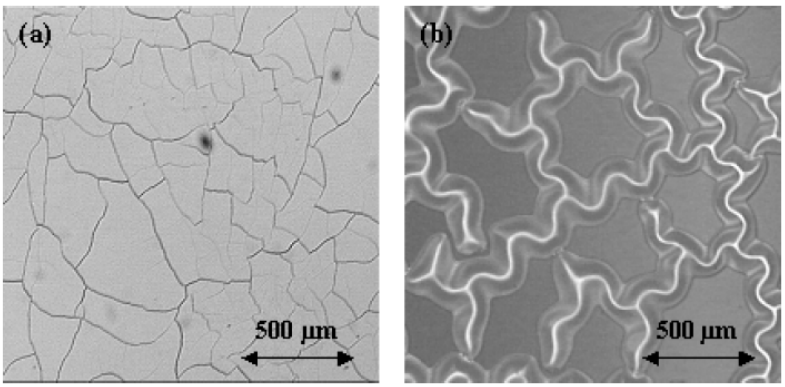

Figure 3.5 *(a) Cracking and (b) buckling of AR-coating [6, fig. 6.9].*

Now the components, which affect on total transmittance of a lens system, are understood. Also the mathematics to calculate it is fairly straight forward and it follows principles of ray tracing.

In lens system there pretty much always occur some unwanted reflections also from so called black parts of the lens system like lens barrel, where the lenses are set, and aperture stops. Even though they are made to be as reflection-free as possible, they still inevitably reflect a tiny bit of light, which then bounces back and forth in lens system leading to glares and other unwanted and uncontrollable lighting phenomena in image forming. These do not affect to stack transmittance per se, but are still important to understand from image quality point of view.

Before the sensor in the imaging system there is usually also an infrared, that is, IR cut(-off) filter. The purpose of it is, as it says in the name, is to block IR-rays from entering to the sensor. If this was not done, it could cause the image to be overexposed, since

most silicon-based sensors, which are most widely used in imaging, are highly sensitive to IR-radiation.

3.4 Imaging Sensor

Basic working principle of an image sensor is, that it collects photons and converts them to electric signal. This can be then further down the line converted to ones and zeros - to a digital signal, which then can be interpreted as an digital image.

Photons, that illumination source has emitted a while back, have experienced reflection from an object and gone through the lens system and IR cut filter, are on the sensor surface sorted by their energies to separate different colours of light to different channels. There are couple of different ways (for example Foveon's layered model [37] and 3CCD with three sensors and dichroic prism or mirror setup to split the light spectrum to sub-spectra [3]) to do this, but most commonly used is so called Bayer filter (figure 3.6) since it is the cheapest to manufacture.

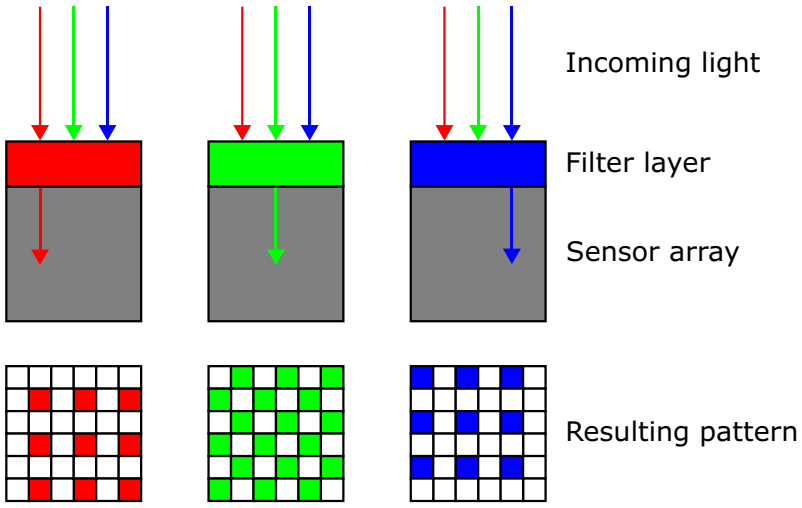

Figure 3.6 *Bayer filter and pattern on a sensor [14].*

Bayer filter works by letting through only certain type of radiation from each of the three different types of colour filters. Filters are arranged so, that no two filter squares next to each other are similar, as seen in figure 3.6. The three colours chosen to filters are red (R), green (G) and blue (B) and they are divided between squares with relations of 25 % - 50 % - 25 %, respectively. As one can notice, there is twice as much green filters in the pattern, also called as mosaic, as there are blues and reds. This is done since human eye is most sensitive to green shades. The greens are differentiated from one another by assigning them to the colour filters in the same row with them, that is, green-red (Gr) and green-blue (Gb). Thus it is possible to monitor efficiency of each colour filter and pixel.

As it was already mentioned, the job of a sensor is to "transform" energy of a photon to energy of an electron. This happens as in any photosensitive sensor: photon hitting photodiode, also known as photosites, excites electron from valence band to conduction band of a semiconductor creating an electron-hole pair and excited electron now creates charge. The measure of how many of the photons of certain wavelength create a charge carrier is called quantum efficiency (QE). Typical QE of mobile sensor is presented in figure 3.7. The sensor used there is ON Semiconductor's model MT9P031 with 5 megapixels (MP). In this particular sensor each pixel is 2.2 x 2.2 μm of size and the size of the sensor itself is 1/2.5 inch (5.7 x 4.3 mm). For comparison some flagship models of largest mobile phone manufacturers nowadays boast up to 40 MP sensors and pixel sizes between 1 and 1.5 μm (per dimension) for their main cameras. Sensors are usually sized around 1/2 inch, which means around 6.4 x 4.8 mm of size.

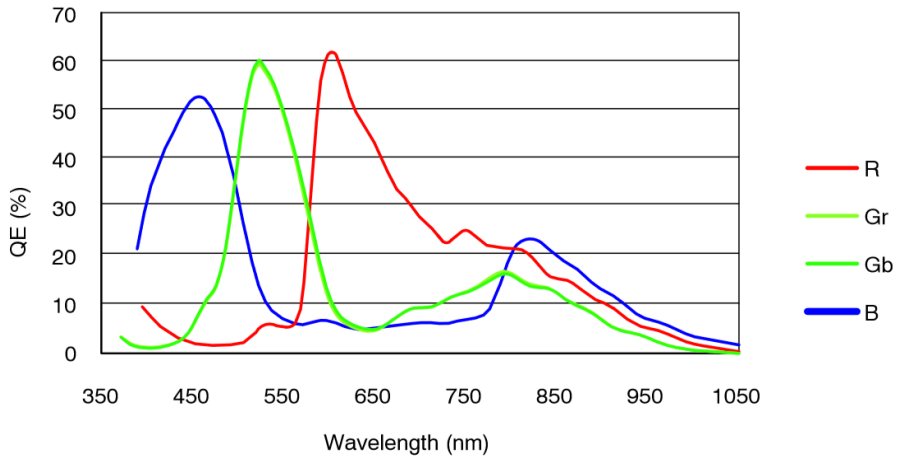

Figure 3.7 *Typical QE plot of a mobile image sensor. Sensor in question is ON Semiconductor's MT9P031 5 MP sensor. [51]*

Larger pixel count or smaller pixel size does not necessarily make sensor absolutely better in every scenario, though. Assume two 10 MP sensors, one of size 1/3 and another of 1/1.5 inch. Here the latter would naturally also have larger pixels. This then in turn means it can collect more light with same aperture and exposure time, since the area where photons are collected, the photosite, is physically larger. This carries to also less noise [13] and wider dynamic range [74] of the camera. The latter means, that details of the scene are not lost as easily in extreme lighting conditions. Smaller pixels are still wanted by imaging community, since it allows for more of them in smaller area, which then will help make the whole system smaller, since optics do not have to cover such large sensor area. It also allows smaller die size and spatial resolution. [74] Also especially in world of mobile imaging, where space within the cell phone itself is extremely limited, small size of everything is highly valued.

Pixel size also effects on so called well capacity. This nickname arises from a metafore, that each pixel is thought as a well or a bucket of sort and it can only store as many electrons in it as there is room for. Effectively what will happen, when well reaches its capacity, the pixel will saturate, meaning that, in an image, it turns white and loses its colour and radiance information. If well is filled up to its capacity and light still keeps coming in and thus well keeps filling up more and more, this can cause charge to flow to adjacent pixels. This phenomenon, called overflow, will cause image artifact known as bloom, also known as shader effect. This means light is spread over the edges of an object even when there is no light actually present in those places. Thus next to pixels or pixel columns are designed so called overflow drains to which excess charge can flow without effecting the neighbouring pixels. Principle of an overflow drain is presented in figure 3.8. Well capacity is also related to dynamic range, as dynamic range can be defined as full well divided by dark noise (noise level of a sensor in an environment, where there is no light). [35]

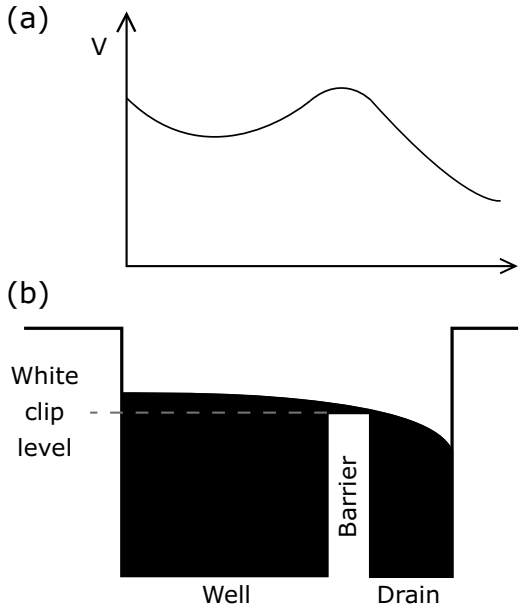

Figure 3.8 *Well, barrier and drain in a pixel presented as (a) a potential well and (b) figuratively. Based on [35, fig. 3-34, 3-35].*

The sensor surface is not made totally out of photosites, but there are also circuitry enabling them to function. This naturally means, that if light hits the circuitry, it is not collected by photosites, which decreases the efficiency of the sensor. Thus on top of Bayer filter lie microlenses. They are usually convex-plano lenses with diameter around tens of micrometers and their purpose is to concentrate light to photosites. [48] Of course, as microlenses are still only lenses, there are still some problems: if light is coming in large AoI to the microlens, this might cause the light to hit neighboring photosite instead of the site it is designed to. This phenomenon is called crosstalk.

When the light finally makes its way to the surface of the actual sensor, there are basically two possible models receiving it: in modern digital camera systems there are mainly used CCD (charge-coupled device) and CMOS (complementary metal-oxide semiconductor) sensors. The latter is so called active pixel sensor (APS) meaning, that the signal from photons is amplified in each pixel separately, when in passive pixel sensors (PPS), as CCD is, the only job of the pixel is to convert photons to electrons and amplification of the signal will happen later on down the image processing pipeline.

In the early days of digital imaging (in the 1960's and 70's) CCD sensor was the weapon of choice for the tech-savvy photo- and videographers as MOS-based (metal-oxide semiconductor) sensors were still not performing up to standards. As CMOSs used PPS technology until 1990's, their image quality was not up to the standards set by CCD sensors. Then it was noticed, that a CMOS APS would increase signal-to-noise ratio and sensor speed, it was widely adopted as a technology beside the CCDs. Both of them are still in use, but consumer products have steered strongly towards CMOS APSs due to their lower power consumption and fast data readout. Amplification in each pixel still has its downsides too: due to multiple amplification sites also noise levels of the signal rise and thus signal-to-noise ratio (SNR) decreases compared to passive pixel CCD sensors. [22]

Another major difference between CCD and CMOS APS is the way charge is read from them. In CCD sensor charge from pixels are collected in row-by-row or column-by-column manner and sent to capacitor and amplifier, where the charges are amplified to the degree the following devices in pipeline require. For CMOS APS the amplification is done straight away in the pixel and also each pixel has a capacitor in it. Then the charges are read parallel from each row, which makes the readout faster than that of a CCD.

There is also a difference on how the light is recorded to the sensor: CCDs collect the light at a single instant for the whole sensor area as they use global shutters. CMOSs on the other hand capture the scene row-by-row. Thus as for CCD the movement of an object is only seen at most as motion blur if it moves fast enough but for CMOS there occurs so called rolling shutter artifact. This seems as if the object is somehow warped for example from corner to corner. This is depicted in figure 3.9.

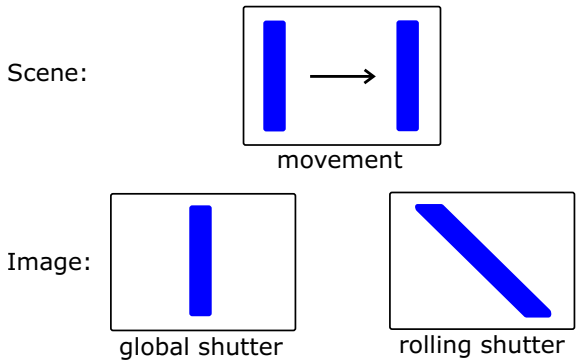

Figure 3.9 *Simplified rolling shutter artefact depicted and compared with global shutter movement capturing.*

The degree of rolling shutter artifact depends naturally on speed and nature of the movement and exposure time. For example rolling fan will show different kind of artifact than car driving by the photographer.

After being amplified and collected, charges from pixels are converted to digital form with analog-to-digital converter (ADC). ADC can nowadays be also integrated to CMOS APS to form digital pixel sensor (DPS), but this seems still to be a more at a study phase rather than utilized in mass production applications. Schematic of ADC is presented in figure 3.10.

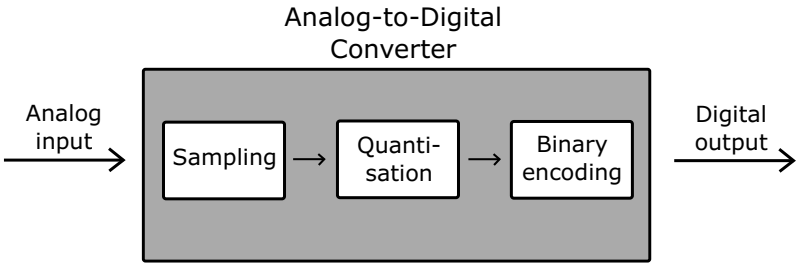

Figure 3.10 *Schematic of an analog-to-digital converter.*

This is the basic principle on which ADCs are based on: ADC takes some analog input signal and then it measures the interval of the signal at some sampling rate based on the resolution of the converter. Quantisation breaks continuous analog signal to discrete signal based on sampling and then signal is given binary value based on the difference of quantised signal and reference signal coming from ADC itself. [32], [36], [68]

In nowadays consumer imaging systems ADC is not actually part of the pixels, but already in the mid-1990's have been presented CMOS APSs with also ADCs is integrated to each pixel [27]. This kind of sensor is called digital pixel sensor, DPS. This is though an interesting research topic in the field and as the efforts for more and more integration

in field of technology are a massive trend, this might be something, that will be seen in consumer products in few years time.

3.5 Noise Sources in Imaging

In imaging noise can be described as unwanted fluctuation in brightness of pixels and it is not part of the scene itself. It can be divided into two categories based on its appearance in the image: random and pattern noise, former of which can be described with statistical processes, but for the latter this cannot be done.

First random noise types are discussed. They are caused by temporal fluctuations in imaging process, hence the group is often given a hypernym of temporal noise. In the imaging system there are plenty of phases at which some component of noise is added to the signal and it starts right at the moment when light hits the sensor. This noise component is so called shot noise and it has two sources: photons of light and dark current and they are related to the photosensitive nature of the sensor. First, photon shot noise (PSN), first discovered by Walter Schottky in 1918 [66], arises from temporal fluctuations in number of photons hitting each pixel at any given time period and thus it is a natural source of noise - and actually only one at that. [79]

For dark current there are three mechanisms of origin and all of them are associated with thermal creation of electrons: generation in depletion region of the semiconductor sensor, in neutral bulk material and generation due to surface states [35]. Dark current is essentially dependent on temperature of the sensor and it can be reduced significantly by proper cooling of the sensor. Vice versa, if cooling is neglected, dark current noise levels can rise considerably, which can then in turn cause notable problems in image quality. [79]

Shot noise is temporally random process and can thus be described mathematically with Poisson distribution. In Poisson statistics variation is equal to mean of signal and thus it can be written

$$\left\langle \mathcal{N}_{shot}^2 \right\rangle = \left\langle \mathcal{N}_{PS}^2 \right\rangle + \left\langle \mathcal{N}_{DC}^2 \right\rangle = \mathcal{N}_{PS} + \mathcal{N}_{DC}, \tag{3.6}$$

where $\mathcal{N}_{shot}$ is shot noise, $\mathcal{N}_{PS}$ photon shot noise and $\mathcal{N}_{DC}$ dark current noise.

Reset noise, as name implies, is related to resetting pixels before light hitting the sensor induces new electron creation. In resetting process there arise thermally induced charge fluctuations in pixels and reset noise decribes this uncertainty of charge that remains in a

pixel after resetting. Reset noise is often also called kTC noise, since variance of noise current, $\mathcal{I}_{reset}$ can be mathematically described with [11], [35]

$$\left\langle \mathcal{I}_{reset}^2 \right\rangle = k_B T C, \tag{3.7}$$

where C is capacitance of photodiode. Thus it can be seen, that reset noise has strong dependence on temperature of system, and hence sufficient cooling is important as it was also for dark current shot noise.

As current of the sensor if amplified, either at pixel as in CMOS APS's case or off the sensor as with CCD, this also creates noise. Amplification induces two kinds of noise: pink and white noise, former of which is also known as $\frac{1}{f}$ noise telling of its relationship with power spectral density of noise. The variance of noise voltage $U_{1/f}$ can be roughly estimated from [57], [79].

$$\left\langle U_{\frac{1}{f}}^2 \right\rangle = \frac{\mathcal{K}}{C_{ox} l w} \frac{1}{f}, \tag{3.8}$$

where $\mathcal{K}$ is process dependent constant, C_{ox} gate capacitance of transistor, l and w length and width of transistor and f noise frequency. White noise then is defined as uniform random noise having same intensity at different frequencies and hence constant spectral power.

In the interface of silicon substrate and oxide film there appear defect (energy) states to which electrons are randomly trapped and released causing $\frac{1}{f}$ noise. $\frac{1}{f}$ noise is usually bigger problem in CMOS APSs, where amplification happens on pixel. [57], [79] Also as it can be seen from equation 3.8, the noise can be reduced by increasing the size of a transistor and thus pixel. Also as noise originates from impurities and defects on the oxide-silicon interface, purity of the interface is also a determining factor in noise levels. During quantisation process in ADC continuous analog signal is converted to discrete digital signal. In this process arises so called quantisation noise due to imperfection of conversion. [35]

This covers temporal noises related to imaging sensors. As mentioned, there are also pattern noises, which form even visible lines or other patterns to the image. Patterns can form either on pixel-to-pixel bases in the dark or when light hits them their responses might differ. Former is called fixed-pattern noise (FPN) as it is spatially fixed as it relates to specific pixels and latter photo-response non-uniformity (PRNU). [35], [79]

FPN arises from manufacturing non-uniformities in transistor parameters and column circuitries. The former, as it is related to each pixel separately can be sampled away pretty efficiently during analog imaging process as latter needs to be compensated in image processing phase. For PRNU there are three parts in the system to factor in: Differences in microlens structure, which could lead to differences in illumination hitting each pixel and photon-electron and electron-voltage conversions can present variations and thus lead to non-uniformities. As it is hard to nominate effect of single cause to the total non-uniformity, the corrections are made as calibration of each individual pixel by using gain maps. [79]

Now the total system noise, $\mathcal{N}_{sys}$, of any system can be characterised as [35]

$$\left\langle \mathcal{N}_{sys} \right\rangle = \sqrt{\left\langle \mathcal{N}_1^2 \right\rangle + \cdots + \left\langle \mathcal{N}_m^2 \right\rangle}, \tag{3.9}$$

where $m \in \mathbb{N}$. Here is noted, that noise components are considered additive.

All of the aforementioned noise components add up to the total noise profile of a device. As it has now been noted, there are some effects related to illuminance and some that will take place regardless. Thus to keep track on the performance of an imaging device, a measure of seriousness of noise is needed - enter signal-to-noise ratio.

3.6 Signal-to-Noise Ratio

If the level of noise is so low compared to the actual signal, that it will not disturb the interpretation of an image at any level, the designer and manufacturers of the device at hand have made an outstanding job. On the other hand, if for example there is notable graininess in the image, there is a problem. The noisiness of an image is measured with signal-to-noise ratio (SNR or sometimes S/N), defined as relation of signal level and isolated noise of a signal. As temporal noise can be described with Poisson distribution, where standard deviation, σ_x, can be derived from the mean, μ_x, of the number of events, n_x, relation becomes [8]

$$\mathrm{SNR} = \frac{\mu_x}{\sigma_x} = \frac{n_x}{\sqrt{n_x}}, \tag{3.10}$$

Even if noise sources were non-temporal, SNR can still be calculated with statistical mean and standard deviation as presented above. There are also other ways of defining SNR (see for example refrence [35]), but definition presented here is used throughout this thesis as the way to calculate absolute measure of SNR.

However, as the dynamic range of a digital camera is fairly wide, it is common to report SNRs as decibels. Hence SNRs presented in this thesis are transformed from absolute to decibel form is done with following equation [47]:

$$\mathrm{SNR}_{dB} = 20 \log_{10}(\mathrm{SNR}). \tag{3.11}$$

For an actual image, SNR is often determined from some small region of interest (ROI), where signal is relatively uniform. Defining SNR from the whole image would be somewhat problematic, since the dynamic range of a typical image is sufficiently high. In a situation, where the dynamic range is fairly low, the calculation can be made from larger area or even from the whole image.

3.7 Image Signal Processing and Auto White Balance

Image signal processing (ISP) means exactly what it sounds: image signal is modified in different manners in order to produce eye-pleasing end result. ISP pipeline consists of plenty of different pieces: demoisaicing, auto focus, auto exposure, auto white balance, different corrections for lens system imperfections such as distortions and shading, denoising, filtering and more. In this thesis most of them are not going to be touched any further than this notion, but auto white balance (AWB) will be used later on so it will be explored further in this Section.

As an object is lit with illuminations of different colour temperature, the colour of the object will seem to change: for colder colour temperatures, object becomes redish and for higher it will seem bluish. Basic principle of AWB is to try to fix this discoloration by comparing colour channels of each pixel with one another, blue channels against blue channels and so forth, and then gain each channel in each pixel so, that the maximum values between different colour channels match with one another. This can be done either with colour channel amplifiers or digitally. [83]

As gaining is done in AWB process, this naturally increases both the actual signal and the noise coming with signal. As an example blue channel is considered: As mentioned in Subsection 2.4.4 short wavelengths have lower spectral powers and as lenses tend to absorb and reflect them more than longer wavelengths. This then results in less photoelectrons in blue channel compared to red and green ones. When considering noise the result from lower spectral power at the surface of the sensor is two-fold: the absolute measure of photon shot noise decreases, but noise components originating from sensor stay stable. Although, as photon shot noise is defined by Poisson statistics, this leads to decreasing SNR even though absolute noise is level is decreasing. Thus then when calculating it

for the whole noise profile, meaning combination of all noise sources, SNR is further decreased. Now as whole signal including full noise profile is amplified, SNR stays the same, but noise becomes much more prominent in absolute measure. This results in notable blue noise in final image, if denoising is not done properly.

4. RESEARCH METHODS

In Chapter 2 there were presented a wide range of different optical and physical properties of glass and polymer optical materials. Part of the reason, why research was done with so broad of a scope was to get good enough understanding of material properties and their differences and similarities to be able to determine further focus of the thesis. An order of magnitude analysis (not presented in this thesis) was conducted after sufficient amount of literature had been studied so the scope could be more precisely defined.

In the analysis it was noticed, that the biggest differences in material characteristics were present in thermal properties and transmittance in UV and IR regions. What comes to thermal differences, they were already fairly well understood within the thesis facilitator. Also to get a good understanding on the effects of the thermal property differences in optics, it would have been necessary to study and produce related optical designs. With these in mind it was decided, that it would not be the best interest of this thesis to focus on thermal properties. Hence the efforts were shifted towards studying transmittance differences and their effects especially in the UV region, since in most consumer applications IR radiation is gotten rid of with IR cut filter as it was mentioned in 3.3.

Other interesting topics would have been for example birefringence and its effects on for example depth data acquisition and water absorption and its effects on refractive index and strain it causes to lens coatings and the lens itself. As birefringence is also caused by strain, these two could somewhat overlap. Also long-term heating and its effects on material transmittance would have been an interesting topic of study, since it is tightly related to the subject matter of the thesis. However the correlation was found so late in the project, that it was no longer practical to incorporate it to the thesis as an experimental study. These three topics are something to study further down the line in more detail.

As it was pointed out in the end of Subsection 2.4.4, high transmittance in UV has potential to reduce blue noise in imaging, especially in low light scenarios. This postulation stands on following reasoning: As it was presented in figure 3.1, it is the case for most illuminants, that for shorter wavelenghts (< 450 nm) spectral power tends to decrease. Also as shown in figure 3.2, also reflectances of different colours tend to somewhat lack the blue end of the spectrum. When it is added to this, that as it is depicted in figures 5.1 and 2.15, also

in many optical materials, transmittance losses are greater at shorter wavelengths. Thus when performing AWB for image, blue channel needs to be boosted more than green and red channels to achieve correct perception of colours in the final image. As signal being amplified also contains noise, this noise is also amplified in the process resulting in more prominent blue noise than green or red ones.

As it was decided, that thermal properties would be merely studied on superficial level, Excel sheet calculations were decided to be an adequate tool for the job. Also some supporting MATLAB-calculations were carried out. The material for calculations was obtained from manufacturer data sheets and should thus be fairly reliable.

The emphasis of experimental part of this thesis was to study the effect of transmittance differences of different materials on noise levels in final image and it was decided, that simulation would be a befitting tool for quantitative studying of the phenomenon. The main argument in favor of simulation in this study is, that the variety of lens stacks, illumination sources and reflectances studied would be achieved with overwhelming ease compared to traditional measurement setup as all parameters could be modified according to needs as study progressed.

The data for noise simulation was obtained from couple of different sources: transmittance data were gotten from suppliers of optical materials, spectral responses of sensors from sensor manufacturers, illumination powers of different illuminants from CIE archives and reflectance spectra from archives of the thesis' facilitator. All the above sources can be seen as reliable and when examining the received data against other literature they held true.

To assist noise simulation further, dark noise level was measured. As far as the simulation goes, it only accounts for the photon induced noise, that is, photon shot noise. All other noise sources, originating from the sensor itself, were then measured to make the noise profile match better with real world situation.

4.1 Calculation of Thermal Defocus

As explained in Subsection 2.5.3 thermal defocus arises from two basic factors: change of refractive index with temperature and change of geometrical shape, that is, thermal expansion or contraction. Naturally change of focal length, as can be noted from equation 2.80 used to define focal change with temperature, is a function of focal length of the lens itself. Thus measurements of the lens were designed to match those of mobile lens designs, meaning curvatures ranging from around 2 mm to 8 mm and thickness of the lens in the middle of the it around 0.4 mm. As it already has been noted, the relative change

of focal length with temperature is actually indifferent of the actual focal length and thus of lens dimensions. This is noted in equation 2.81. In this thesis, both the relative and absolute results are be presented, since the absolute measure is important in analysis of the reliability of the lens system, especially in fixed-focus solutions.

Calculations were done for temperature range of 10 - 50 °C. This is fairly narrow of a range, but it was problematic to find accurate data for plastics reaching over these temperature limits. As both CTE and $\frac{dn}{dT}$ tend to increase as temperature rises and vice versa, if temperature gap was to be increased, the advantage of glasses would become even more prominent. If gap was widened from high temperature end, increase would be even greater than if the widening would be done from low temperature end.

As these calculations are fairly superficial, they do not depict any actual optical system design. Also the absolute results gotten from calculations fit only for one type of lens with certain properties and measures, whereas the relative results are indifferent of the lens shape. Nonetheless, the point of these calculations is merely to show, that there is a certain measure of thermal defocus taking place with different materials. Also understanding of the differences in material thermal properties is gained to help decision making in optical design phase.

4.2 Noise Simulation

Image noise simulation, as any simulation, is to correspond to the functions of natural world. General structure of the simulation is demonstrated in flow chart in figure 4.1. The simulation can be divided to three sectors based on where the different blocks would fall in an actual camera pipeline: what happens before sensor, on and after it.

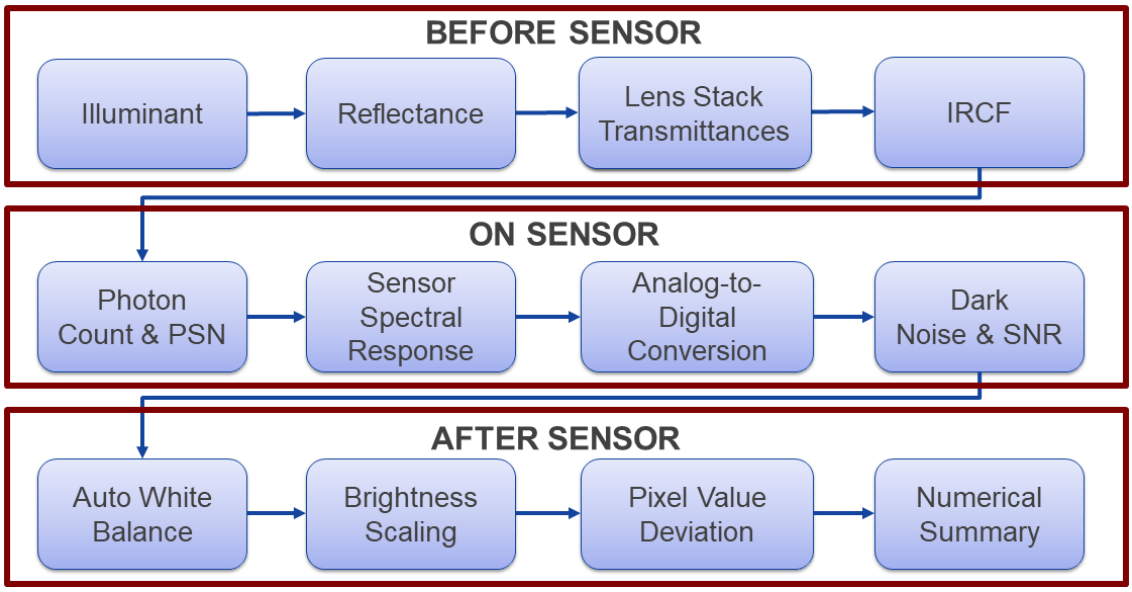

Figure 4.1 *Flow chart of noise simulation.*

Simulation follows the path of photons from illumination source to and through the lens system of a camera after which they reach the sensor. At sensor they are converted to electrons and later on voltage and to digital form. Different noise sources are taken account to at suitable positions. After digitalisation of the signal, it goes through very primitive ISP consisting only of AWB. Brightness scaling is also done to make visual noise comparison of images from different stacks easier as they would otherwise have different mean values and hence different brightnesses. In the end some mathematical analysis on image is done.

All components of the simulation need to be well defined and noise free for being able to isolate the effect of transmittance differences on noise. Hence for the surfaces from which the light is reflected, known reflectance specta from Gretag-Macbeth ColorChecker (figure 3.2 (a)) were chosen and illumination spectra were picked from CIE stardard illuminants. Reflectances could have also been chosen from multispectral images, but this would have complicated SNR calculations. This is related to defining region of interest of which the calculation would be done.

Image in the simulation is created as a matrix. For each pixel there are three values, one for each color channel. In principle in the simulation it is possible to include more color channels to the data, but as in MATLAB only three colour channel image has ready made functions to display it, the decision was made to stick with three channel model. As in the real world most imaging sensors display four different color channels, two of them being green, these two are averaged allowing again the use of MATLAB's ready made image displaying features.

As shown in the figure 4.1, light goes through three major damping factors between its emission from illuminant and its arrival to the surface of the sensor: it is reflected from surface after which it travels through lens stack and IR cut filter. Damping of the illumination spectral power is depicted in figure 4.2. In the figure there is not seen the effect of IR cut filter as in the simulation it is replaced with ideal fully transparent element, thus making spectral power identical to the lowest plot.

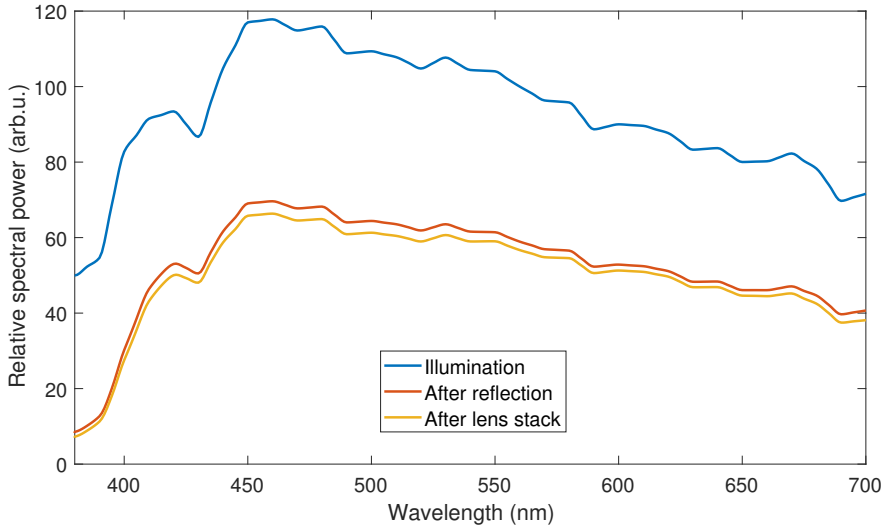

Figure 4.2 *Damping of spectral power from the illuminant through the reflection and lens stack to the sensor.*

In figure 4.2 there is used reflectance from neutral grey patch of Gretag-Macbeth ColorChecker (see figure 3.2) and lens stack of six 0.4 mm thick AR-coated lenses of EP-5000R, which is one of the studied plastic materials. Similar graphs were also used during simulation build up to visually check the correctness transmittance of modelling.

AR-coating's reflectance data was acquired via ready MATLAB function grabit.m [73]. With said function one sets points following a plot with known axes after which grabit.m saves them as number pairs or, in a way, coordinates. This way data set describing a plot is obtained. Similarly the data for ON Semiconductor's sensor was attained with grabit.m.

Naturally data acquisition with grabit.m brings some inaccuracy to the results. However, as both sensor and AR-coating data are used similarly for all lens materials and other variables, they will not affect very drastically to the comparison of materials, which is the main point of the thesis.

4.2.1 Modeling of Photon Shot Noise

The simulation itself does not include any fancy mathematical tools, since most of it is fairly straight forward matrix multiplication and addition. Main problem in constructing the simulation, was to be assured of the validity of the noise modeling.

As photon shot noise is temporal noise, it can be described with Poisson statistics with mean at zero. Thus when illumination power reaching the sensor is known exactly, it can be written that

$$\sqrt{\langle \mathcal{N}_{PS}^2 \rangle} = \sigma_{x,PS} = \sqrt{n_x}, \tag{4.1}$$

meaning, that standard deviation of PSN is equal to the square root of the number of photons hitting the sensor. As temporal noise is additive noise (truly random and does not depend on the state of the system) it can simply be added to the original signal. As mentioned PSN has mean of zero and standard deviation dependent on the original signal itself.

4.2.2 Measurement and Simulation of Dark Noise

Dark noise here stands for all sensor related inconsistency in the image, that occur when there is no light coming to the sensor. The measurement of dark noise was conducted in set up, where sensor was covered with thick fabric to block light from hitting the sensor. Then sets of images were captured with two different analog gain and exposure time settings to present well lit and low light scenarios, that is, respectively best and worst case scenarios in the noise point of view. Images were captured in room temperature without any cooling for the sensor. Thermal noise component should still be fairly constant as the sensor temperature was monitored and it appeared as being relatively stable, fluctuating around or less than $1°C$ of the mean temperature. On the other hand this represents a normal use case of a sensor, where it is being used in room temperature and hence its temperature can change a bit during its use, even when it is cooled down in the camera setup.

Image data gathered for the dark noise characterisation was of 10-bit form with artificial black level offset at 64, which then should be the expectation value, that is, mean of the measurement. Black level offset is done, since if black level was strictly zero, noise of sensor would inevitably result in also some negative values, which would be somewhat problematic from ISP point of view. Black level at zero would also result in distorting the noise profile of the signal as presented in figure 4.3.

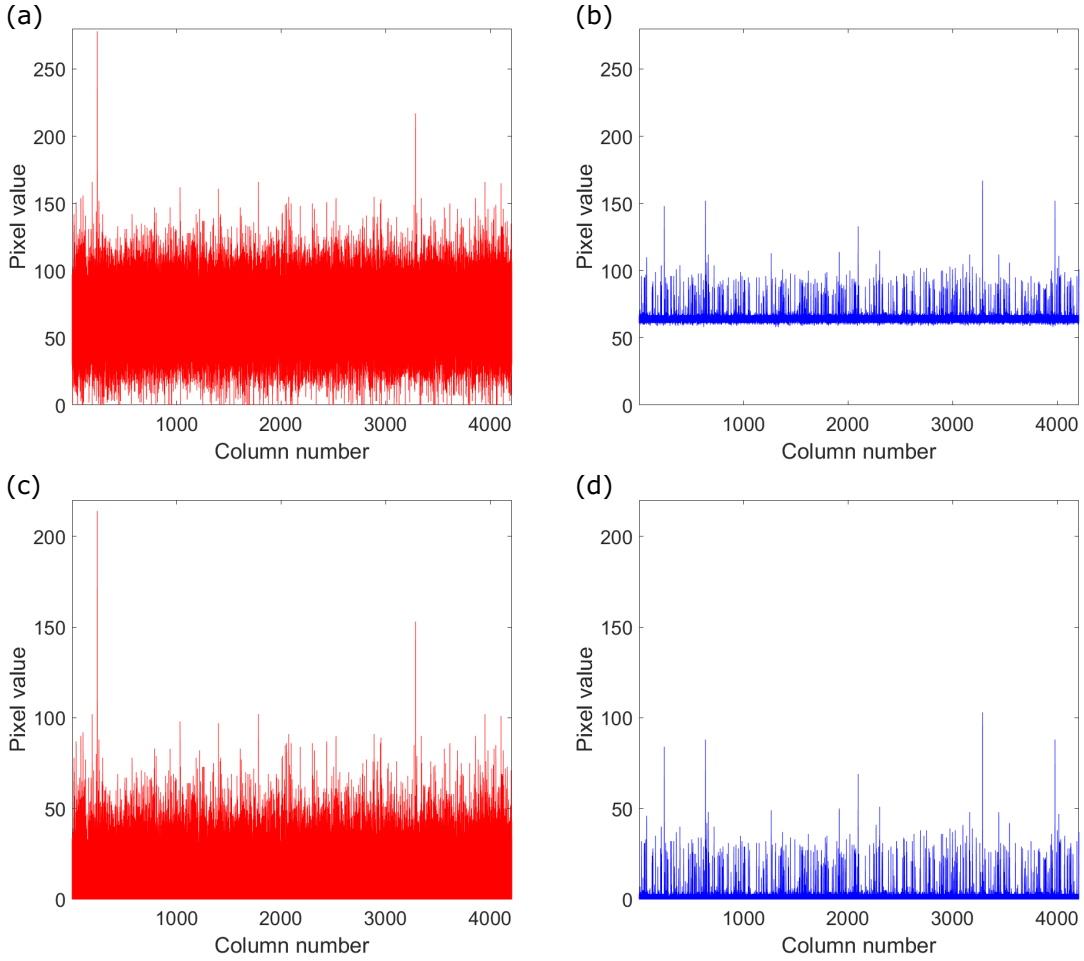

Figure 4.3 *(a), (b) When black level is intentionally set high enough above zero the whole noise profile can be measured. (c), (d) When black level is set at zero, part of noise profile of the sensor is lost. Images for (a) and (c) have been captured with 16x analog gain and 8.3 ms exposure time and for (b) and (d) with 1x gain and 30.3ms exposure.*

In the figure 4.3 in each subfigure there are presented all 13 128 960 pixels (3120 x 4208 pixel sensor) of one of the captured images per camera settings. Sensor used in experiment was Samsung S5K3M3SM24. First images were captured with 1x analog gain and 30.3 ms exposure time and 113 images were taken in total making the total sample size about 1.5 billion pixels. Second set of images had settings changed to 16x analog gain and 8.3 ms exposure time and total of only 100 images were captured. Still even this adds up to about 1.3 billion pixel sample size. What comes to the two different imaging settings, the first represents a low gain - medium exposure time situation and second then a high gain - short exposure time set up. This ends up to two different noise profiles, first representing a well lit and stable object and second a low light and maybe movement capture. Former of these is from final image quality point of view pretty much optimal situation and latter rather problematic.

In subfigures from second measurement (with short exposure time) it can be noticed, that there are very few spikes going way off from the otherwise pretty constant noise front. Then again in first setup (with longer exposure time) there are quite a bit more spikes that reach to higher pixel values than the other noise profile. Most probably these spikes in pixel values are not part of the noise profile but rather incoming photons, which means, that the measurement setup has not been completely dark as it should have been. On behalf of this proposition also speaks the fact, that in first set up exposure times were longer thus enabling more photons to hit the sensor.

When calculating mean values and standard deviations for both setups from all of the images captured, means came out as 63.8632 and 62.1841 and standard deviations as 0.3171 and 2.8538 for first and second set up, respectively. These results are fairly well in line with the set offset value of 64.

When comparing subfigures 4.3(a) and (b) it can be also noticed, that in (a) black level offset at 64 almost fully compensates for the maximum "negative" noise components. As in subfigure (b), offset of 64 seems as totally overdone and it could be decreased easily by around 50. This would widen the dynamic range of the image and thus allow for better details in low light.

In the simulation merely the statistical characteristics, that is, mean and standard deviation are being used to describe dark noise with the help of random number generator of MATLAB. As also black level correction was calculated from the images as mean value of the pixels, it has been taken into account by decreasing the dynamic range. This is also the case in an actual camera.

Combining the two noise sources, PSN and dark noise, is in the simulation is just a summation as they are additive. Hence in the end there is assigned a total noise value for each colour channel in each pixel forming the full noise profile for the image.

As it can be seen in images captured with low gain and long exposure time, the noise is relatively nonexistent. Hence as the simulation was run with these noise characteristics, only effects of PSN were notable. Thus in Section 5.3, where results of simulation are discussed, said results are obtained by using high gain and long exposure time dark noise measurements. This can be though either as photographic worst case scenario, what comes to lighting, or as presenting a low-end sensor performance found in cheaper end products. On the other hand the low levels of dark noise measured tell, that in high-end sensors the sensor-related noise performance is, in good imaging conditions, excellent.

4.2.3 Limitations of the Simulation

The purpose of a simulation is to represent real world as accurately as possible, within reason. As anyone, who has studied science, knows, there will inevitably be some uncertainty and inaccuracy in simulations as no scientific model is perfect. Also as mostly in real life, time and resources to perfect a simulation is limited. Hence some approximations and simplifications need to take place. In this thesis, these approximations can be somewhat divided into two categories depending on whether they effect the modelling of the sensor or the optical path of light.

As an observant reader might have noticed in the beginning of this section, there was mentioned, that each pixel in the simulation holds values for all three colour channel. However, when looking at figure 3.6, one can detect, that in actual sensors using Bayer filters, only one colour filter is placed on one pixel. In real life this results in mosaicing, which needs to be handled in ISP. Part of the purpose of this simulation was to display visual effects on noise, that different transmittances might have. There might have been some minor differences as how the image would look like, if mosaicing and demoisaicing were present. Numerical results though should remain intact, since they were calculated for each channel separately. Also as the areas of channels were equal in size and hence the amount of incoming photons is the same for every channel, without taking into account PSN. Also in real sensor some of the surface area is occupied by metal wiring used to transfer charge created in photosites. This mostly effects on the efficiency of the sensor and hence does not effect the results significantly.

As it was discussed in Section 3.4, each pixel has so called full well capacity, that effects on dynamic range of the sensor. In real life if well is filled to saturation, it might leak some of the photoelectrons to its neighbouring pixels resulting in blooming effect. This effect is called electronic crosstalk to distinguish it from optical crosstalk, which will be discussed later in this Subsection. In this simulation no crosstalk whatsoever is modelled, and what comes to saturation of pixels, this simulation only cuts off the excess photons. This means, that pixel that is right at saturation limit does not seem different than one, that is "more" saturated.

Also different noise sources could have been modelled one by one, for more accurate noise profile, but this would not probably have very big of a difference in results, as all temporal noise components are taken into account with dark noise measurement and PSN modelling. Of course, as measurement was conducted in certain conditions, this dark noise level only applies to these conditions limiting the use cases of the simulation or on the other hand lowering the accuracy of it in different environments. Also in the simulation stable temperature was assumed.

When examining the optics pipeline, it is inevitably clear, that simulation does not consider any actual optical design, but rather just bunch of uniform lenses stacked on top of one another. All of the lenses are considered being of equal thickness and all of them being of the same glass or polymer material. This presents multiple issues comparing to real cameras.

The one maybe most related to optical design is that dispersion of light in optical materials tends to increase non-linearly when wavelengths get shorter as depicted in figure 4.4. In the figure dispersion graphs of studied materials are presented, with the exception of Zeonex material, which has been changed from K26R to novel T62R due to lack of dispersion data for K26R. Material properties are otherwise very similar between the two, so the change is hence well justified in this case. This dispersion property presents a design issue at least with flint materials and hence this might reduce usability of some materials in some lens designs and applications.

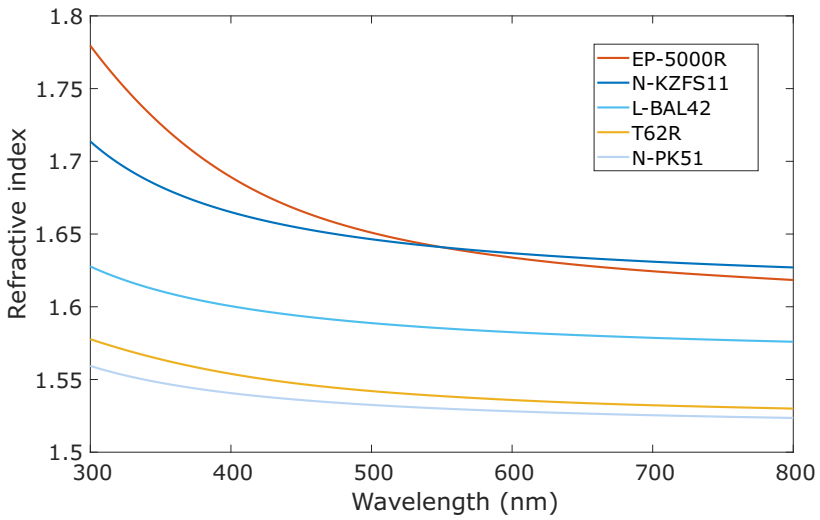

Figure 4.4 *Dispersion graphs of studied materials. Zeonex K26R has been replaced with T62R due to lack of former's dispersion data.*

Simulation assumes, that light is coming to the lens stack at normal angle and this is the direction at which all reflectances (and hence tranmittances) are calculated. As reflections actually happen at every lens-air interface and from non-ideal black parts of the lens barrel, reflected rays would be left bouncing around in the barrel. This leads to them arriving to the sensor to random places from uncontrollable directions hence interfering with ideal image formation. Also absorption of light in lenses would be slightly increased, if AoI was anything but zero, as light would travel longer distance inside the lens. Non-zero AoI also decreases performance of AR-coatings as discussed in Section 3.3.

Changing AoIs also have effect on how light refracts or reflects from microlenses on the

surface of colour filters of a sensor. For large AoIs in some regions of the sensor, usually near the edges, light might get refracted to totally different photosite as it was supposed to. This leads to activation of wrong "coloured" pixel and thus distorts the colour of the image in that region. This phenomenon is now called optical crosstalk. Neither microlenses nor optical crosstalk is modelled in this simulation.

Light is modelled hitting the sensor uniformly to each pixel. In real world though, the edges of sensor are usually more poorly illuminated than the center and hence the image might seem somewhat darker on the edges.

IR cut filter is modelled as a box filter, meaning 100 $\%$ of light passes it before 700 nm mark, where it cuts everything off. Normally IR cut filters are made of thin glass, and thus reflect some light. Also the cut off is not totally sharp and depending on application, cut off might happen as early as in 650 nm. For these uncertainties it was left as more of a "place holder" for actual IR cut filter data to take its place in later versions of simulation.

As simulation presumes lens stack ideal, it assumes no aberrations discussed in Section 2.5. Although they are not that important in relation to investigating the effects of transmittance differences and their consequences, it would be good idea to include them in more comprehensive version of sensor simulation. One reason pleading for this is for example curviness of the focal plane resulting from multiple lenses and their different aberration corrections will locally effect on sharpness of focus.

5. RESULTS

The main goal of the thesis was to develop a broad understanding on the similarities and differences of optical grade plastics and glasses as materials: what are their strengths and limitations with respect to different applications. As is was described in the beginning of Chapter 4, based on order of magnitude analysis, studying of thermal defocus and effects of short wavelength transmittance differences were decided as the main objectives of this thesis. In this Chapter the obtained results are presented.

The glass materials studied in this thesis are Ohara's L-BAL42 [49] and Schott's N-PK51 [61]. Plastic materials then are Zeon's Zeonex K26R cyclo olefin polymer [85], Mitsubishi Gas Chemical Company's Iupizeta EP-5000R polycarbonate [16], [17] and N-KZFS11 [61]. Some key values for these materials are presented in table 5.1. Materials have been decided so, that first the plastic has been chosen and then the glasses have been matched for similar refractive indices: Zeonex has been chosen as a bench mark and top level optical polymer and Iupizeta as a commonly used one. From glasses it can be said, that out of the three L-BAL42 is most widely used in optics and all three are suitable for precision molding. Also Zeonex, N-PK51 and L-BAL42 can be counted as a crown materials and Iupizeta and N-KZFS11 as flint. Relevant thermal properties and optical characteristics are presented in table 5.1

Table 5.1 *Optical and thermal properties of compared materials. Upper part of table consists of crown materias and lower part of flint materials.*

Material	n	V_d	CTE ($10^{-6}/°C$)	dn/dT ($10^{-6}/°C$)
Zeonex K26R	1.535	56	60	-130
N-PK51	1.529	77	12	-7.7
L-BAL42	1.583	60	7.2	4.6
Iupizeta EP-5000R	1.635	24	66	-120
N-KZFS11	1.638	42	6.6	4.2

What needs to be accounted for these materials and when comparing transmittances is, that it is customary for glass manufacturers to give transmittances as internal transmittances

and on the other hand polymer manufacturers as total transmittances. Thus here total transmittances have been converted to internal transmittances with equation 2.71. This makes glasses and plastics fairly comparable, as Schott AG uses this formula to transfer their measurement results of total transmittance to internal trasmittances for their brochures [65]. Total transmittances of materials studied have been presented in figure 5.1.

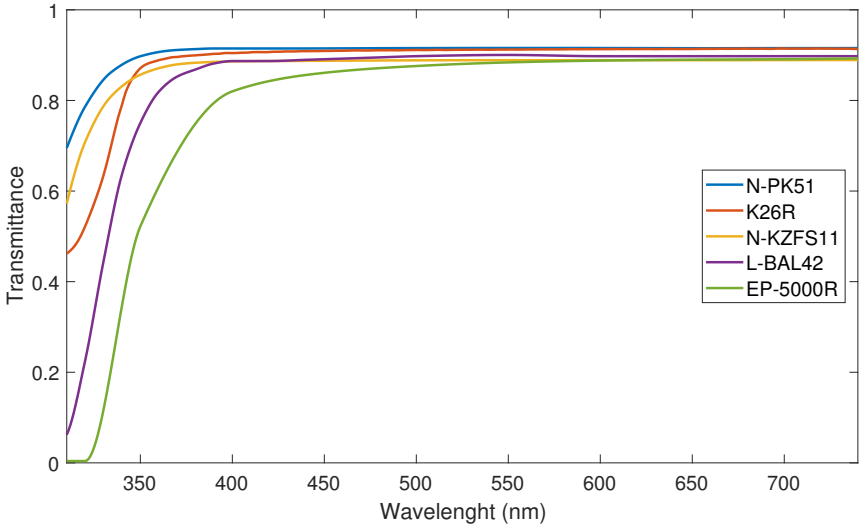

Figure 5.1 *Total transmittances of studied materials at 3 mm sample thickness.*

Transmittances were also originally given for different thicknesses ranging from 1 to 10mm depending on the material. All transmittances were hence recalculated for 3 mm thickness, as this was the thickness of studied plastic materials given by manufacturers, by using Beer-Lambert law (equation 2.72).

5.1 Thermal Defocus

Thermal focal change was, already based on literature, expected to be more prominent in plastic materials. Same result was found in the calculations of this thesis as presented in figure 5.2. In calculations equations 2.80 for absolute and 2.81 for relative thermal defocus were used.

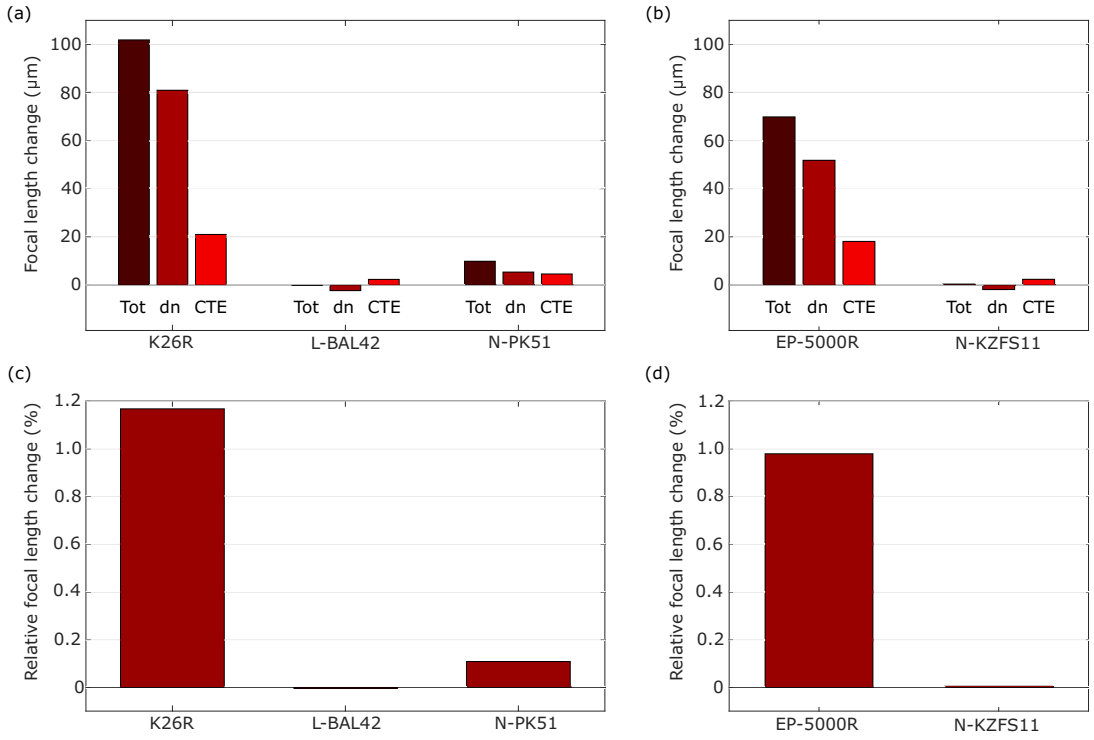

Figure 5.2 *Focal length changes of studied materials. In (a) and (c) there are compared crown materials and in (b) and (d) flint ones. In (a) and (b) there are represented the absolute focal length changes and their factors and in (c) and (d) relative total focal length changes with temperature change from 10 to 50 °C.*

Figure 5.2 tells common story with optical materials: thermal stability of glass is far superior compared to that of any optical polymer. In imaging solutions having autofocus function, this might not be that fatal of a flaw, but with fixed focus solutions, this needs to be accounted for very carefully in optical design. Lens specifications for calculations were following: $T_i = 10$°C and $T_f = 50$°C, thickness = 0.4 mm, and radii of curvature $R_1 = 3$ mm and $R_2 = 8$ mm resulting to 8-9 mm focal lengths for crown and 7-7.5 mm for flint materials.

Absolute focal length changes (figures 5.2 (a) and (b)) are related to lens dimensions, but as already discussed in 2.5.3, relative changes are indifferent to lens dimensions. Thus from the figure it can be seen, that for studied polymer materials thermal focal length change in this temperature range is around 1 % and for studied glasses it fluctuates in between 0 and 0.1 %.

It was mentioned in Subsection 2.3.1, that mostly in glasses the effects of thermal change in refractive index and thermal expansion work to opposite directions and for plastics to same directions in forming the thermal defocus. For studied plastics this seems to hold true as shown in figure 5.2. For glasses then, one exception is seen in Schott N-PK51,

where both factors have effect in the same direction. When some other glasses were studied it was noticed, that this is not totally uncommon, but it happens from time to time. Still it seems, that even in these scenarios, glasses are about 10 times less sensitive to temperature changes in what comes to their focal length change with 10 - 50 °C range. Most stable glasses, as Ohara's L-BAL42, they are effectively not influenced at all by thermal changes in their environments making them optimal for wide temperature range, such as automotive, or fixed focus applications.

5.2 Short Wavelength Transmittance

In figure 5.1 is shown, that depending on the material, transmittances start to decline when moving to shorter wavelengths starting as early as around 550 nm for EP-5000R and then somewhere between 350 and 390 nm for the other materials. Most of this lower transmittance can be attributed to increased absorption and scattering in materials in UV-region as discussed in Subsections 2.2.1 and 2.3.1. As absorption is exponentially dependent on distance travelled in material as shown by Beer-Lambert law (equation 2.72), transmittance in short wavelengths improves drastically when thickness of a lens is decreased from 3mm to more portable 0.4mm. Also with good AR-coatings interface reflection losses can be minimized as shown in figure 3.3. These transmittances are presented in figure 5.3.

Transmittances have been calculated so, that first internal transmittances have been calculated for right thickness by using modified Beer-Lambert law for two thicknesses in equation 2.73 and then losses after AR-coating on both sides have been subtracted from the transmittance. AR-coating used for calculations is Edmund Optics' VIS-EXT also presented in figure 3.3.

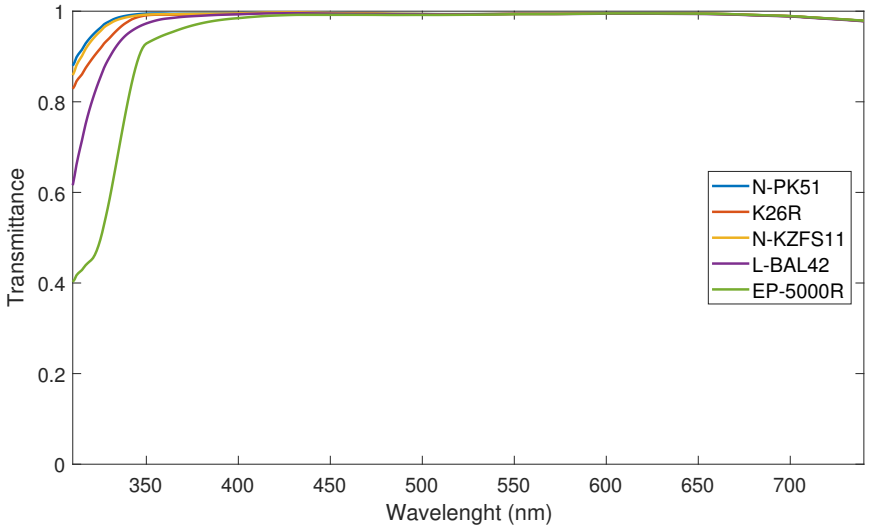

Figure 5.3 *Transmittances of studied materials with AR-coating at 0.4 mm thickness.*

As it is presented in figure 3.3, VIS-EXT is usually applied on Schott N-BK7 glass substrate. Hence it might not be, as is, optimally suitable for here studied materials, but it still gives a good benchmark on how well optimized AR-coatings could work with these materials. However it seems, that in reality broad band AR-coatings for plastics substrates might not be as good as the ones made for glass substrates. Hence, what comes to AR-coatings, in this thesis is presented the best case scenario for polymers. [2], [21]

There are quite many different possible combinations on how, with these five materials alone, one could build a lens stack. As full glass stacks are still a bit far fetched idea, at least in mobile cameras in which the focus will now be, willingly pairing two glass materials is here avoided. However, full glass stacks will appear in comparisons between full plastic and hybrid stacks, but there only one glass material is used for simplicity's sake. In figure 5.4 are presented transmittances for crown materials with high transparency paired with EP-5000R: there are two different plastic-glass pairs, EP-5000R–L-BAL42 ((a)-(b)) and EP-5000R–N-PK51 ((c)-(d)) and for comparison also EP-5000R–K26R plastic-plastic pair ((e)-(f)). In subfigures (a), (c) and (e) are presented transmittances and in (b), (d) and (f) the comparison with stack, that have different amount of glass in them (or K26R acting as "glass" in last three subfigures). Illuminant used for these results is D65 CIE standard illuminant corresponding sun light. The lens stacks have been identified so, that the number of glass lenses stands before letter G and for plastics then in front of P. As K26R is, in a way, replacing glass elements, the number of such elements stands also in front of G.

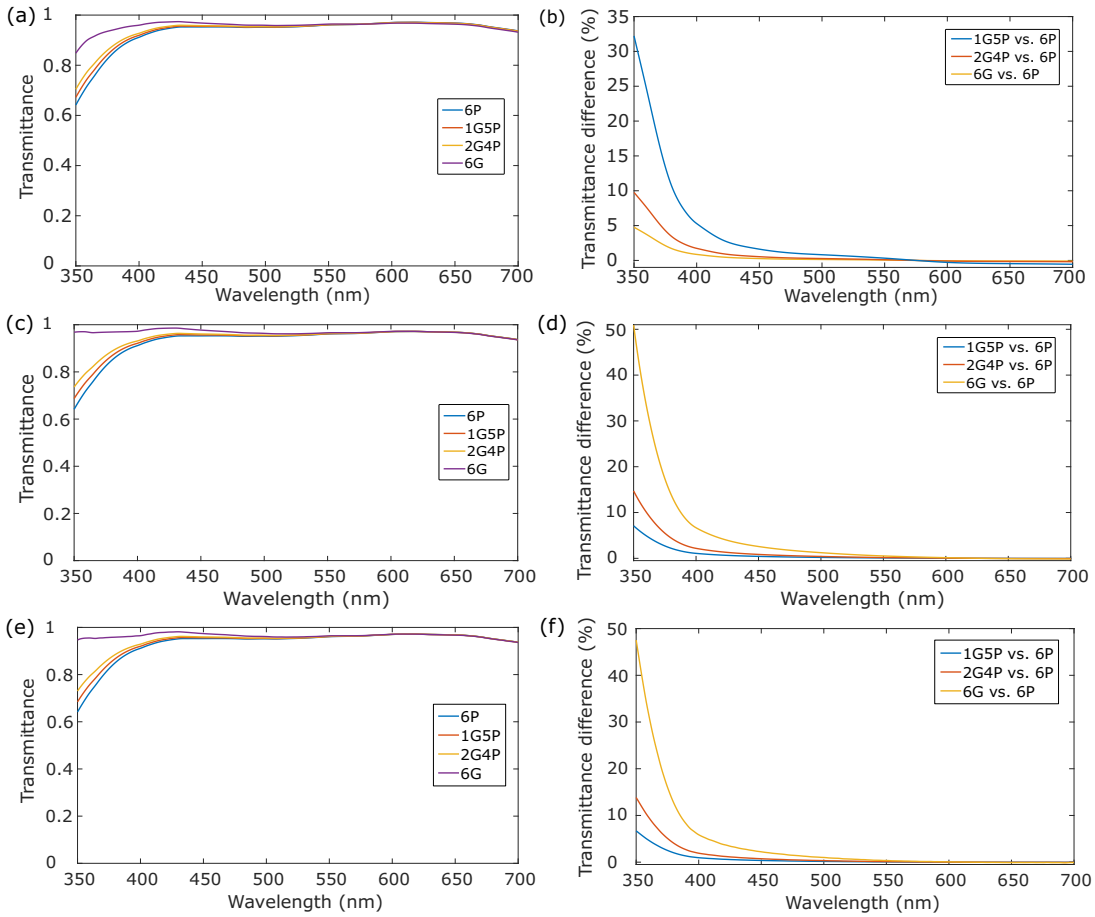

Figure 5.4 *Transmittances of different crown high transparency material containing lens stacks and how they compare with each other. In (a)-(b) are presented material pair EP-5000R – L-BAL42, in (c)-(d) EP-5000R – N-PK51 and in (e)-(f) EP-5000R – K26R.*

From all three different combinations, there is a more or less notable difference in stack transmittances and as expected, the difference is greater the shorter the wavelengths get in the considered band.

For flint glass materials similar results are presented in figure 5.5. In subfigures (a)-(b) are presented material pair N-KZFS11 – EP-5000R and in (c)-(d) N-KZFS11 – K26R. Actually pairing two flint materials as in (a)-(b) would not make that much sense, but here the purpose of EP-5000R is to mimic widely used crown polymer, Mitsui Chemicals' APL5014CL [46], which has very similar transmittance qualities to those of EP-5000R. Thus these results give a good approximation on the how a real pairing could behave. Here an observant reader might think, why then APL5014CL's own transmittance properties are not being used. For this relevant and important question, the answer is, that accurate and original data was neither found online or gotten from manufacturer. Also, in subfigures (c) and (d) it is good to note the differing y-axis ticks from other result plots.

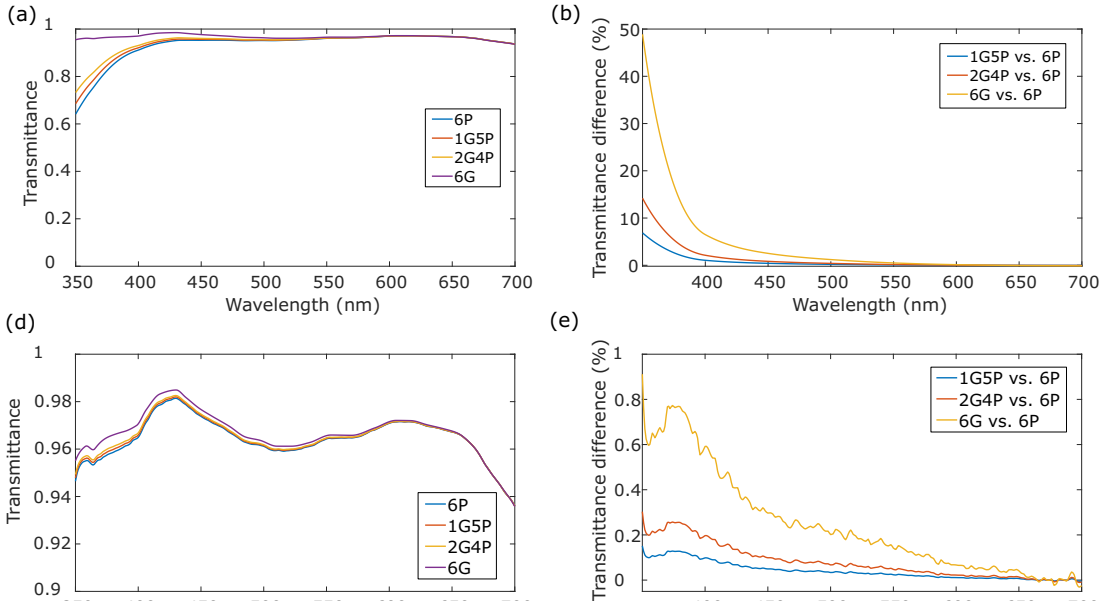

Figure 5.5 *Transmittances of different flint glass containing lens stacks and how they compare with each other. In (a) is presented material pair N-KZFS11 – EP-5000R and in (c) N-KZFS11 – K26R.*

Numerical transmittance results from both crown and flint materials have been gathered to the table 5.2. In upper part of the table are presented the results of crown materials and in lower part flint ones.

Table 5.2 *Transmittance differences, $\Delta\mathcal{T}$, between different lens stack structures at 380 nm and mean differences over visible (VIS) light band (380-700 nm).*

Lens materials	Lens structures	$\Delta\mathcal{T}$ @380nm (%)	$\overline{\Delta\mathcal{T}}$ over VIS (%)
EP-5000R – L-BAL42	1G5P vs. 6P	1.7	0.2
	2G4P vs. 6P	3.4	0.4
	6G vs. 6P	10.7	1.1
EP-5000R – N-PK51	1G5P vs. 6P	2.2	0.3
	2G4P vs. 6P	4.4	0.6
	6G vs. 6P	13.9	1.7
EP-5000R – K26R	1G5P vs. 6P	2.0	0.2
	2G4P vs. 6P	4.1	0.5
	6G vs. 6P	12.7	1.5
N-KZFS11 – EP-5000R	1G5P vs. 6P	2.1	0.3
	2G4P vs. 6P	4.3	0.6
	6G vs. 6P	13.6	1.7
N-KZFS11 – K26R	1G5P vs. 6P	0.13	0.03
	2G4P vs. 6P	0.26	0.07
	6G vs. 6P	0.77	0.20

Spectral power is related to number of photons with equation 3.2. Also the sensor pixels expressly detect the photons and not so much their energies, and also PSN is correlated with variance in photon count over time. Hence in figure 5.6 are presented, for different lens stack combinations, the number of photons for one nanometer wavelength band arriving to the surface of the sensor. Absolute results are presented in (a), (c) and (e) and then relative differences in photon counts in (b), (d) and (f). Results are presented for three illuminants: in (a)-(b) are shown results for A, in (c)-(d) D65 and in (e)-(f) F2 illuminant. As other parameters go, spectral reflectance of Gretag Macbeth's neutral grey patch was used and the material pair in question was EP-5000R – N-PK51.

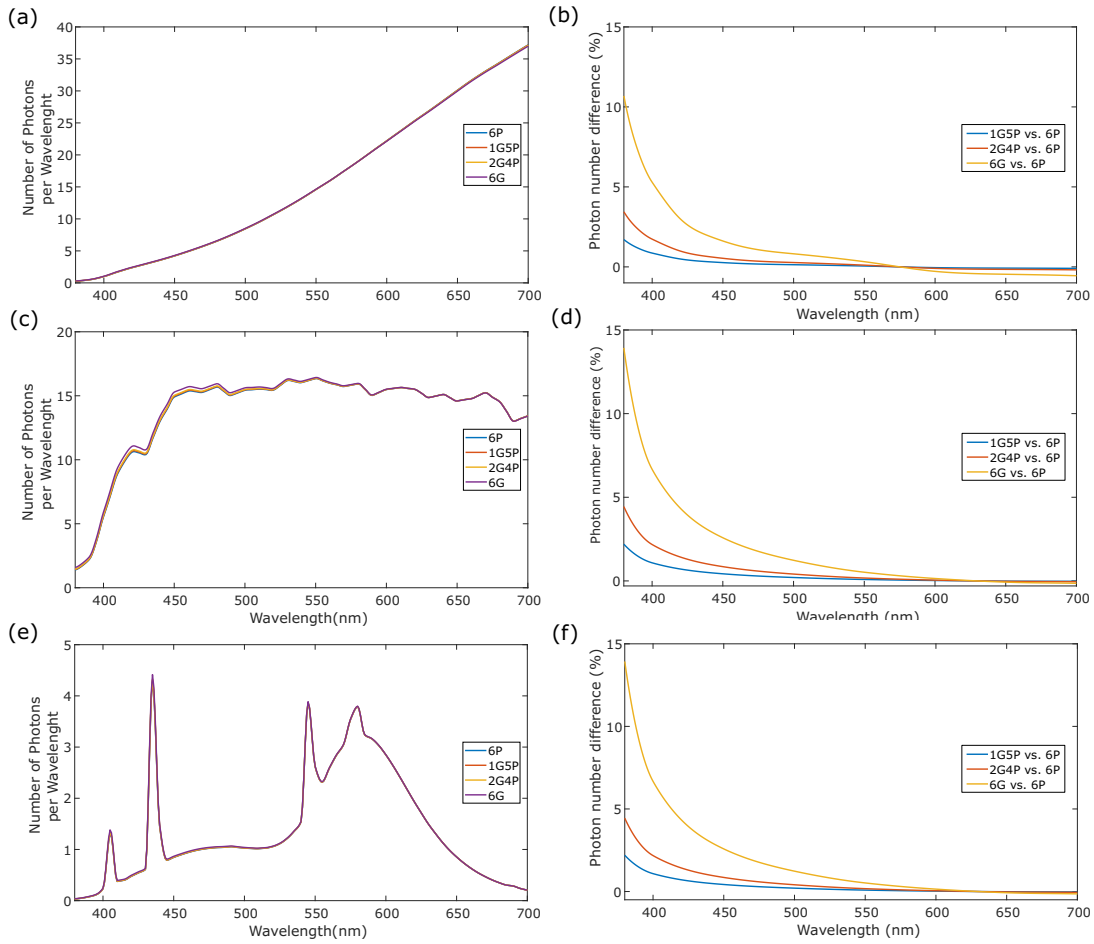

Figure 5.6 *Photon counts for different CIE illuminants at the sensor surface after six lens EP-5000R – N-PK51 lens stack. In (a)-(b) are presented A illuminant, (c)-(d) D65 and in (e)-(f) F2. (a), (c) and (e) represent the absolute number of photons per one nanometer wavelength band and (b), (d) and (f) the comparison of these photon counts between different lens stack structures.*

From absolute results it can be seen, that photon counts overlap very strongly for all illuminants and lens stack combinations. Still some minor differences can be seen in relative results: D65 and F2 illuminants yield almost identical relative photon count results and A illuminant seems to lead to smallest advantage for glass. It actually turns out, when comparing relative results with figure 5.4 (d), where relative spectral power differences of EP-5000R – N-PK51 material pair was compared under D65 illuminant, that relative results achieved here under D65 illuminant (subfigure (d) here) yield exactly the same outcome. This can be mathematically established by calculating relative photon number count from equation 3.2 as follows:

$$\frac{n_{x,j} - n_{x,i}}{n_{x,i}} = \frac{\Phi_{E,j} - \Phi_{E_i}}{\Phi_{E_i}}. \tag{5.1}$$

Hence results presented here can be thought as appendices to the ones displayed in figures

5.4 and 5.5. Thus greatest differences between glass and plastic materials arise with D65 and F2 illuminants. However, it must be noted, that D65 presents throughout the spectrum more than three times as many photons hitting the pixels as F2. Hence according to definition of SNR in equation 3.10 this should yield to higher SNR, based on PSN alone, with D65 compared to F2 illuminant.

How do these differences in transmittance and photon count then translate to final image then? In figure 5.7 are presented Gretag-Macbeth checker's (a) blue and (b) neutral grey patch appearance differences between 6P and 6G stacks made of EP-5000R and N-PK51 without noise. There are also shown how the patch would look like without lenses to give raise to any transmittance losses. The material pair was chosen, since it presents the greatest transmittance differences, so there would be the best chance to see visual differences resulting from different transmittances. Illuminant used was CIE D65 with spectral power corresponding to 800 digital units.

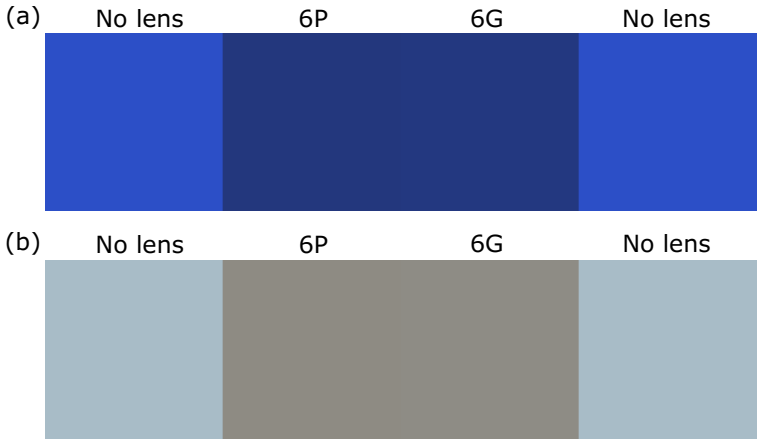

Figure 5.7 *Gretag-Machbeth ColorChecker's (a) blue and (b) grey patches seen with and without AR-coated lenses. On the both edges there are presented how the colour would look like without lenses under D65 illuminant and in the middle is the brightness comparison between AR-coated 6P and 6G lenses. Lens materials used were EP-5000R as plastic and L-BAL42 as glass.*

Between 6P and 6G stacks there is only slight, but still visible (at least on a bright computer screen), difference in blue and grey patch appearance. As neither the numerical results do present that big of a difference between the two stacks, lack of visual distinguishability is expexted.

Interestingly in subfigure (b) the grey patch does not seem that grey without the lenses. This is most certainly due to the uneven spectral power distribution of the used D65 illuminant as seen in figure 3.1.

Then again, one might wonder if AR coatings were to be removed altogether, what would

happen to the results. In figure 5.8 are presented the blue patches through stacks made of non-AR-coated EP-5000R and AR-coated L-BAL42.

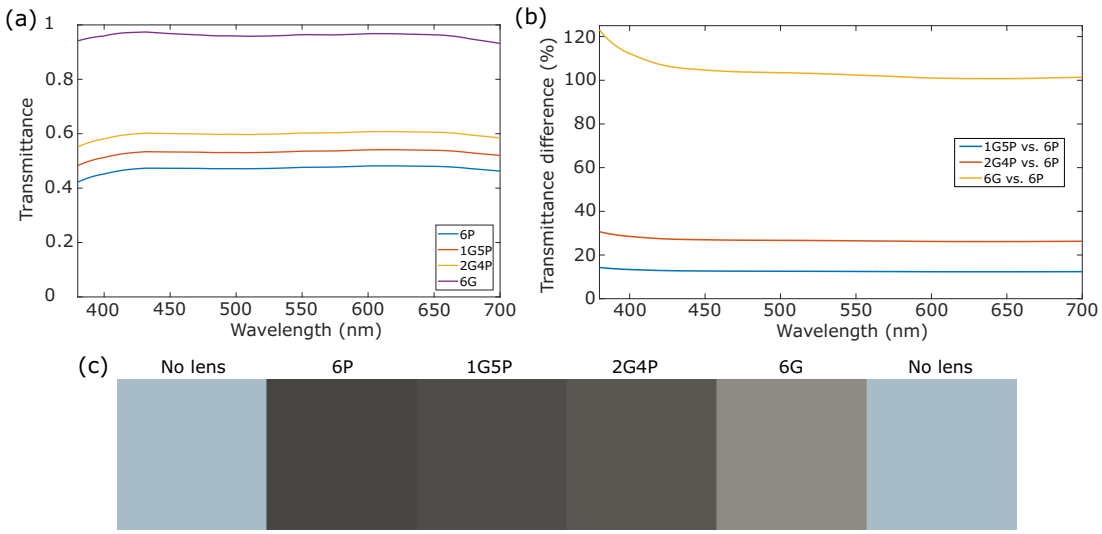

Figure 5.8 *Lens stack (a) transmittances, (b) comparisons against 6P stack and (c) Gretag-Macbeth neutral grey patch as seen through different lens stack structures and without lenses on the edges. Plastic lenses used for these calculations are not AR-coated, but glass lenses are.*

In figure 5.8 already with one lens plastic-to-glass replacement there is possible to see very visible result in the shade of grey. Thus an important take away here is, that well done AR-coating has a great importance in lens stack transmittance. Without a proper coating the cumulative 8-10 % per lens transmittance loss adds up so much, that even half of the original illumination can get cut off. This is especially important to keep in mind, since the AR-coatings of polymers might not perform as well as ones for glasses as pointed out earlier in this Section.

5.3 Noise

The core premise of the experimental part of this thesis was, that interchanging plastic and glass parts in a lens stack could have an effect on the noisiness of the final image. Especially of the blue channel was considered interesting as the largest differences in transmittance were seen in short wavelength regions. In this Section are presented some visual and numerical results for different lighting conditions, with respect to both illuminants and illumination levels, and lens stack structures.

Illumination level refers to relative illumination power, which has been scaled to match 10-bit digital data form. This means that 1024 is the maximum illumination value of a pixel, thus making it the saturation level. This maximum value can be, in the simulation,

surpassed though with enough noise, but those pixels still saturate, so there is no visual difference between them.

As mentioned in Section 3.4, digital values are created in ADC from charge coming the pixel. In nowadays pixels full well capacity is somewhere around 8000 charge carriers per 1 μm^2 of pixel area. Thus, if a 1.25 μm^2 pixel is considered, in ADC a conversion of roughly 10 charge carriers to one data unit is carried out. This conversion is done for all of the charge received from the pixel giving the pixel its digital 10-bit value. Thus, when there is more light and hence more charge carriers are created in a pixel, the higher the digital value also becomes.

In this simulation noise properties are studied in three different lighting conditions. Good lighting is represented by digital value of 800, mediocre lighting by 500 and poor lighting conditions by 50 digital units.

In this simulation scaling from charge carrier number to digital values is done so, that pixels getting the most light reach the set value, for example 800, and others, without noise, will settle to some lower value depe. Scalon the amount of light receiveding inding s also done between lens stacks so, that the stack transmitting most will reach the set maximum illumination value and others are scaled downwards accordingly.

Lens structures are all comprised of six individual lenses, which can be made either of glass or plastic. Number of glass lenses is marked with G and plastic lenses then with P: for example, 2G4P lens stack would have two lenses made of glass and four of plastic. Six lenses were chosen as total number as it is the number of lenses used nowadays in most high-end mobile cameras.

In the simulation ON Semiconductor's MT9P031-D 5MP CMOS digital imaging sensor's spectral response was used, so other sensors would lead to different results. Also dark (sensor-generated) noise was measured from Samsung S5K3M3SM24 sensor, so the results do not depict any particular sensor per se, but are rather a result of combining properties of two different sensors. Naturally optimal scenario would have been to take both characteristics from one sensor, but this was not managed to obtain. As object reflectance Gretag-Macbeth ColorChecker's neutral grey patch was used.

Results have been aquired by using a generated flat coloured 0.64 MP image in calculations meaning, that each pixel coloured the same without noise. Image size was chosen as is, since SNR results could be repeated with three decimal points meaning, that statistical fluctuations in noise were effectively cancelled out with adequate number of generated data points. As the numerical results are relatively vast, here are only presented some selected parts of them and they are fully visible in appendix A.

In the tables 5.3 and 5.4 are presented results for two of the lens stacks, full glass (6G) and full plastic (6P), made of material pair L-BAL42 – EP-5000R. As mentioned, these are a pair of often used moldable glasses and plastics. In table 5.3 are presented the SNR results of both lens stacks and in 5.4 these results are compared between stacks.

Table 5.3 *SNRs obtained from the simulation for different lighting conditions and lens stack structures. Materials used are L-BAL42 (G) and EP-5000R (P) and results are shown for blue (B), green (G) and red (R) channels.*

Illuminant	Relative illumination power (*arb.u.*)	SNRs					
		6P			6G		
		B	G	R	B	G	R
A	800	36.303	39.938	44.307	36.340	39.946	44.296
	400	31.632	35.542	40.301	31.672	35.552	40.288
	50	14.952	19.204	24.491	14.997	19.215	24.476
D65	800	42.755	43.163	43.293	42.837	43.196	43.294
	400	39.052	39.503	39.648	39.143	39.529	39.647
	50	23.694	24.214	24.382	23.799	24.244	24.379
F2	800	35.541	37.403	37.516	35.549	37.416	37.522
	400	33.233	35.325	35.453	33.309	35.340	35.460
	50	20.631	23.330	23.498	20.729	23.350	23.499

As given by equation 3.10 the highest SNRs are achieved with high illumination levels. This can also be observed in table 5.3. Result is seen both with illumination power and spectral power distribution among wavelengths: for example CIE A illuminant's spectral power, and thus number of photons, increases as wavelenghts get longer and this can be seen as worst SNRs in blue and best in red channels. Then when illuminants have more evenly distributed spectral powers as with D65 and F2, it is seen, that SNRs between different channels are also fairly equal. Here is also seen the difference between the number of photons between F2 and D65 as pointed out in figure 5.6. As F2 has around three times less photons per wavelength band, it is seen here as decreased SNR compared to one achieved with D65.

There is a widely recognised industry standard of SNR of 10 for highest noise level producing still somewhat usable images. In table 5.3 there can be noted, that even in very low light conditions this SNR level is not achieved. As simulation describes pretty much optimal scenario, when considering lens transmittances, this result is fairly expected. However, there is still seen a great imbalance between channels, especially with

illuminant A. In this case it basically translates to more blue noise than red or green with A illuminant. For daylight and fluorescent illuminants this imbalance is not by far as bad, so there different coloured noises should be fairly well balanced.

This same trend also holds for different material combos: SNRs are pretty close of those presented in table 5.3 for all materials. Also a wide trend can be seen, that lens stacks made of high transmissive materials (different glasses and Zeonex K26R), SNRs are consistently higher than for stacks made of only EP-5000R (or APL5014CL). This result comes basically from the definition of SNR (equation 3.10) and it can be verified from table 5.4, where SNRs of lens stack structures having different number of high and lower transmissive materials are compared.

Table 5.4 *Comparison of 6G and 6P lens stack SNR results. Materials used are L-BAL42 (G) and EP-5000R (P) and results are shown for blue (B), green (G) and red (R) channels.*

Illuminant	Relative illumination power (*arb.u.*)	SNRs 6G vs. 6P (%)		
		B	G	R
A	800	0.10	0.02	-0.02
	400	0.13	0.03	-0.03
	50	0.30	0.06	-0.06
D65	800	0.19	0.05	0.00
	400	0.23	0.07	0.00
	50	0.45	0.13	-0.01
F2	800	0.19	0.03	0.01
	400	0.23	0.04	0.01
	50	0.47	0.09	0.01

In table 5.4 it is broadly seen, that in both green and blue channels a full glass stack results in better SNR than a full plastic stack. Of course, same holds, when glass is replaced with K26R as it has glass-like transmittance qualities. As it can be noticed in figure 5.4, EP-5000R transmits long wavelengths a bit better, than some glasses and this results in slight defeat of full glass stack in red channel SNR comparison with A illuminant, where, as mentioned, spectral power is disproportionately concentrated to long wavelengths. For other used illuminants, however, the situation is then stabilized to different stacks having almost equal SNRs in red channel.

As it is possible to see in appendix A, that there is some advantage gained in blue and green channels even with only one or two high transmittance elements compared to full

EP-5000R stack. However, even the whole lens stack is made of high transmittance material, the maximum advantage gained for blue channel is between 0.47 and 0.76 %. These results were achieved by using F2 illuminant. Second greatest differences were achieved with D65 and then smallest differences were noticed with A illuminant. The most advantage, materialwise, in blue channel is gained with N-PK51, then second best material of the ones compared seems to be N-KZFS11, then K26R and worst performance of high transmittance materials had L-BAL42, results from which were already partly presented above.

For green channel the results for full high transmittance material stacks landed between 0.13 and 0.24 % in favor for high-transmittance materials and order of materials' performances stayed the same. With green channel though D65 illuminant achieved greatest difference, most likely due to its spectral power peaking in middle of visible wavelength region.

There is a slightly odd occurence with green channels of every material pairing studied in this thesis: worst SNRs are achieved with 1G5P lens stack structures. This might be due to an increasing tail in green channel QE after 650 nm: as EP-5000R transmits red light a bit better than high transmittance materials, this overpowers the green channel QE spike around 540 nm, where transmittances of different materials are pretty much equal. Then when second plastic element is replaced with high transmittance material, these tail loses its dominance and the transmittance difference and green QE spike together prevail.

For blue channels it seems, that independent of high transmittance material, there is some advantage gained in comparing SNRs to the full EP-5000R stack even when only one lens is replaced. However, the advantage gained is only 0.1-0.6 ‰with A illuminant and maximum of 1.0 ‰with N-PK51 material and D65 and F2 illuminants. As these results may not have been so significant as it was postulated at some point of the thesis making, they are still conclusive.

Low light scenarios are known to be problematic in terms of blue noise. It was also predicted earlier in this thesis, that higher transmittance would increase SNRs relatively more in low light compared to well lit scenario. This was also found to hold as for all materials there was a clear increase, especially with full glass or K26R stacks relative to full EP-5000R stacks in SNRs in all channels.

What comes to visible results, as one could guess after seeing numerical results, no visible difference was seen in terms of noise even between full high transparency material stack and full EP-5000R stack. In figure 5.9 are presented RGBs ((a) and (b)) and grey scale images of blue channels ((c) and (d)) of 6P and 6G stacks of EP-5000R and N-PK51, respectively. Between these two materials the numerical results differed the most, so if

there was a possibility to see some differences in noise visually, this pair was the best chance. In these images D65 was used as illuminant.

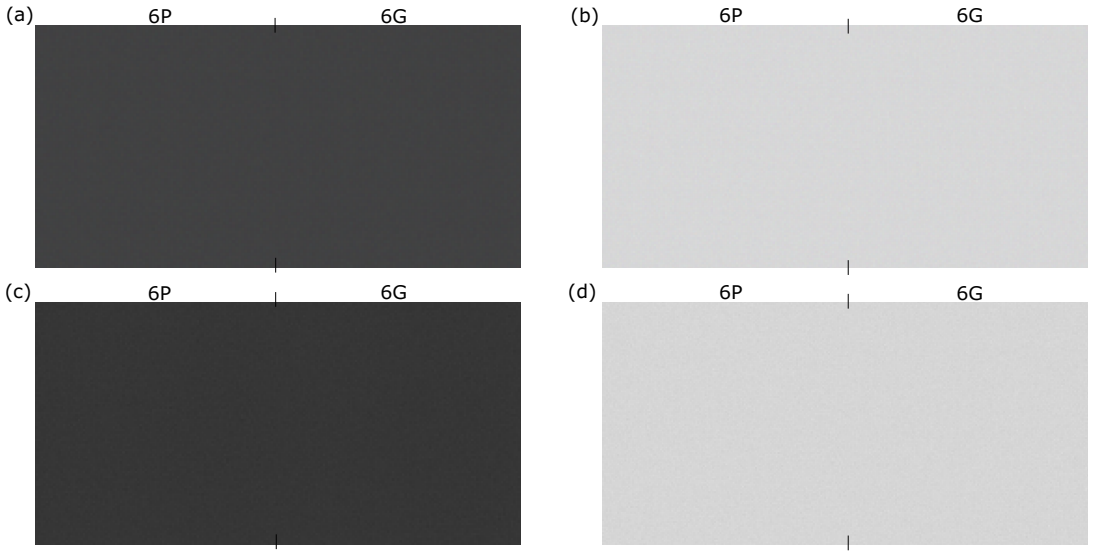

Figure 5.9 *Zoomed in (a)-(b) RGBs and (c)-(d) grey scale images of blue channels. All comparable images present relatively equal amounts of noise. Material pairs in all images are EP-5000R (P) and N-PK51 (G) to maximize SNR differences between materials. Images are created under D65 illuminant.*

For either only blue channel subfigures or full RBG images there are no detectable differences in noise levels of any sorts, when comparing between full glass and full plastic stacks. In RGBs there also seems to be pretty equal amount of all coloured noises and not any overpowering of blue noise independent of illumination power. This observation is well in correlation with the numerical results (for this material pair they are found in appendix A, but similar results for EP-5000R and L-BAL42 were presented in table 5.3).

The distribution of pixel values between different stacks was also studied and histrograms for each channel is presented in figure 5.10. In subfigure (a) are presented distributions for blue channels, in (b) for green and in (c) for red channels.

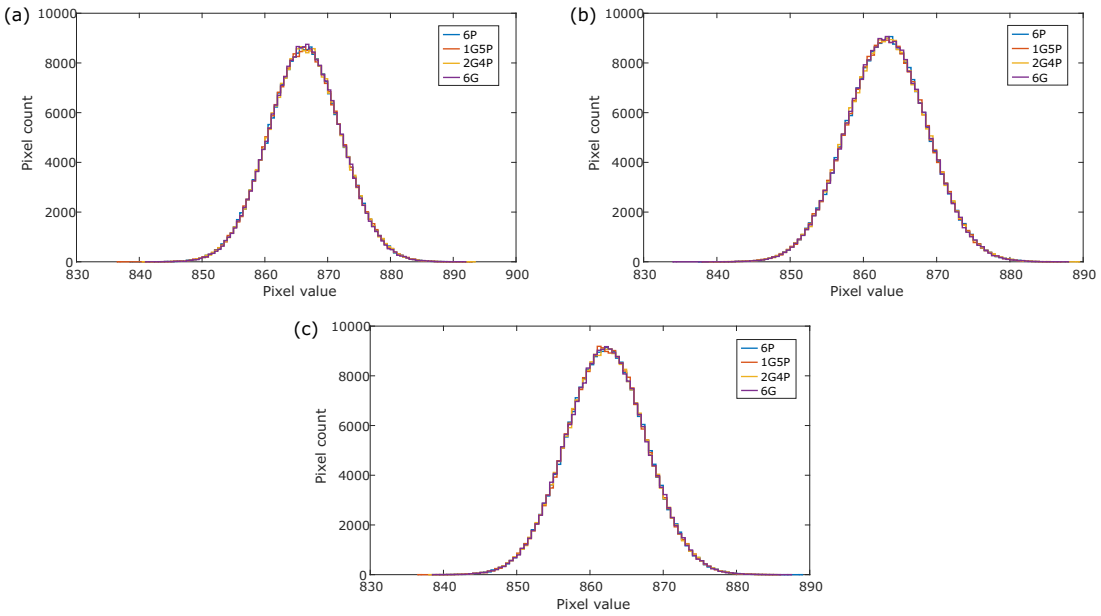

Figure 5.10 *Distribution of pixel values in (a) blue, (b) green and (c) red channels for 6P, 1G5P, 2G4P and 6G stacks. Materials used are EP-5000R (P) and N-PK51 (G). Illuminant used is CIE D65.*

Also in histograms in figure 5.10 there can be seen no particular differences between distribution of pixel values between different lens stacks structures. Also standard deviations (STD) calculated from the signals present only minor differences: for blue channel in 6P stack standard deviation is 5.81 and for 6G stack it is 5.75, which translates to roughly 1 % advantage for glass stack. For green channel STDs are 5.56 and 5.53 and for red channels 5.46 and 5.47 for full plastic and full glass stacks, respectively.

On the other hand, when examining the numerical results of illuminant A, there is a clearer difference in SNRs between channels. As it turns out, in images with this illuminant, there is a visible blue noise predominance. This is shown in figure 5.11, where 6P lens stacks made of EP-5000R are imaging a grey patch from Gretag-Macbeth ColorChecker. It is seen, that actually blue channel and its noise is gained so overwhelmingly, that the whole image ends up appearing bluish rather than grey.

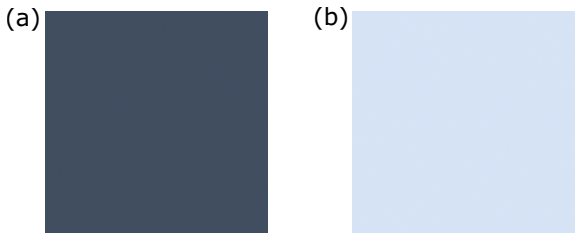

Figure 5.11 *RGBs of 6P stacks made of EP-5000R with A illuminant, where overpowering blue is seen to turn the images bluish. In subfigure (a) illumination power is 200 and in (b) 800 digital units.*

To emphasise the importance of good AR-coating even more, in figure 5.12 there are comparisons between 6P stack made of non-AR-coated EP-5000R and AR-coated 6G stack of L-BAL42. In (a) are compared zoomed RGBs and in (b) zoomed grey scale images of blue channels. Also in figure below are presented distributions of pixel values for (a) blue, (b) green and (c) red channels for same four lens stacks as histograms.

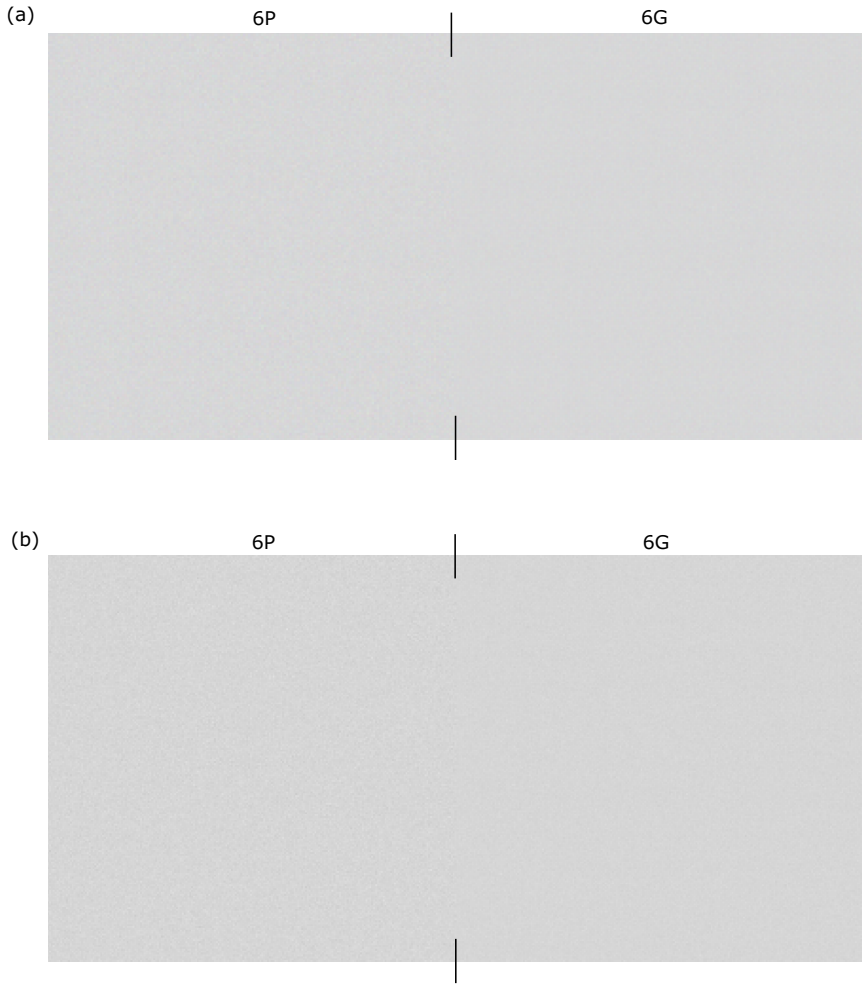

Figure 5.12 *Comparison of worst and best case scenarios. In (a) are presented zoomed RGBs and in (b) zoomed grey scale images of blue channels. Non-AR-coated 6P stacks (material EP-5000R) present visibly more noise than AR-coated 6G stacks (material L-BAL42).*

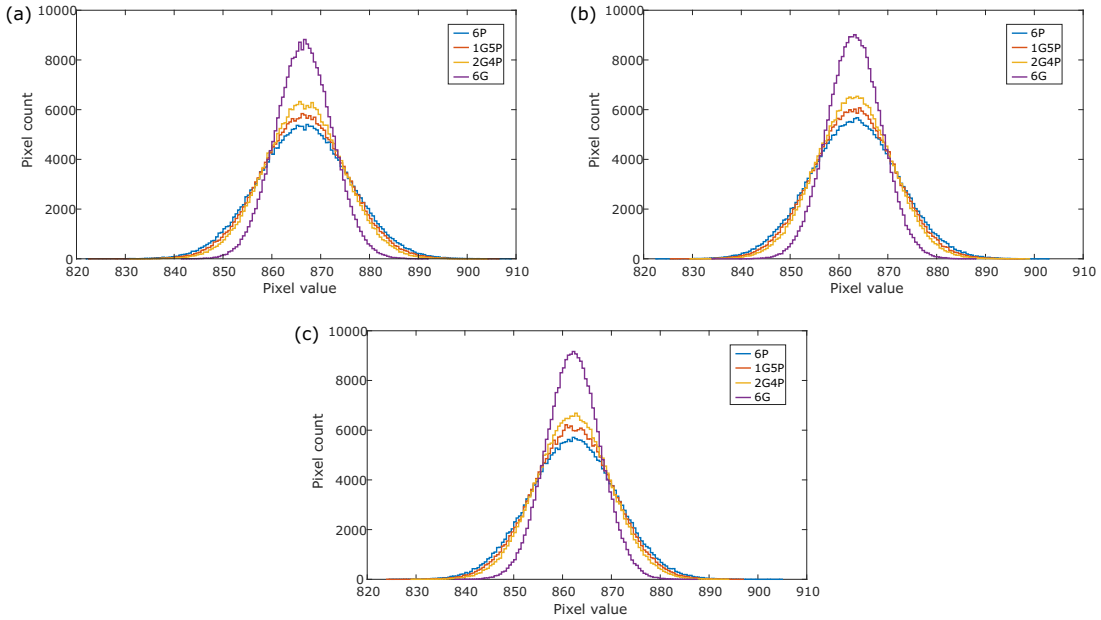

Figure 5.13 *Distribution of pixel values in each channel for different lens stack structures. In (a) is presented blue channels, in (b) green and in (c) red channels. Materials used were non-AR-coated EP-5000R (P) and AR-coated L-BAL42 (G). Results were received under D65 illuminant.*

In figure 5.12 there can be seen visible difference in noise levels in both blue channels and RGBs: AR-coated materials present significantly less noise. This speaks on the importance of the proper AR-coating on the materials. In case of these conditions, the mean difference between lens stack transmittances over visible light range was about 104 %. SNRs for non-AR-coated lenses were around 38 and for AR-coated ones around 43, making SNRs for every channel 12-13 % higher for AR-coated stack. Hence, it is no wonder, that no visible differences were found in comparisons between different, optimally AR-coated lens stacks. Also in figure 5.13 it is clearly detected, that the more AR-coated elements the stack has, the closer the most of the pixel values are distributed to the mean value of the signal.

6. DISCUSSION

In Section 5.1 results of thermal stability calculations were presented. They concluded pretty effectively, that what comes to thermal performance parameters, glasses are in multiple ways far superior in comparison with plastics.

For thermal defocus the biggest difference comes in the form of thermal instability of refractive index, which can be more than 30 times higher with even the best of optical polymers, such as Zeonex. Also in most cases in glasses this change in refractive index works to compensate the thermal expansion of the material, thus making glass basically immune to temperature changes. In the worst case for glass, it still has 10 times better focal stability, even in fairly narrow range of 10 to 50 °C studied in this thesis. For wider ranges this difference would only increase and as plastics tend to react more agressively to thermal changes as temperatures rise, the difference would increase somewhat exponentially.

As changes in temperature effect also the geometrical shape of a lens with CTE, this makes optical plastics also more prone to cracking of coatings. This arises from differences in materials' expansion rates, which then induce stress into the coating layers. This stress is mathematically 5-15 times higher for plastics. And this is not the only thing in which glass has the upper hand, what comes to AR coatings.

It was found in the late phases of the thesis process, that at least according to one manufacturer [2], Zeonex cannot be coated as well as N-BK7, as what comes to AR coating performance in the edges of the visible light range. As very little data of AR coating performances for optical plastics was found, it cannot be said for certainty, that AR coatings for plastics cannot be made as good as ones for glasses, but rather more studies need to be conducted. There is also a possibility, that not all glasses can be coated as well as N-BK7. The thickness of sample could have some effect on the coating performance of the material as well, and like things listed previously in this paragraph, this has not been taken into account in this thesis. With these in mind, the results obtained here, can be thought as a best case scenario for both materials, but even more so for the plastics.

In Sections 5.2 and 5.3 results for differences in material transmittances and their effects on noise creation were presented. Here a clear link between higher transmittance of materials

and better SNR was verified. However, the differences between materials were not nearly as great as it was first expected. This was mostly, because the material data first received was later found inconsistent and thus deemed unreliable for the research. This fault was, however, found so late in the process, that simulation and all other parts of the thesis were so far in progress, that the direction of the study was decided to keep as is. Also as material producers usually give their transmittance values for thicker samples, at least for use in mobile cameras, they cannot be judged as received. Still valuable information and understanding has been obtained and future work can be based on the simulation and findings of the thesis.

What comes to the transmittance and noise results themselves, it was found, that well designed optical polymer can possess glass-like transmittance properties, at least in the visible light region. However, it can be concluded, that most top tier plastics work as crown materials with low refractive index and low diffraction. As it can be seen from the figure 2.15, flint polymer materials, such as polystyrene and polycarbonate, latter of which EP-5000R presents, have notably weaker transmittance than flint glass like N-KZFS11 introduced in this thesis. This can be, however, at least partially attributed to higher Abbe number of N-KZFS11, 42, as it was only 24 for EP-5000R. When examining for example glasses in Schott's Abbe diagram [61], it can be seen, that glasses for this low Abbe numbers also have rather weak internal transmittance in short wavelength region. Then again, these glasses have refractive indices up to two, when EP-5000R only has n =1.635, thus making it hard to make this apples-to-apples comparison. Rather again, this tells from the versatility of glass as a optical material.

For the diversity of glasses also speaks figure 2.3, where a much larger variety of glasses to choose from for different optical characteristics is seen. This gives plenty more design freedom for optical designers to do their job, and as design specifications, especially for mobile camera lenses, get more and more demanding a good selection of materials will be much appreciated. Mostly this tightening happens in refraction related parts of the design, as z-height, that is, the height of the camera module is decreased, and apertures are increased. Thus here the higher refractive index plays crucial role, as the path of light can be changed within shorter distance, meaning thinner lenses or wider AoIs for the lenses of same thicknesses.

In the the process of modelling noise there were many simplifications made, which naturally affect the end results. However, they have more or less similar effect on all optical materials studied, so the relative results should be reliable from that point of view. What comes to reliability of the absolute results obtained, the most significant effect comes from the simulated dark noise as it was measured as worst case scenario to make its effects clearer in the simulation and in the results. Thus in real world the effect of sensor noise to

SNR is mostly less than what it was found here.

Glasses have displayed some advantages over optical polymers, what comes to optical characteristics. However, there are still some areas, where improvements need to take place in order to glass to gain market share from plastics.

First and foremost prices of the components would need to come down. This goes both for the material expenses themselves and lens production costs. From Ohara's pricing chart from the year 2018 [50], for example L-BAL42 falls to 35-60 $/lb price category, whereas polymer prices range from less than 0.50 $/lb for polycarbonate (2011) [71] to 15-18 $/lb for Zeonex (2000) [67]. As these prices are somewhat outdated, there has likely been a some changes, but these can be taken as guidelines. Price for normal borosilicate glass can be as cheap as 0.75$/lb (2011) [71], but mostly they are not suitable for molding.

The second price component is then related to the manufacturing process of optical components. Plastic lenses are injection molded, which makes them fast to manufacture as no high temperatures and pressures, and hence no long cooling times are needed. For glass lenses even with the most modern technology alone the high transition temperatures and pressures needed to make glass suitable for molding take time to reach. Also the cooling process takes more time to avoid refractive index shifts. Hence unit cost of plastic lens usually comes to be a great deal more affordable than one for glass.

Also in some specific applications weight of glass might come into play as a restricting factor as glasses usually have 2-3 times higher specific gravity than plastics [60, p. 21]. In most cases, though, this problem can be somewhat reduced as glass lenses can be made thinner due to better refractive qualities.

7. CONCLUSIONS

The main objective of this thesis was to study the differences between optical glasses and polymer materials in mass-produced imaging applications. As subject matter itself was fairly vast, first mainly physical and optical characteristics of the materials were studied on more of a superficial level.

To determine a better focus for the experimental part of the thesis a order of magnitude analysis was conducted. In this analysis four characteristics caught interest: thermal characteristics, short wavelength trasmittance, birefringence and water absorption. Out of these two thermal and transmittance properties were decided on to being the topics of interest and studies of birefringence and water absorption were postponed for the time after thesis.

As thermal differences of plastic and glass materials were already fairly well understood within the thesis facilitator, it was decided to only make some simple calculations on the thermal characteristics and focus efforts more on trasmittance comparisons. It was postulated, that differences in short wavelength transmittance could induce differences in image noise performance. This assumption lead to decision to start crafting a basic digital camera simulation, where path of photon from the illuminant to image sensor would be traced. On and after the sensor photoelectrons created and digitalised would then be converted to numerical and visual data on how noise effects the final image after some elementary ISP steps. The simulation itself was executed with MATLAB.

The results of thermal studies were well in line with literature and prior knowledge. Glasses showed high thermal stability in their optical qualities like refractive index, geometric change and focal length change with temperature, whereas even the best plastics turned out to be inferior to glasses in all of the studied thermal properties.

In transmittance comparisons plastics held their ground remarkably better and when in came to short wavelength transmittance, the best optical polymers performed even better than one commonly used glass. Noisewise there was no remarkable difference in results: numerical SNRs per colour channel differed around 0.8 % at maximum for the advantage of glass in six lens full glass stack versus full plastic stack comparisons. Also it was

found, that incorporating high transmittance materials to the lens stack resulted in bigger relative increase in SNRs in low light scenarios as it was postulated. However, none of the aforementioned results yielded to any visual difference between noise levels in different lens stack structures with well AR-coated materials.

These results were obtained, however, with an assumption, that all materials studied could be AR-coated as well as N-BK7 glass. In the late phases of thesis process, though, it was discovered, that this might not be possible for polymers, as even Zeonex could not be this well coated according to one coating manufacturer. Hence there might be some room for the more visible differences, if this presents to hold true for other plastics as well. This is backed up by simulations done between non-AR-coated plastic and AR-coated glass, where significant visual and numerical differences were obtained. Still more research on the AR-coatings on different materials needs to be done.

It was also found, that at least Zeonex loses a significant part of its transmittance, when it is kept in high temperatures for extended periods of time. There are studies showing significantly smaller transmittance decrease on glasses during thermal aging process, which could also add up to noise differences in some applications, in which long product lifetime meets high temperature requirements. As an example from this could be driver monitoring cameras attached to the dashboard of a car. There is still very little research to be found on the effects of thermal aging either for optical glasses or plastics, so this would be an interesting subject for further investigation.

REFERENCES

[1] R. Abd-Allah, "Solarization behaviour of manganesecontaining glass: An experimental and analytical study," *Mediterranean Archaeology and Archaeometry*, vol. 9, no. 1, pp. 37–53, 2009.

[2] AccuCoat Inc. Multilayer anti-reflective coating on Zeonex − AC110. [Online]. Available: https://accucoatinc.com/anti-reflective-coatings/ac_110/

[3] Adept Turnkey Pty Ltd. The 3CCD colour advantage: Let the benefits speak for themselves. [Online]. Available: http://www.adept.net.au/news/newsletter/201203-mar/article_3ccd_colour.shtml#dichroic

[4] APN MJM, from Wikimedia Commons. [Online]. Available: https://upload.wikimedia.org/wikipedia/commons/0/09/Crystal_on_graph_paper.jpg

[5] ASTM. (2003) G17303 standard tables for reference solar spectral irradiances: Direct normal and hemispherical on 37ř tilted surface. [Online]. Available: http://www.eng.uc.edu/~beaucag/Classes/SolarPowerForAfrica/BookPartsPVTechnical/AppendixA1StandardAM0andAM1p5.pdf

[6] S. Bäumer, Ed., *Handbook of plastic optics*. Wiley-VCH, 2005.

[7] E. C. Beder, C. D. Bass, and W. L. Shackleford, "Transmissivity and absorption of fused quartz between 0.22 μ and 3.5 μ from room temperature to 1500 °c," *Appl. Opt.*, vol. 10, no. 10, pp. 2263–2268, Oct 1971. [Online]. Available: http://ao.osa.org/abstract.cfm?URI=ao-10-10-2263

[8] J. Beutel, H. L. Kundel, and R. L. Van Metter, *Handbook of Medical Imaging, Volume 1 - Physics and Psychophysics*. SPIE, 2000.

[9] M. Born and E. Wolf, *Principles of Optics*, 7th ed. Cambridge University Press, 1999.

[10] P. Bouguer, "Essai d'optique sur la gradation de la lumière," Paris, France, 1729. [Online]. Available: https://books.google.fi/books?id=JNkTAAAAQAAJ&pg=PA1&redir_esc=y#v=onepage&q&f=false

[11] I. G. Calizo, "Reset noise in CMOS image sensors," Master's thesis, San Jose State University, 2005. [Online]. Available: https://scholarworks.sjsu.edu/etd_theses/2746/

[12] Cardinal Glass Industries. Technical Service Bulletin, Haze in Glass Products. [Online]. Available: http://www.cardinalcorp.com/source/pdf/tsb/cg/CG07_01-2016.pdf

[13] P. B. Catrysse and B. A. Wandell, "Roadmap for CMOS image sensors: Moore meets Planck and Sommerfeld."

[14] Cburnett [GFDL (http://www.gnu.org/copyleft/fdl.html), from Wikimedia Commons. Bayer pattern on sensor profile. [Online]. Available: https://upload.wikimedia.org/wikipedia/commons/1/1c/Bayer_pattern_on_sensor_profile.svg

[15] CIE International Commission on Illumination, "Cie 15: Technical report: Colorimetry," 2004.

[16] M. E.-P. Company. Polycarbonate resin (iupilon novarex xantar). [Online]. Available: https://www.m-ep.co.jp/en/pdf/product/iupi_nova/pc.pdf

[17] M. G. C. Company. Iupizeta ep-5000. [Online]. Available: https://chfile.cn.gcimg.net/gcwthird/day_20170228/84ec6d194er7a96df39d7k76e0087519.pdf

[18] G. Diener, "Superluminal group velocities and information transfer," *Physics Letters A*, vol. 223, no. 5, pp. 327 – 331, 1996. [Online]. Available: http://www.sciencedirect.com/science/article/pii/S0375960196007670

[19] Diverse Optics. Specifications of optical grade polymers and glass. [Online]. Available: http://diverseoptics.com/wp-content/uploads/2012/02/Specifications_of_Optical_Grade_Polymers_and_Glass.pdf

[20] N. Domíngues, D. Mayershofer, C. Garsia, and J. Asara, "Accurate polarimeter with multicapture fitting for plastic lens evaluation," *Optical Engineering*, vol. 55, 2016. [Online]. Available: https://doi.org/10.1117/1.OE.55.2.024102

[21] Edmund Optics. Application notes: Anti-reflection (ar) coatings. [Online]. Available: https://www.edmundoptics.com/resources/application-notes/optics/anti-reflection-coatings/

[22] A. El Gamal and H. Eltoukhy, "Cmos image sensors: An introduction to the technology, design, and performance limits, presenting recent developments and future directions." *IEEE CIRCUITS & DEVICES MAGAZINE*, 2005. [Online]. Available: https://ieeexplore.ieee.org/stamp/stamp.jsp?tp=&arnumber=1438751

[23] EMPIR PhotoLED, "Future photometry based on solid-state lighting products," January 2018. [Online]. Available: http://photoled.aalto.fi/material/15SIB07_PhotoLED_Publishable_Summary_Jan2018.pdf

[24] G. J. M. Fechine, R. M. S., R. M. Souto Maior, and C. L. H., "Surface characterization of photodegraded poly(ethylene terephthalate). The effect of ultraviolet absorbers," *Polymer*, vol. 45, no. 7, pp. 2303–2308, March 2004.

[25] R. P. Feynman, R. Leighton, and M. Sands, *Feynman Lectures on Physics, Volume I*. Basic Books, 2013. [Online]. Available: http://www.feynmanlectures.caltech.edu/

[26] ——, *Feynman Lectures on Physics, Volume II*. Basic Books, 2013. [Online]. Available: http://www.feynmanlectures.caltech.edu/

[27] B. Fowler, A. El Gamal, and D. X. D. Yang, "A CMOS Area Image Sensor wit Pixel-Level A/D Conversion," *IEEE International Solid-State Circuits Conference*, Ferburary 1994. [Online]. Available: https://ieeexplore.ieee.org/stamp/stamp.jsp?tp=&arnumber=344659

[28] Georgia State University, College of Arts and Sciences, Department of Physics and Astronomy. Maxwell's equations. [Online]. Available: http://hyperphysics.phy-astr.gsu.edu/hbase/electric/maxeq.html

[29] ——. Radiant Flux. [Online]. Available: http://hyperphysics.phy-astr.gsu.edu/hbase/vision/radiant.html

[30] D. T. Gillespie, A. L. Olsen, and L. W. Nichols, "Transmittance of optical materials at high temperatures in the 1-μ to 12-μ range," *Appl. Opt.*, vol. 4, no. 11, pp. 1488–1493, Nov 1965. [Online]. Available: http://ao.osa.org/abstract.cfm?URI=ao-4-11-1488

[31] GS Plastic Optics. Transmission curves. [Online]. Available: https://www.gsoptics.com/transmission-curves/

[32] D. O. Guaraglia and J. L. Pousa, *Introduction to Modern Instrumentation - For Hydraulics and Environmental Sciences*. De Gruyter, 2014. [Online]. Available: https://app.knovel.com/hotlink/khtml/id:kt010REA33/introduction-modern-instrumentation/analog-digital-conversion

[33] E. Hecht, *Optics*, 5th ed. Pearson Education Ltd., 2017.

[34] P. Hofmann, *Solid state physics: an introduction*, 1st ed. Weinheim: Wiley-VCH, 2008.

[35] G. C. Holst and T. S. Lomheim, *CMOS/CCD Sensors and Camera Systems*, 2nd ed. JCD Publishing and SPIE Press, 2011.

[36] P. Horowitz and W. Hill, *Art of Electronics*, 3rd ed. Cambridge University Press, 2016.

[37] P. M. Hubel. Foveon technology and the changing landscape of digital cameras. [Online]. Available: http://www.foveon.com/files/CIC13_Hubel_Final.pdf

[38] HunterLab. (2008) Insights on Color, Haze. [Online]. Available: https://www.hunterlab.se/wp-content/uploads/2012/11/Haze.pdf

[39] I. S. Kroch, via Wikimedia Commons. [Online]. Available: https://upload.wikimedia.org/wikipedia/commons/b/b3/Astigmatism.svg

[40] E.-S. Kang, J.-U. Park, and B.-S. Bae, "Effect of organic modifiers on the thermo-optic characteristics of inorganic-organic hybrid material films," *Journal of Materials Research*, vol. 18, no. 8, pp. 1889–1894, August 2003.

[41] W.-C. Kim and N.-C. Park, "Effect of birefringence of lens material on polarization status and optical imaging characteristics," *Optics Communications*, vol. 413, pp. 329 – 335, 2018. [Online]. Available: http://www.sciencedirect.com/science/article/pii/S0030401817312002

[42] S. Lan and E. Samad, "Low-birefringence lens design for polarization sensitive optical systems," *Proc.SPIE*, vol. 6289, 2006. [Online]. Available: https://doi.org/10.1117/12.679416

[43] Y. Lin, J. P. You, Y. Lin, N. T. Tran, and F. G. Shi, "Development of high-performance optical silicone for the packaging of high-power LEDs," *IEEE Transactions on Components and Packaging Technologies*, vol. 33, no. 4, pp. 761–766, Dec 2010. [Online]. Available: https://ieeexplore.ieee.org/document/5499035

[44] Lyon, R. F., Public domain, via Wikimedia Commons. [Online]. Available: https://upload.wikimedia.org/wikipedia/commons/a/ad/Gretag-Macbeth_ColorChecker.jpg

[45] C. S. McCamy, H. Marcus, and J. G. Davidson, "A color-rendition chart," *Journal of Applied Photographic Engineering*, vol. 2, no. 3, pp. 95 – 99, 1976. [Online]. Available: http://www.cis.rit.edu/~cnspci/references/mccamy1976.pdf

[46] *APEL Cyclo Olefin Copolymer (COC): datasheet*, Mitsui Chemicals. [Online]. Available: https://www.mitsuichem.com/en/service/pdf/apel_j.pdf

[47] J. Nakamura, *Image Sensors and Signal Processing for Digital Still Cameras*. Boca Raton, FL: CRC Press, April 2005. [Online]. Available: https://books.google.fi/books?id=UY6QzgzgieYC&pg=PA79&redir_esc=y#v=onepage&q&f=false

[48] P. Nussbaum, V. R., H. P. Herzig, M. Eisner, and S. Haselbeck, "Design, fabrication and testing of microlens arrays for sensors and microsystems,"

Pure Appl. Opt., vol. 6, pp. 617–636, August 1997. [Online]. Available: https://www.suss-microoptics.com/suss-microoptics/technical-publications/Microlens_Arrays_for_Sensors_and_Microsystems.pdf

[49] *L-BAL42: datasheet*, Ohara Corporation. [Online]. Available: https://www.oharacorp.com/pdf/elbal42.pdf

[50] Ohara Corporation. Optical glass chart. [Online]. Available: https://www.oharacorp.com/pdf/pricing-chart-2018-01.pdf

[51] ON Semiconductor. Mt9p031. [Online]. Available: http://www.onsemi.com/pub/Collateral/MT9P031-D.PDF

[52] K. E. Oughstun and N. A. Cartwright, "On the Lorentz-Lorenz formula and the lorentz model of dielectric dispersion," *Optics Express*, vol. 11, no. 13, pp. 1541–1546, 2003. [Online]. Available: https://www.osapublishing.org/oe/abstract.cfm?uri=oe-11-13-1541

[53] L. S. Pedrotti, in *Fundamentals of Photonics*. SPIE - The international society for optics and photonics, ch. Basic Geometrical Optics. [Online]. Available: http://spie.org/publications/fundamentals-of-photonics-modules

[54] M. Philip and F. Al-Azzawi, "Effects of natural and artificial weathering on the physical properties of recycled poly(ethylene terephthalate)," *Journal of Polymers and the Environment*, Feb 2018. [Online]. Available: https://doi.org/10.1007/s10924-018-1191-x

[55] M. Planck, "Über das Gesetz der Energieverteilung im Normalspektrum (German) [On the law of distribution of energy in the normal spectrum]," *Annalen der Physik*, vol. 309, no. 3, pp. 553–563, 1901.

[56] M. Pokrass, Z. Burshtein, and R. Gvishi, "Thermo-optic coefficient in some hybrid organic/inorganic fast sol-gel glasses," *Optical Materials*, vol. 32, no. 9, pp. 975–981, July 2010. [Online]. Available: https://doi.org/10.1016/j.optmat.2010.01.038

[57] B. Razavi, *Design of Analog CMOS Integrated Circuits*. McGraw-Hill, 2001. [Online]. Available: http://d1.amobbs.com/bbs_upload782111/files_24/ourdev_521342.pdf

[58] P. J. Rogers and M. Roberts, in *Handbook of Optics*, 3rd ed. New York, NY, USA: McGraw-Hill, Inc., 2010, vol. 2, ch. Thermal Compensation Techniques. [Online]. Available: http://www.photonics.intec.ugent.be/education/IVPV/res_handbook/v1ch39.pdf

[59] M. Schaub, J. Schwiegerling, E. Fest, A. Symmons, and R. H. Shepard, *Molded Optics: Design and Manufacture*. CRC Press, 2011.

[60] M. P. Schaub, *Design of Plastic Optical Systems*. SPIE, 2009.

[61] Schott AG. Interactive abbe diagram. [Online]. Available: https://www.schott.com/advanced_optics/english/knowledge-center/technical-articles-and-tools/abbe-diagramm.html

[62] ——. Optical glass data sheets. [Online]. Available: https://www.schott.com/d/advanced_optics/ac85c64c-60a0-4113-a9df-23ee1be20428/1.3/schott-optical-glass-collection-datasheets-english-17012017.pdf

[63] ——. Technical information, advanced optics, TIE-27: Stress in optical glass. [Online]. Available: https://www.schott.com/d/advanced_optics/1275dc1e-ef01-45d1-a88a-79deec322443/1.1/schott_tie-27_stress_in_optical_glass_us.pdf

[64] ——, "Technical information, advanced optics, TIE-35: Transmittance of optical glass." [Online]. Available: https://www.schott.com/d/advanced_optics/e434285e-65f6-4f21-a1b8-af282e17629c/1.1/schott_tie-35_transmittance_of_optical_glass_us.pdf

[65] ——, "Optical filter glass," 2015. [Online]. Available: https://www.us.schott.com/d/advanced_optics/a0c882b3-5169-4430-9770-1725a13c62da/1.3/schott-optical-filter-glass-description-2015-us.pdf

[66] W. Schottky, "Über spontane Stromschwankungen in verschiedenen Elektrizitätsleitern (German)," *Annalen der Physik*, vol. 362, no. 23, pp. 541–567, 1918.

[67] Schut, Jan H., Plastic Technology. New cyclic olefins. [Online]. Available: https://www.ptonline.com/articles/new-cyclic-olefins

[68] H. Spieler, *Semiconductor Detector Systems*. Oxford University Press, 2005. [Online]. Available: https://app.knovel.com/hotlink/khtml/id:kt004NBZL1/semiconductor-detector/digitization-pulse-height

[69] N. Sultanova, S. Kasarova, and I. Nikolov, "Advanced applications of optical polymers," *Bulgarian Journal of Physics*, vol. 40, no. 3, p. 258264, 2013.

[70] ——, "Advanced applications of optical polymers," *Bulgarian Journal of Physics*, vol. 43, no. 3, pp. 243–250, 2016.

[71] A. Symmons and R. Pini, "Precision molded glass challenges plastic optics," p. 42, 2011. [Online]. Available: https://www.laserfocusworld.com/articles/2011/07/molded-optics-precision-molded-glass-challenges-plastic-optics.html

[72] B. Tatian, "Fitting refractive-index data with the sellmeier dispersion formula," *Appl. Opt.*, vol. 23, no. 24, pp. 4477–4485, Dec 1984. [Online]. Available: http://ao.osa.org/abstract.cfm?URI=ao-23-24-4477

[73] The MathWorks, Inc., "GRABIT." [Online]. Available: https://se.mathworks.com/matlabcentral/fileexchange/7173-grabit

[74] C. Ting, P. B. Catrysse, A. El Gamal, and B. A. Wandell, "How small should pixel size be?" *Proceedings SPIE*, vol. 3965, January 2000. [Online]. Available: https://doi.org/10.1117/12.385463

[75] G. F. Tjandraatmadja and L. S. Burn, in *Durability of Building Materials and Components 8*, M. A. Lacasse and D. J. Vanier, Eds. Ottawa, ON, Canada: Institute for Research in Construction, 1999, ch. The effects of ultraviolet radiation on polycarbonate glazing, pp. 884–898. [Online]. Available: https://www.irbnet.de/daten/iconda/CIB1832.pdf

[76] C. Tsai, W. Cheng, J. Chang, S. Huang, J. Liou, G. Chen, Y. Huang, J. Wang, and W. Cheng, "Thermal-stability comparison of glass- and silicone-based high-power phosphor-converted white-light-emitting diodes under thermal aging," *IEEE Transactions on Device and Materials Reliability*, vol. 14, no. 1, pp. 4–8, March 2014. [Online]. Available: https://ieeexplore.ieee.org/document/6257458

[77] G. Upender, S. Ramesh, M. Prasad, V. Sathe, and V. Mouli, "Optical band gap, glass transition temperature and structural studies of $(100 - 2x)TeO_2 - xAg_2O - xWO_3$ glass system," *Journal of Alloys and Compounds*, vol. 504, no. 2, pp. 468–474, 2010. [Online]. Available: http://www.sciencedirect.com/science/article/pii/S0925838810013587

[78] W. von Sellmeier, "Zur Erklärung der abnormen Farbenfolge im Spectrum einiger Substanzen (German)," *Annalen der Physik*, vol. 219, no. 6, pp. 272–282, 1871.

[79] X. Wang, "Noise in sub-micron cmos image sensors," Ph.D. dissertation, Technische Universiteit Delft, Enschede, Netherlands, 2008. [Online]. Available: https://pdfs.semanticscholar.org/e3d3/dfa28ba90fd6d38ed4bf350a24aa309e18fd.pdf

[80] M. J. Weber, *Handbook of Optical Materials*. CRC Press, 2003.

[81] f. W. C. WolfWings [Public domain]. [Online]. Available: (a)https://upload.wikimedia.org/wikipedia/commons/5/5b/Pincushion_distortion.svg,(b) https://upload.wikimedia.org/wikipedia/commons/6/63/Barrel_distortion.svg

[82] E. Yousif and R. Haddad, "Photodegradation and photostabilization of polymers, especially polystyrene: review," *SpringerPlus*, vol. 2, no. 398, 2013.

[83] L. Yung-Cheng, C. Wen-Hsin, and C. Ye-Quang, "Automatic white balance for digital still camera," *IEEE Transactions on Consumer Electronics*, vol. 41, no. 3, pp. 460–466, Aug 1995.

[84] Zeon Corporation Specialty Plastics and Components Division, "Introduction of zeonexő T62R + recommended molding condition (unpublished)."

[85] *New high-performance thermoplastics for next-generation*, Zeon Specialty Materials. [Online]. Available: http://www.zeon.co.jp/content/200323391.pdf

[86] L. Zhang and W. Liu, "Precision glass molding: Toward an optimal fabrication of optical lenses," *Frontiers of Mechanical Engineering*, vol. 12, no. 1, pp. 3–17, Mar 2017. [Online]. Available: https://doi.org/10.1007/s11465-017-0408-3

APPENDIX A. NUMERICAL RESULTS FROM SNR SIMULATIONS

Table 1 *SNRs obtained from the simulation for different lighting conditions and lens structures for L-BAL42 and EP-5000R materials.*

Illuminant	Relative illumination power (*arb.u.*)	SNRs											
		6P			1G5P			2G4P			6G		
		B	G	R	B	G	R	B	G	R	B	G	R
A	800	36.303	39.938	44.307	36.305	39.931	44.286	36.301	39.941	44.308	36.340	39.946	44.296
	400	31.632	35.542	40.301	31.634	35.536	40.280	31.631	35.546	40.301	31.672	35.552	40.288
	50	14.952	19.204	24.491	14.953	19.197	24.471	14.953	19.209	24.471	14.997	19.215	24.476
D65	800	42.755	43.163	43.293	42.765	43.159	43.275	42.769	43.171	43.298	42.837	43.196	43.294
	400	39.052	39.503	39.648	39.063	39.500	39.630	39.068	39.512	39.652	39.143	39.529	39.647
	50	23.694	24.214	24.382	23.707	24.210	24.364	23.715	24.224	24.385	23.799	24.244	24.379
F2	800	35.541	37.403	37.516	35.548	37.397	37.498	35.549	37.408	37.522	35.549	37.416	37.522
	400	33.233	35.325	35.453	33.242	35.320	35.435	33.244	35.330	35.458	33.309	35.340	35.460
	50	20.631	23.330	23.498	20.642	23.325	23.481	20.650	23.337	23.503	20.729	23.350	23.499

Table 2 *Comparison of 1G5P, 2G4P and 6P against 6P lens stack SNR results for L-BAL42 and EP-5000R.*

Illuminant	Relative illumination power (*arb.u.*)	SNRs								
		1G5P vs. 6P (%)			2G4P vs. 6P (%)			6G vs. 6P (%)		
		B	G	R	B	G	R	B	G	R
A	800	0.01	-0.02	-0.05	0.00	0.01	0.00	0.10	0.02	-0.02
	400	0.01	-0.02	-0.05	0.00	0.01	0.00	0.13	0.03	-0.03
	50	0.01	-0.04	-0.08	0.00	0.02	0.00	0.30	0.06	-0.06
D65	800	0.02	-0.01	-0.04	0.03	0.02	0.01	0.19	0.05	0.00
	400	0.03	-0.01	-0.05	0.04	0.02	-0.01	0.23	0.07	0.00
	50	0.05	-0.01	-0.07	0.09	0.04	0.02	0.45	0.13	-0.01
F2	800	0.02	-0.02	-0.05	0.02	0.01	0.02	0.19	0.03	0.01
	400	0.02	-0.02	-0.05	0.03	0.01	0.02	0.23	0.04	0.01
	50	0.05	-0.02	-0.07	0.09	0.03	0.02	0.47	0.09	0.01

Table 3 *SNRs obtained from the simulation for different lighting conditions and lens structures for N-PK51 and EP-5000R materials.*

Illuminant	Relative illumination power (*arb.u.*)	SNRs											
		6P			1G5P			2G4P			6G		
		B	G	R	B	G	R	B	G	R	B	G	R
A	800	36.300	39.935	44.304	36.309	39.933	44.289	36.312	39.946	44.315	36.378	39.967	44.322
	400	31.629	35.539	40.298	31.638	35.537	40.282	31.643	35.551	40.308	31.712	35.574	40.315
	50	14.949	19.201	24.487	14.958	19.198	24.473	14.964	19.214	24.498	15.040	19.239	24.506
D65	800	42.746	43.154	43.284	42.763	43.153	43.270	42.775	43.169	43.298	42.876	43.199	43.312
	400	39.039	39.491	39.636	39.059	39.491	39.622	39.073	39.508	39.650	39.184	39.541	39.665
	50	23.677	24.197	24.365	23.700	24.198	24.353	23.718	24.217	24.380	23.844	24.255	24.398
F2	800	35.535	37.398	37.510	35.549	37.395	37.496	35.557	37.408	37.524	35.642	37.427	37.537
	400	33.224	35.316	35.444	33.240	35.314	35.430	33.250	35.328	35.458	33.345	35.350	35.473
	50	20.613	23.312	23.480	20.634	23.312	23.469	20.651	23.328	23.496	20.770	23.358	23.515

Table 4 *Comparison of 1G5P, 2G4P and 6P against 6P lens stack SNR results for N-PK51 and EP-5000R.*

Illuminant	Relative illumination power (*arb.u.*)	SNRs								
		1G5P vs. 6P (%)			2G4P vs. 6P (%)			6G vs. 6P (%)		
		B	G	R	B	G	R	B	G	R
A	800	0.02	-0.01	-0.04	0.03	0.03	0.02	0.21	0.08	0.04
	400	0.03	-0.01	-0.04	0.04	0.03	0.03	0.26	0.10	0.04
	50	0.06	-0.01	-0.06	0.11	0.07	0.05	0.61	0.20	0.08
D65	800	0.04	0.00	-0.03	0.07	0.04	0.03	0.30	0.10	0.06
	400	0.05	0.00	-0.03	0.09	0.04	0.04	0.37	0.13	0.07
	50	0.10	0.01	-0.05	0.18	0.08	0.06	0.71	0.24	0.14
F2	800	0.04	-0.01	-0.04	0.06	0.03	0.04	0.30	0.08	0.07
	400	0.05	-0.01	-0.04	0.08	0.03	0.04	0.36	0.10	0.08
	50	0.10	0.00	-0.05	0.18	0.07	0.07	0.76	0.19	0.15

Table 5 *SNRs obtained from the simulation for different lighting conditions and lens structures for K26R and EP-5000R materials.*

Illuminant	Relative illumination power (*arb.u.*)	SNRs											
		6P			1G5P			2G4P			6G		
		B	G	R	B	G	R	B	G	R	B	G	R
A	800	36.303	39.937	44.306	36.309	39.933	44.290	36.310	39.945	44.316	36.366	39.959	44.321
	400	31.632	35.542	40.300	31.639	35.538	40.284	31.640	35.550	40.410	31.700	35.566	40.315
	50	14.952	19.204	24.490	14.958	19.200	24.476	14.962	19.213	24.500	15.027	19.230	24.506
D65	800	42.749	43.157	43.287	42.763	43.154	43.272	42.772	43.168	43.299	42.859	43.190	43.311
	400	39.043	39.495	39.640	39.059	39.493	39.625	39.070	39.507	39.653	39.166	39.532	39.664
	50	23.682	24.202	24.370	23.701	24.201	24.358	23.715	24.217	24.384	23.824	24.245	24.397
F2	800	35.537	37.400	37.512	35.548	37.395	37.512	35.554	37.407	37.524	35.628	37.420	37.535
	400	33.227	35.319	35.447	33.240	35.316	35.432	33.247	35.328	35.459	33.330	35.343	35.471
	50	20.620	23.319	23.487	20.637	23.316	23.474	20.650	23.330	23.501	20.753	23.351	23.514

Table 6 *Comparison of 1G5P, 2G4P and 6P against 6P lens stack SNR results for K26R and EP-5000R.*

Illuminant	Relative illumination power (*arb.u.*)	SNRs								
		1G5P vs. 6P (%)			2G4P vs. 6P (%)			6G vs. 6P (%)		
		B	G	R	B	G	R	B	G	R
A	800	0.02	-0.01	-0.04	0.02	0.02	0.02	0.17	0.05	0.03
	400	0.02	-0.01	-0.04	0.03	0.02	0.02	0.22	0.07	0.04
	50	0.04	-0.02	-0.06	0.07	0.05	0.04	0.50	0.14	0.07
D65	800	0.03	-0.01	-0.03	0.05	0.03	0.03	0.26	0.08	0.05
	400	0.04	0.00	-0.04	0.07	0.03	0.03	0.31	0.09	0.06
	50	0.08	0.00	-0.05	0.14	0.06	0.06	0.60	0.18	0.11
F2	800	0.03	-0.01	-0.04	0.05	0.02	0.03	0.26	0.05	0.06
	400	0.04	-0.01	-0.04	0.06	0.02	0.04	0.31	0.07	0.07
	50	0.08	-0.01	-0.05	0.15	0.05	0.06	0.64	0.14	0.12

Table 7 *SNRs obtained from the simulation for different lighting conditions and lens structures for N-KZFS11 and EP-5000R materials.*

Illuminant	Relative illumination power (*arb.u.*)	SNRs											
		6P			1G5P			2G4P			6G		
		B	G	R	B	G	R	B	G	R	B	G	R
A	800	36.300	39.935	44.304	36.308	39.932	44.288	36.311	39.945	44.314	36.376	39.966	44.322
	400	31.628	35.539	40.298	31.638	35.536	40.282	31.642	35.550	40.308	31.710	35.572	40.316
	50	14.948	19.200	24.487	14.957	19.198	24.473	14.963	19.213	24.498	15.037	19.237	24.506
D65	800	42.746	43.154	43.284	42.763	43.153	43.270	42.774	43.169	43.298	42.873	43.197	43.312
	400	39.039	39.491	39.636	39.059	39.491	39.622	39.072	39.507	39.650	39.180	39.539	39.665
	50	23.677	24.197	24.365	23.699	24.198	24.353	23.717	24.216	24.380	23.840	24.254	24.398
F2	800	35.535	37.398	37.510	35.548	37.395	37.496	35.556	37.408	37.524	35.640	37.426	37.537
	400	33.224	35.317	35.444	33.240	35.314	35.430	33.250	35.328	35.458	33.342	35.349	35.472
	50	20.614	23.313	23.481	20.634	23.312	23.470	20.651	23.328	23.497	20.767	23.357	23.515

Table 8 *Comparison of 1G5P, 2G4P and 6P against 6P lens stack SNR results for N-KZFS11 and EP-5000R.*

Illuminant	Relative illumination power (*arb.u.*)	SNRs								
		1G5P vs. 6P (%)			2G4P vs. 6P (%)			6G vs. 6P (%)		
		B	G	R	B	G	R	B	G	R
A	800	0.02	-0.01	-0.04	0.03	0.03	0.02	0.21	0.08	0.04
	400	0.03	-0.01	-0.04	0.04	0.03	0.03	0.26	0.09	0.04
	50	0.06	-0.01	-0.06	0.10	0.07	0.05	0.60	0.19	0.08
D65	800	0.04	0.00	-0.03	0.07	0.03	0.03	0.30	0.10	0.06
	400	0.05	0.00	-0.03	0.08	0.04	0.04	0.36	0.12	0.07
	50	0.09	0.00	-0.05	0.17	0.08	0.06	0.69	0.23	0.14
F2	800	0.04	-0.01	-0.04	0.06	0.03	0.04	0.29	0.08	0.07
	400	0.05	-0.01	-0.04	0.08	0.03	0.04	0.36	0.09	0.08
	50	0.10	-0.01	-0.05	0.18	0.06	0.07	0.74	0.19	0.14

Table 9 *SNRs obtained from the simulation for different lighting conditions and lens structures for N-KZFS11 and K26R materials.*

Illuminant	Relative illumination power (*arb.u.*)	SNRs											
		6P			1G5P			2G4P			6G		
		B	G	R	B	G	R	B	G	R	B	G	R
A	800	36.367	39.961	44.304	36.364	39.954	44.289	36.356	39.963	44.315	36.376	39.966	44.322
	400	31.700	35.567	40.298	31.697	35.560	40.282	31.689	35.569	40.308	31.710	35.572	40.316
	50	15.025	19.232	24.487	15.021	19.224	24.473	15.015	19.234	24.498	15.037	19.237	24.506
D65	800	42.860	43.191	43.293	42.858	43.185	43.278	42.850	43.194	43.304	42.873	43.197	43.312
	400	39.165	39.532	39.646	39.164	39.526	39.631	39.157	39.535	39.657	39.180	39.539	39.665
	50	23.822	24.245	24.377	23.820	24.238	24.363	23.814	24.248	24.388	23.840	24.254	24.398
F2	800	35.630	37.423	37.518	35.627	37.416	37.503	35.619	37.424	37.529	35.640	37.426	37.537
	400	33.330	35.345	35.453	33.328	35.338	35.438	33.320	35.346	35.464	33.342	35.349	35.472
	50	20.750	23.350	23.493	20.747	23.342	23.480	20.741	23.352	23.505	20.767	23.357	23.515

Table 10 *Comparison of 1G5P, 2G4P and 6P against 6P lens stack SNR results for N-KZFS11 and K26R.*

Illuminant	Relative illumination power (*arb.u.*)	SNRs								
		1G5P vs. 6P (%)			2G4P vs. 6P (%)			6G vs. 6P (%)		
		B	G	R	B	G	R	B	G	R
A	800	-0.01	-0.02	-0.04	-0.03	0.00	0.02	0.02	0.01	0.04
	400	-0.01	-0.02	-0.04	-0.03	0.01	0.03	0.03	0.01	0.04
	50	-0.03	-0.04	-0.06	-0.07	0.01	0.05	0.08	0.03	0.08
D65	800	0.00	-0.02	-0.04	-0.02	0.01	0.02	0.03	0.01	0.04
	400	0.00	-0.02	-0.04	-0.02	0.01	0.03	0.04	0.02	0.05
	50	-0.01	-0.03	-0.06	-0.03	0.01	0.05	0.08	0.04	0.09
F2	800	-0.01	-0.02	-0.04	-0.03	0.00	0.03	0.03	0.01	0.05
	400	-0.01	-0.02	-0.04	-0.03	0.01	0.03	0.04	0.01	0.05
	50	-0.01	-0.03	-0.06	-0.04	0.01	0.05	0.08	0.03	0.09